Conserved regulatory motifs and resistance mechanisms of the MET receptor tyrosine kinase

by
Gabriella Estevam

DISSERTATION
Submitted in partial satisfaction of the requirements for degree of
DOCTOR OF PHILOSOPHY

in

Biochemistry and Molecular Biology

in the

GRADUATE DIVISION
of the
UNIVERSITY OF CALIFORNIA, SAN FRANCISCO

Approved:

DocuSigned by:
Natalia Jura
E438674A382B42F...

Natalia Jura
Chair

DocuSigned by:
James Fraser
DocuSigned by:
David Morgan
AAC13F29657E472...

James Fraser

David Morgan

Committee Members

Acknowledgements

I would like to begin by thanking my advisor and mentor, professor James Fraser. He accepted me into his lab in one of the most challenging times of my graduate career, when I was making a scientific pivot, but that did not deter him from placing immense trust in me and allowing me to lead a new project in the lab. He has shown true generosity, and with his mentorship I have grown as a scientist and individual. In the Fraser lab, I have had the opportunity to explore multiple facets of biochemistry, biophysics, and molecular biology, but always with a supportive base, encouragement, and respect. I've learned so much from my time in the Fraser Lab and James himself, mainly in regard to leadership and how to approaches scientific questions and challenges. As I graduate now, I am happy to say I'm more inspired and excited by research than ever before, and I am beyond grateful for his influence.

I'd like to thank my thesis committee, professor Natalia Jura and professor Dave Morgan, who have been consistent supporters throughout graduate school. They have believed in me, provided me scope, collaboration, advice, and mentorship both in my project and career. Their time, attention, and inclusively has been critical in my growth, and their labs have been welcoming spaces as I've developed broader skills. It has been a privilege and joy working with them.

Edmond Linossi has been not only a fantastic collaborator but also a mentor to me. His patience, moral and scientific support, communication, and careful attention to detail in literature has molded how I think about kinase function, kinetics, and signaling. It is an understatement to say he has been generous with his time in meeting as team MET nearly every week of our collaboration. It has been an honor.

Of course, without mentors past I would not be writing this thesis. Professor Michael Stone gave me my first start in basic science research as second year student in college. Michael entrusted me with several projects over the years, and with his mentorship I developed a strong foundation in biophysics. I'm proud to say my passion for structural biology and biochemistry started in the

Stone Research Group. There, Christina Palka was my first graduate student mentor, and to her I owe my pipetting skills and enthusiastic approach to research - to this day she is one of my role models. I would also like to thank professor Carrie Partch for her support and encouragement in applying to and attending graduate school. From her, I learned the fundamentals of kinases and kinetics I use and think about to this day, and it has been a pleasure attending her seminars here at UCSF. During my time at UCSC, Yulianna Ortega and Xingci Situ were fundamental in supporting my undergraduate research through the STEM Diversity Programs. They taught me to never close an opportunity on myself and their work has, and continues, to make an important impact on young scientists.

Next, I'd like to thank Fraser Lab members, both current and former, who have made it a positive and fulfilling environment. I want to particularly thank Erin Thompson, Jenna Pellegrino, Jennifer Michaud, John D. Lee, Lena Bergmann, José Luis Olmos Jr., Eric Greene, Christian Macdonald, Stephanie Wankowicz, Galen Correy, Daphne Chen, and Leah Roe. Willow Coyote-Maestas, has also been a DMS mentor to me - we've had good scientific banter and brainstorming over the years, and I'm happy to see him now as a professor.

Outside of lab, I would like to Henry Ng, Manuela Ritcher, Natalie Whitis, Amanda Chung, Brendan Nichols, Michael Schoof, and Ben Herken for their presence and friendship in my life, especially in the early years of graduate school before I essentially disappeared into the lab and stopped having a social life. I would also like to thank Daphne Chen, Leah Roe, Jenna Pellegrino, and José Luis Olmos Jr. for being my friends both inside and outside of lab.

Last, but in no way least, I'd like to thank my family. My mom, Adriana Orru, and dad, Rogerio Estevam, have made immeasurable sacrifices for me and my brother, Jonathan. Their outstanding bravery, dedication, and resilience is why I'm here. They taught me strong values and have always supported and believed in me. I am so proud of them and beyond grateful. Words will never be enough. Thank you.

Contributions

Chapter 1

Gabriella O. Estevam, Edmond M. Linossi, Christian B. Macdonald, Carla A. Espinoza, Jennifer M. Michaud, Willow Coyote-Maestas, Eric A. Collisson, Natalia Jura, James S. Fraser (2023). Conserved regulatory motifs in the juxtamembrane domain and kinase N-lobe revealed through deep mutational scanning of the MET receptor tyrosine kinase domain.BioRxiv.

Chapter 2

Gabriella O. Estevam, Edmond M. Linossi, Jingyou Rao, Christian B. Macdonald, Ashraya Ravikumar, Karson Chrispens, Willow Coyote-Maestas, Harold Pimentel, Eric A. Collisson, Natalia Jura, James S. Fraser.

Conserved regulatory motifs and resistance mechanisms of the MET receptor tyrosine kinase

Gabriella Orru Estevam

Abstract

MET is a receptor tyrosine kinase (RTK) responsible for initiating signaling pathways involved in development and wound repair. MET activation relies on ligand binding to the extracellular receptor, which prompts dimerization, intracellular phosphorylation, and recruitment of associated signaling proteins. Mutations, which are predominantly observed clinically in the intracellular juxtamembrane and kinase domains, can disrupt typical MET regulatory mechanisms. Understanding how juxtamembrane variants, such as exon 14 skipping (METΔEx14), and rare kinase domain mutations can increase signaling, often leading to cancer, remains a challenge. While ATP-competitive tyrosine kinase inhibitors (TKIs) offer growing potential for effectively targeting oncogenic MET, this too is limited by the emergence of resistance mutations with no treatment reference.

In chapter 1, I perform a parallel deep mutational scan (DMS) of MET intracellular kinase domain in two fusion protein backgrounds: wild type and METΔEx14. This comparative approach has revealed a critical hydrophobic interaction between a juxtamembrane segment and the kinase C-helix, pointing to differences in regulatory mechanisms between MET and other RTKs. Additionally, this study uncovered a β5 motif that acts as a structural pivot for kinase domain activation in MET and other TAM family of kinases. Lastly, a number of previously unknown activating mutations were identified, aiding the effort to annotate driver, passenger, and drug resistance mutations in the MET kinase domain.

Building upon this foundation, in chapter 2, I extended this DMS to study TKI resistance in the kinase domain against 11 MET inhibitors to reveal unique and shared resistance mechanisms

across inhibitor types. Leveraging this dataset as a reference, differential sensitivities to inhibitor pairs were explored to establish an experimental framework for assessing idiosyncratic resistance mutations, inhibitor combinations, and sequential treatments based on mutational sensitivity, location, and frequency within the screen, which hopefully can serve as a tool in future drug design.

Table of Contents

List of Figures

Chapter 1: Conserved regulatory motifs in the juxtamembrane domain and kinase N-lobe revealed through deep mutational scanning of the MET kinase domain

Contributing authors

Gabriella O. Estevam[1,2], Edmond M. Linossi[3,4], Christian B. Macdonald[1], Carla A. Espinoza[2,3,4], Jennifer M. Michaud[1], Willow Coyote-Maestas[1,7], Eric A. Collisson[5,6], Natalia Jura[5,6], James S. Fraser[1,7,*]

Affiliations

1. Department of Bioengineering and Therapeutic Sciences, University of California, San Francisco, San Francisco, United States

2. Tetrad Graduate Program, University of California San Francisco, San Francisco, United States

3. Cardiovascular Research Institute, University of California San Francisco, San Francisco, United States

4. Department of Cellular and Molecular Pharmacology, University of California San Francisco, United States

5. Helen Diller Family Comprehensive Cancer Center, University of California, San Francisco, United States

6. Department of Medicine/Hematology and Oncology, University of California, San Francisco, United States

7. Quantitative Biosciences Institute, University of California, San Francisco, United States

* - jfraser@fraserlab.com

Introduction

Receptor tyrosine kinases (RTKs) are transmembrane proteins that play an essential role in the initiation and regulation of signaling pathways (Lemmon and Schlessinger., 2010). Most RTKs are activated upon extracellular ligand binding, promoting a relay of intracellular phosphorylation events that drive signaling (Lemmon and Schlessinger., 2010). Mutations that allow RTKs to signal independent of ligand or other typical regulatory mechanisms are commonly identified in cancer (Duplaquet et al., 2018; Saraon et al., 2021; Comoglio et al., 2018). The transition from physiological ligand-dependent to pathological ligand-independent signaling is exemplified by the RTK, MET (**Figure 1.1**). Kinase activity of MET is normally activated by dimerization due to binding of hepatocyte growth factor (HGF) to the MET extracellular binding domain (Linossi et al., 2021). The resultant signaling is crucial for pathways implicated in development and wound repair (Trusolino et al., 2010; Petrini, 2015; Kato, 2017).

In contrast to physiological HGF-regulated activity, MET oncogenic activity arises through a variety of mechanisms such as gene amplification, mutations, gene fusions, and HGF autocrine loops (Duplaquet et al., 2018; Comoglio et al., 2018; Saraon et al., 2021; Kang et al., 2023). In MET fusions, replacement of the extracellular domain (ECD) and transmembrane domain by an in-frame translocation generates proteins with constitutive oligomerization of the intracellular domain (ICD), which leads to kinase domain (KD) activation (Sun et al., 2023; Liu et al., 2022). While MET fusions are rare in patients, they are important tools in studying MET activation in cellular models (Park et al., 1986; Vigna et al., 1999; Pal et al., 2017). A more common mutation in cancer is METΔEx14, a splicing variant that skips the entire exon 14 coding region, resulting in a shorter ICD missing approximately half of the juxtamembrane domain (JM) upstream of the kinase domain (KD) (Ma et al., 2003; Kong-beltran et al., 2006; Frampton et al., 2015) (**Figure 1.1**). The METΔEx14 variant maintains the ligand-binding ECD and is oncogenic in part due to a combination of increased ligand sensitivity and reduced degradation due to the loss of a Cbl ubiquitin ligase interaction (Frampton et al., 2015; Abella et al., 2005; Pechard et al., 2001;

Kong-beltran et al., 2006). Finally, as in many RTKs, distinct cancer-associated missense mutations are increasingly mapped to the MET kinase domain (Duplaquet et al., 2018; Chiara et al., 2003). Annotation of the status of these mutations as driver, passenger, or resistance mutations remains a significant challenge for the use of targeted therapies (Lu et al., 2017; Fernandes et al., 2021).

Here, we use deep mutational scanning (DMS) (Fowler and Fields, 2014) to screen a nearly comprehensive set of MET kinase domain mutations. Previous DMS studies have identified potential activating mutations and provided insight on the allosteric regulation of other kinases (Brenan et al., 2016; Ahler et al., 2019; Persky et al., 2020; Chakraborty et al., 2021; Hobbs et al., 2022). A phenotypic and inhibitor resistance DMS in the Ser/Thr kinase ERK2, reported tumor-associated mutations enriched at recruitment domains, in addition to identifying mutations that confer resistance without direct drug-protein interactions (Brenan et al., 2016). Similarly, when compared across Ser/Thr kinases like ERK2 and BRAF, and Tyr kinases like EGFR and ABL1, screens against CDK4/6 highlighted a "pocket protector" position near the ATP-binding site, and a generalizable allosteric, activating "keymaster" position within the N-lobe of kinases as sites of drug resistance (Persky et al., 2020). DMS of the Tyr kinase, SRC, elucidated a coordinated role between the F pocket and the SH4 domain to stabilize SRC's closed conformation (Ahler et al., 2019). Moreover, mutations to SRC autoinhibitory regions were identified as general resistance hotspots (Chakraborty et al., 2021). DMS of an ancestral reconstruction of the Syk-family kinases, AncSZ, revealed mutations that improve bacterial protein expression, in addition to finding commonalities between AncSZ and eukaryotic Syk kinases at regulatory regions like the αC-β4 loop (Hobbs et al., 2022). Together, these studies have been critical in illuminating novel features across Tyr and Ser/Thr kinases, which we now build on for the RTK family with MET.

To identify residues that have a direct effect on kinase function, we leveraged the murine Ba/F3 cell line as a selection system. The Ba/F3 cell line has been used as a model to study RTK

signaling because it exhibits: (1) undetected expression of endogenous RTKs including Met, (2) addiction to exogenous interleukin-3 (IL-3) for signaling and growth, and (3) dependence on exogenous kinase expression for growth in the absence of IL-3 (Daley and Baltimore, 1988; Warmuth et al., 2007; Koga et al., 2022). IL-3 withdrawal therefore serves as a permissive signaling switch that allows for the effective readout of variants that alter kinase-driven proliferation (Melnick et., al 2006). Here, we used the TPR fusion of the MET ICD (TPR-MET) to screen for potential activating and inactivating mutations in the KD. The TPR-MET fusion provides the advantage of studying MET's kinase domain in a cytoplasmic, constitutively oligomerized, active, and HGF-free system (**Figure 1.1**) (Cooper et al., 1984; Park et al., 1986; Peschard et al., 2001; Rodrigues and Park, 1993; Vigna et al., 1999; Mak et al., 2007; Pal et al., 2017; Lu et al., 2017; Fujino et al., 2019). This system also affords enough dynamic range to identify mutations that cause increased proliferation (Melnick et., al 2006). We also assessed the impact of exon 14 loss (ΔEx14) on the MET kinase mutational landscape to better understand this oncogenic lesion. Our comprehensive interrogation of the MET kinase domain reveals novel regulatory regions and acts as a reference for rare activating mutations in both wild type and ΔEx14 backgrounds.

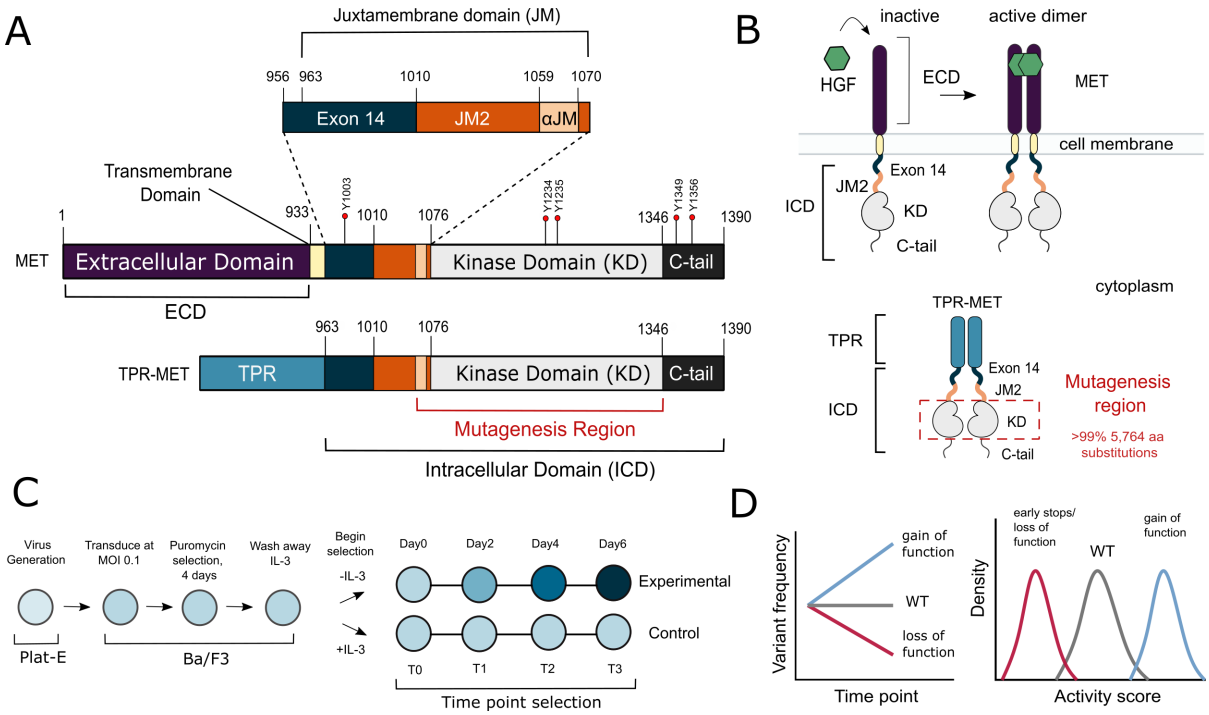

Figure 1.1. MET domain boundaries and DMS experimental workflow. (A) Domain boundaries of the full-length MET receptor (MET) and TPR-MET fusion (TPR-MET). Extracellular domain (ECD) and intracellular domain (ICD) are distinguished with important phosphorylation sites highlighted in red. Juxtamembrane domain (JM) boundaries are sectioned to annotate the exon 14 coding region and the remainder of the JM (JM2), which includes an JM-helix (JM). (B) Schematic of the full-length, membrane-associated MET receptor with posited MET ECD dimerization upon hepatocyte growth factor (HGF) binding; schematic of the cytoplasmically expressed, constitutively dimerized TPR-MET construct. The DMS mutagenesis region of the kinase domain (KD) is boarded in red. (C) Experimental screen workflow applied to generate and express kinase domain variants prior to selection, beginning with virus generation in Plat-E cells, transduction into Ba/F3 cells at a 0.1 multiplicity of infection (MOI), puromycin selection to enrich for positively infected cells, followed by the IL-3 selection process and time point collection for deep sequencing. (D) Post-selection method for analyzing and validating activity scores based on observed variant frequencies at each time point, measured as a slope which can then be plotted as a distribution.

Results

Measurement of MET kinase domain variant activities in a wild type intracellular domain

To perform a DMS in TPR-MET, we generated a site saturation mutagenesis DNA library of the MET KD (**Figure 1.1**). Our library also included the final alpha-helix of the JM region (JM), which is resolved in most crystal structures, and is just upstream of the KD. Our variant library carried >99% of all possible missense mutations from positions 1059-1345 of human MET, including two internal controls: a WT-synonymous substitution at each position and premature stop codons every eleven positions (24 total). These controls allow us to use deep sequencing to estimate the fitness of WT and null variants, respectively. The library was cloned into the TPR fusion background containing the remaining JM (aa 963-1058), upstream of the JM and KD, and the complete C-terminal tail (aa 1346-1390) downstream of the KD (**Figure 1.1**). We transduced the library into Ba/F3 cells using retrovirus (**Figure 1.1**). Cells were grown in the presence and absence of IL-3 and samples were deep sequenced at distinct timepoints to identify variant frequencies (**Figure 1.1**). We then measured variant fitness scores using Enrich2 (Rubin et al., 2017) for each selection condition (**Figure 1.2**).

As expected, we observed no selection in the IL-3 control condition and a low correlation was observed across replicates (Pearson's r = 0.30). In this condition, all variants, including premature stop codons, displayed near WT-like fitness (**Supplemental Figure 1.7**). In contrast, for the condition where IL-3 was withdrawn, we observed strong evidence of functional selection. There are large differences between the fitness distributions for WT-synonymous, missense, and nonsense mutations. Nonsense mutations are strongly loss-of-function (LOF) (**Supplemental Figure 1.7**). Very few missense mutations are more fit than the average synonymous (WT) variants, which indicates that gain-of-function (GOF) mutations are rare. In addition fitness estimates for specific mutations across replicates of this treatment are strongly correlated (Pearson's r = 0.96) (**Figure 1.2, Supplemental Figure 1.7**).

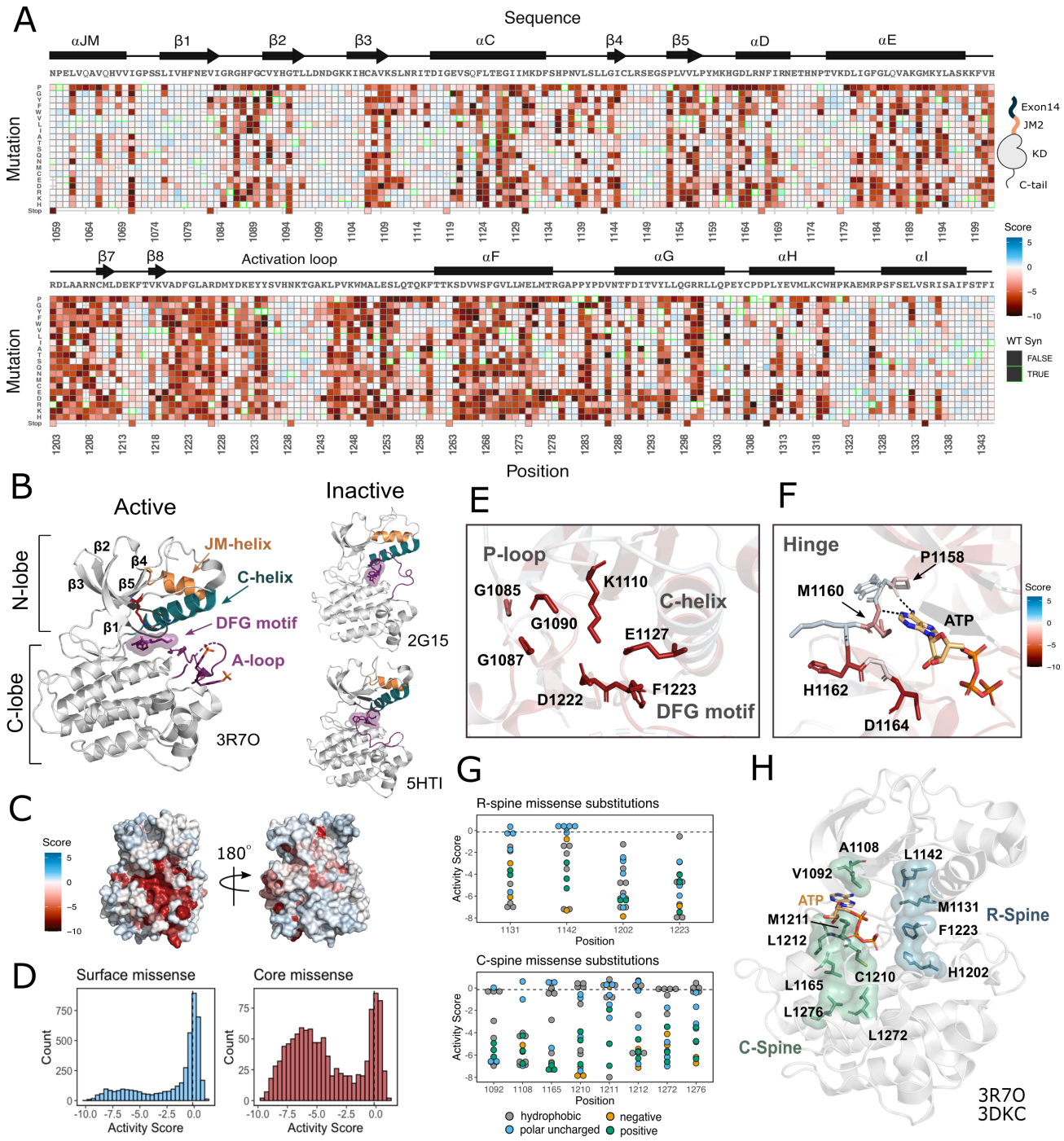

Figure 1.2. Measured effect of MET kinase domain variants across 287 amino acid positions in the context of the full-length juxtamembrane. (A) Activity score heatmap of MET kinase domain variants. WT-synonymous substitutions are outlined in green. (B) Active structure of the MET kinase domain (PDB 3R7O), and two representative inactive structures (PDB 2G15, 5HTI) with motif details highlighted. (C) Surface representation of average activity scores mapped on an active structure (PDB 3R7O). (Figure caption continued on the next page).

(Figure caption continued from the previous page). Synonymous and nonsense mutations were left out of the averaging and surface representation. Residues at the N- and C-term that were not screened, but modeled in the crystal structure are in white and not considered in the averaging and mapping.(D) Comparison of surface and core residues activity score distributions. A vertical dashed line in both graphs represents the mean score of WT-synonymous mutations. (E) Catalytic site and key residues involved in ATP binding and stabilization. Average score of variants mapped onto an active structure (PDB 3R7O). (F) Hinge region residues involved in ATP binding and stabilization. Average score of variants mapped onto an active structure (PDB 3R7O), and overlaid with the ATP molecule of the ATP-bound MET structure (PDB 3DKC). (G) Activity scores and physiochemistry of variants shown for each residue position of the R- and C- spine of MET. (H) R-spine (blue) and C-spine (green) residues highlighted on an active structure (PDB 3R7O) overlaid with the ATP molecule of the ATP-bound MET structure (PDB 3DKC).

Mutational landscape of the MET kinase domain

MET contains a canonical tyrosine kinase domain, sharing structural and conformational hallmarks with other protein kinases (Linossi et al., 2021; Schiering et al., 2003; Wang et al., 2005). Kinase domains have a conserved hydrophobic core with several motifs that are important for folding, stability, conformational transitions, and catalysis. The conformational transition between an active and inactive state relies on the hinge-like closure of the N- and C-"lobes" around an ATP-bound catalytic site. The N-lobe is a dynamic unit comprised of five β-sheets and the C-helix, while the C-lobe is a more rigid unit composed of seven -helices connected by loops (Kornev et al, 2006; Kornev et al, 2008). Two hydrophobic "spines" (the R- and C-spine) assemble across the lobes as the kinase transitions to an active state (Taylor & Kornev, 2011; Hu et al., 2014; Taylor et al., 2015). The transitions from inactive to active states of MET are typical for a tyrosine kinase: the C-helix moves to an "in" position, positioning E1127 to form a salt-bridge with K1110. In addition, the flip of the DFG (residues 1222-1224) motif aligns F1223 with the rest of the R-spine and permits hydrogen bonds between D1222 and ATP (Kornev et al, 2006).

Our DMS results highlight that the conserved regulatory and catalytic motifs in MET are highly sensitive to mutation (**Figure 1.2**). Catalytic site residues involved in either the chemical step of phosphate transfer or the conformational adaptation to ATP binding, such as K1110, E1127,

D1222, and G1224, are intolerant of amino acid substitutions (**Figure 1.2**). Residues surrounding the kinase "hinge", which are involved in coordinating the adenosine potion of ATP (Azam et al., 2008; Dar and Shokat, 2011), are more tolerant to mutation (**Figure 1.2**). This tolerance is especially prominent in residues that make backbone interactions with ATP. Variants in R-spine residues are strongly enriched in loss-of-function (LOF) fitness values. This result speaks to the importance of residue identity, not just physicochemical characteristics in the function of MET. R-spine residues F1223 and H1202 are part of the catalytic DFG and HRD motifs and do not tolerate any mutations (**Figure 1.2**). For R-spine residues M1131 and L1142 positions, only a small number of polar uncharged substitutions show WT-like fitness (**Figure 1.2**). Surprisingly, the MET C-spine was only moderately sensitive to mutations, with most hydrophobic and polar uncharged amino acid substitutions showing WT-like fitness (**Figure 1.2**). We performed a sequence alignment of human RTK kinase domains for both the R- and C-spines, referenced to the MET kinase domain sequence (**Supplemental Figure 1.8**) to explore whether there was greater evolutionary conservation for the R-spine than the C-spine for MET. Consistent with our results, the C-spine was less conserved, but is enriched for hydrophobic residues (**Supplemental Figure 1.8**). These results indicated that key catalytic and regulatory motifs display varying sensitivity. The R-spine and catalytic residues are more highly constrained, whereas C-spine and hinge residues can tolerate a greater number of semi-conservative mutations.

On balance, most solvent exposed and loop regions were more permissive to mutations (**Figure 1.2**). However, certain key regulatory elements stand out, with stronger mutational sensitivity than might be expected based on structural features alone. For example, the C-helix-β4 loop which is important in C-helix modulation and regulation in many kinases (Chen et al., 2007; Yeung et al., 2020), showed LOF effects in agreement with the previously described "ΦxHxNΦΦx" motif (Yeung et al., 2020). Similarly, the glycine residues in the "GxGxxG" motif of the P-loop, which gates ATP entry into the active site, were intolerant to substitutions. Two other relatively immutable sites included Y1234 and Y1235, in the activation loop (A-loop) of MET. The phosphorylation of these residues is required for stabilizing the A-loop in an extended

conformation that enables substrate binding and efficient catalysis (Ferracini et al, 1991; Naldini et al, 1991). Collectively, this deep mutational scan confirms the importance of canonical kinase features and provides a reference point for discovering previously unexplored features of the MET kinase.

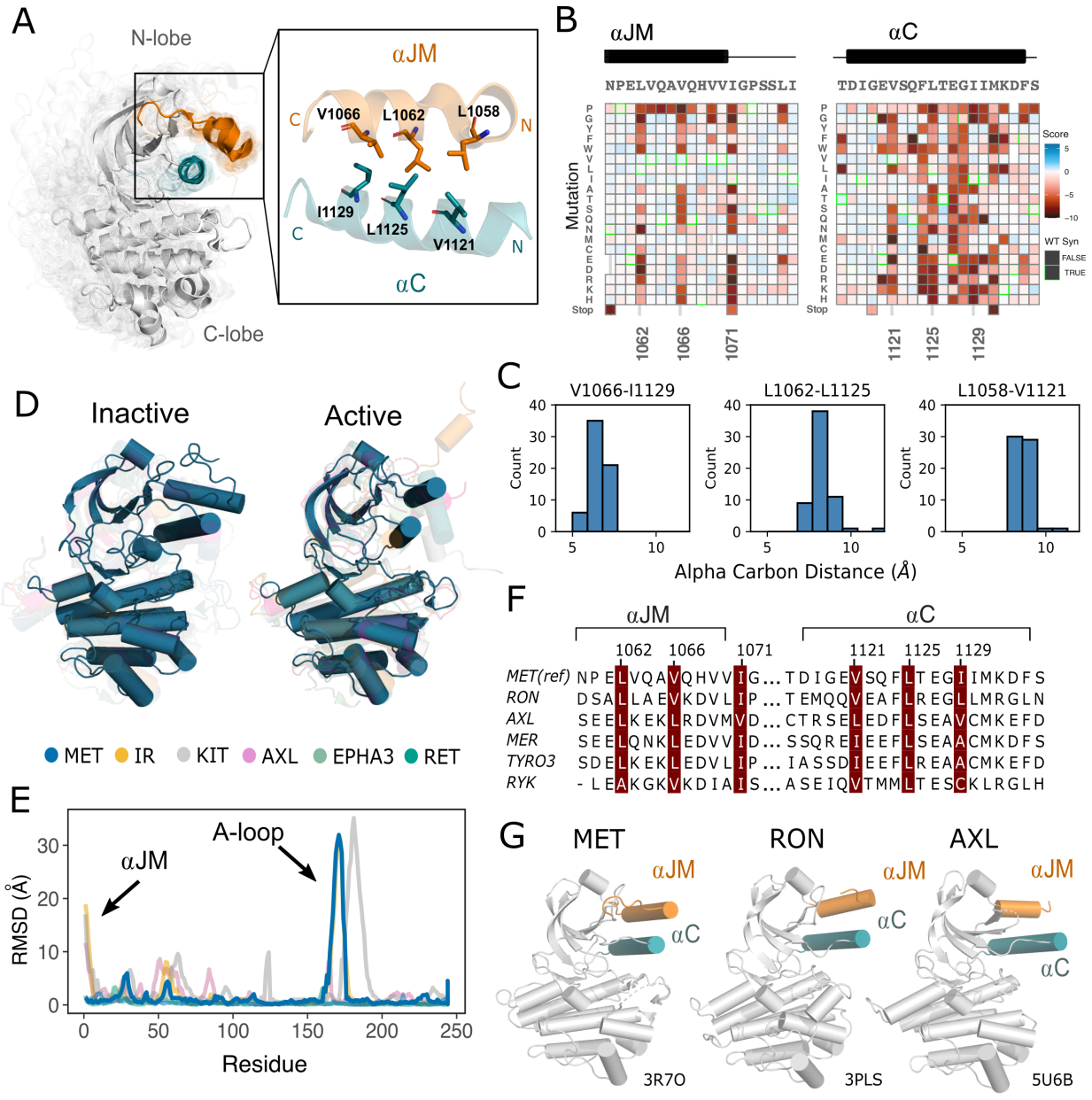

Figure 1.3. Essential JM and C-helix interactions revealed through variant and structural analysis. (A) Ensemble of 93 MET kinase domain crystal structures available in the PDB. All structures, independent of conformation, were locally aligned to JM residues 1059-1070 (all resolved JM and JM-helix residues in orange), and C-helix residues 1117-1134 (teal). In solid gray is a representative active structure (PDB 3R7O). Residues involved in the JM and C-helix interface. (Figure caption continued on the next page).

(Figure caption continued from the previous page). (B) Heatmap sections of the JM-helix and C-helix from the MET ICD screen. (C) Distribution of alpha carbon distances for residues in the JM-helix and C-helix interface, shown for 63 MET crystal structures in the ensemble with residues modeled for positions 1058, 1062, 1066, 1121, 1125, 1129. Distances are independent of conformation. (D) Global alignment of inactive and active RTK kinase domain structures with resolved JM regions. (E) Residue-by-residue, backbone RMSD comparisons of inactive and active structures of MET, AXL, IR, EPHA3, KIT, and RET. (F) MuscleWS alignment of human MET and TAM family juxtamembrane helix sequences. (G) Crystal structures of MET (PDB 3R7O), RON (PDB 3PLS), and AXL (PDB 5U6B) kinase domains, with JM-helix (orange) and C-helix (teal) highlighted. The inactive conformation of AXL shows an JM-helix and C-helix hydrophobic interaction similar to MET, but unlike MET, these interactions are slightly pivoted by a JM-helix turn in its active conformation.

Critical contacts between the JM- and C-helices provide insight into potential juxtamembrane regulation of MET

Given the importance of juxtamembrane (JM) regions in controlling the activation of many RTKs (Hubbard et al 2004; Zhang et al., 2006; Jura et al., 2009; Cabail et al., 2015; Wybenga-Groot et al., 2001; Wiesner et al., 2006) and the prevalence of exon 14 skipping within the JM of MET in cancer (Lu et al., 2017), we were interested in how patterns of mutational sensitivity from the DMS could relate the JM to the activation mechanism of MET. The MET JM (aa 956-1075) is predicted to be largely unstructured, but a small region (aa 1059-1070) folds into an alpha helix (JM) that packs on top of the C-helix of the kinase domain, forming a hydrophobic interface (**Figure 1.3**). Since we included JM in the DMS library, we examined the pattern of substitutions for this region and the C-helix. We observed a strong hydrophobic preference along both the JM and C-helix residues comprising this interface (**Figure 1.3**). The adjacent JM residue 1071 also strongly prefers hydrophobic residues. This residue does not interact with C-helix, but evidently plays an important role in maintaining interactions with a hydrophobic patch in the N-lobe that includes residues L1076, L1097, and V1158. This result indicates the importance of burying the hydrophobic surfaces of the N-lobe, and C-helix in particular, for maintaining an active kinase in the TPR-MET background.

Since the C-helix conformation is a strong predictor of activity in kinases (Ung et al., 2018;

Modi and Dunbrack, 2019), and is often modulated by protein-protein interactions or autoregulatory domains (Huse & Kuriyan, 2002), we hypothesized that these hydrophobic contacts might form preferentially in active MET kinase. The precedence for this idea comes from structural studies of RTK ICDs in the EGF, PDGF, EPH, and IR families (Zhang et al., 2006; Jura et al., 2009; Griffith et al., 2004; Wybenga-Groot et al., 2001; Wiesner et al., 2006; Li et al, 2003; Cabail et al., 2015). For example, in EGFR the JM stabilizes an active, asymmetric head-to-tail dimer (Zhang et al., 2006; Jura et al., 2009). In IR, the JM engages with C-helix to maintain an inactive state, until JM- C-helix interactions are released and swapped to stabilize an active kinase dimer (Cabail et al., 2015). In contrast, in FLT3 the JM packs against the catalytic cleft to stabilize an inactive KD confirmation (Griffith et al., 2004). To test how MET kinase activation is linked to JM conformation, we compared the 93 crystal structures of the MET kinase domain with a modeled portion of its JM, as a MET pseudo-ensemble (**Figure 1.3**). We aligned these structures on the N-lobe to eliminate the effect of the changes in relative N- and C-lobe alignment that occurs with activation. Despite large changes in the relative position of the C-lobe, corresponding to active and inactive structural hallmarks, there was little JM conformational variability or dependence on active/inactive state (**Figure 1.3**). Rather, JM consistently packed against C-helix and maintained the hydrophobic interface across all structures (**Figure 1.3**).

To compare the MET JM- C-helix to other RTK JM-KD interactions, we compiled a set of human RTK kinase domain crystal structures that contain a modeled JM, and have both active and inactive structures available in the PDB. Within this set, IR and KIT displayed large conformational variability of the JM between active and inactive states, but MET stood out again in low conformational variability independent of the kinase activation state (**Figure 1.3**). Indeed, when we examined JMs and kinase domains in a protein sequence alignment of all RTK, we observed that while C-helix is conserved across RTKs, only MET (MET, RON), TAM (TYRO3, AXL, MER), and the RYK pseudokinase harbor an JM with a hydrophobic sequence pattern (**Figure 1.3**). Together, the mutational sensitivity and structural conservation of MET's JM- C-helix interface point to a model, that may be shared with RON and TAM family RTKs,

where JM- C-helix contacts are maintained in both the active and inactive state and are important for TPR-MET stability and activity.

β5 P1153 is a structural pivot for the MET kinase domain N-lobe

Although most regions of high sensitivity from the DMS impinge on well-described aspects of kinase activation, P1153 stood out as a previously unremarked upon position with extremely low tolerance to mutation in our DMS (**Figure 1.4**). Only proline was tolerated in this position. P1153 is located in the β4-β5 region, which plays a role in C-helix coordination and R-spine support (McClendon et al., 2014; Meharena et al., 2013; Taylor and Kornev, 2011). The β4 strand is connected to C-helix and influences activity through regulatory mechanisms such as the "molecular break" in RTKs like FGFR, or through cis- and trans- protein interactions (Chen et al., 2007; Yeung et al., 2020). The β5 strand engages with C-helix, the hinge, and harbors the disease-associated "gatekeeper" position (Azam et al., 2008). The immutability phenotype was especially notable because P1153 is not conserved across kinases (**Supplemental Figure 1.9**).

To test the importance of this residue in a more physiological membrane-bound context, we expressed WT and P11553L variants of the full-length (FL) MET receptor in HEK293 cells. Based on the DMS in Ba/F3 cells, we expected that P1153 mutations would not signal or express poorly in this context. Indeed, relative to the WT MET receptor, P1153L expressed equivalently, but dramatically reduced signals for phosphorylation of the MET activation loop tyrosines, a marker of active MET signaling (**Figure 1.4**). To test whether this importance extended to another MET family member, RON receptor, which also has proline residue at the equivalent position, we tested and observed similar results. Notably, in RON the equivalent proline mutation also significantly compromised receptor expression (**Supplemental Figure 1.9**). These experiments provided initial validation that the results from the TPR-MET construct would translate to a full-length MET receptor context, and indicated the family-specific functional importance of proline in this position ,of the β4-β5 loop.

Next we analyzed the structural environment of P1153. It packs in a hydrophobic cluster with the resistance-associated β3- C-helix "keymaster" position (L1112 in MET) (Persky et al., 2020) and F1124 of C-helix. The hydrophobic packing around P1153 by F1124 and L1112 changes across MET active and inactive structures (**Figure 1.4**). As C-helix adopts an active "in" or inactive "out" conformation, L1112 rotates inward toward the core of the N-lobe to replace F1124 and maintain the hydrophobic environment around P1153 (**Figure 1.4**). The maintenance of hydrophobic contacts across these conformational changes led us to re-examine the relative lack of sequence conservation of P1153 (Supplemental Data Figure 1.11). We compiled a set of representative kinase domain structures from each RTK family, as well as those that have had DMS studies performed previously, and analyzed the Ramachandran angles of the analogous residue in the β4-β5 loop. Although most kinases have a non-proline amino acid at that position, the analogous residues cluster around or inside the proline-permissive contour of Ramachandran space (**Figure 1.4**). Interestingly, while no other RTK family aside from MET and TAM family kinases have a proline at the β4-β5 loop position, most do have a proline exactly one position upstream. This shift occurs both in sequence and in structure: the upstream proline does not participate in the hydrophobic pivot observed here for P1153 in MET (**Figure 1.4**). This analysis suggests that the MET and TAM families represent a subset of RTKs that have evolved the surrounding sequence to accommodate only proline in this structurally restrained region of the β4-β5 loop, explaining the immutability in our DMS experiment.

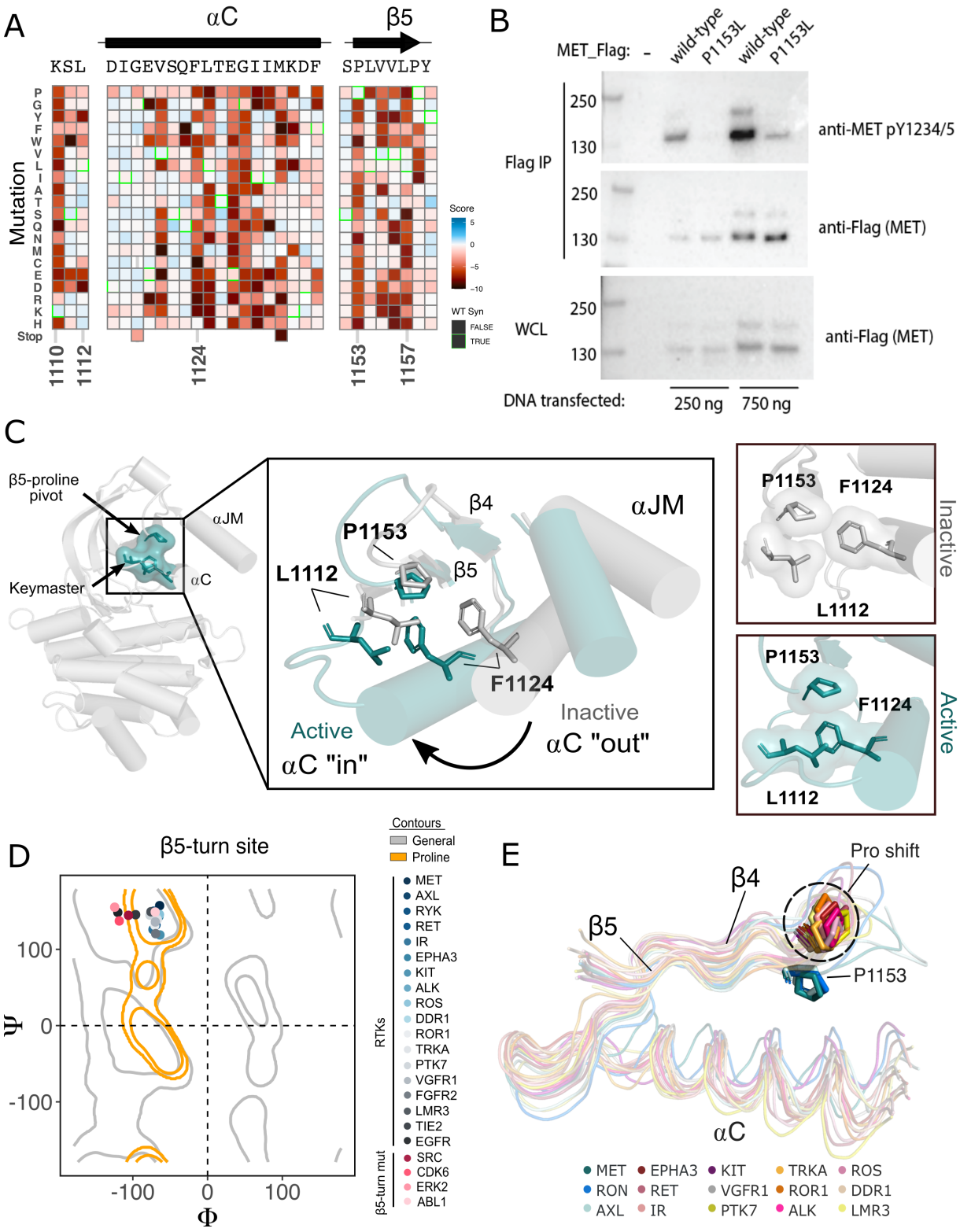

Figure 1.4. β5 Proline motif is an activation pivot for the MET kinase domain. (A) Respective sections of the MET ICD heatmap. (B) FLAG-IP western blot of the P1153L mutation post 24hr expression in HEK293 cells. (Figure caption continued on the next page).

(Figure caption continued from the previous page). (C) Residues of the MET P1153 N-lobe network displayed in an active (PDB 3R7O) and inactive structure (PDB 2G15). Surface representation of residues involved in the P1153 network. (D) Ramachandran plot and structural position of P1153 in MET and one representative kinase domain of each RTK subfamily. (E) Structural representation of the RTK Pro shift of the β4-5 loop. One representative RTK kinase domain from each sub-family is locally aligned to β4-5 of MET.

Mutational landscape of the MET kinase domain in the absence of the exon 14 coding region

Exon 14 skipping, which maintains the ECD and transmembrane region while truncating the ICD at the JM, is one of the most common driver mutations observed in MET(Fernandes et al., 2021; Lu et al., 2017). The oncogenic effect is thought to, at least partially, result from removal of the docking site for Cbl, a ubiquitin ligase responsible for MET lysosomal degradation (Mak et al., 2007; Peschard et al., 2001; Petrelli et a., 2003; Abella et al., 2005; Kong-Beltran et al., 2006). Based on previous findings showing a TPR-METΔEx14 growth advantage over the MET receptor and METΔEx14 receptor, and TPR-MET in anchorage-independent assays of AALE cells (Lu et al., 2017) and fibroblasts (Vigna et al.,1999), we tested whether there was also a growth advantage in Ba/F3 cells (**Figure 1.5**). Counter to expectations, we did not observe a discernible growth differential for TPR-METΔEx14 relative to TPR-MET (**Figure 1.5, Supplemental Figure 1.11**). It is important to note that exon 14 skipping normally occurs in the context of the full length protein, not in fusions such as TPR-MET. Therefore, the lack of a growth rate difference may be due to the need for Cbl regulation to occur at the plasma membrane (Mak et al., 2007) or due to other aspects of the Ba/F3 system. Although the lack of a growth differential means an exon 14-specific mechanism cannot be fully addressed in this experimental format, KD mutational responses are still representative and comparable.

We performed a parallel DMS of the MET KD in the background of an exon 14-skipped ICD (TPR-METΔEx14) (**Figure 1.5**). Most regions implicated in the TPR-MET DMS were similarly sensitive in the TPR-METΔEx14 (**Figure 1.5, Supplemental Figure 1.11**). For example, the

P1153 β4-β5 loop site was also intolerant to mutations in TPR-METΔEx14 (**Supplemental Figure 1.11**). Similarly, the R- and C-spine were sensitive to physicochemical changes outside of hydrophobic and polar uncharged substitutions (**Supplemental Figure 1.11**). To identify specific mutations of the KD that are uniquely sensitive to the presence or absence of exon 14, we filtered variants with the largest differences in activity scores between TPR-MET and TPR-METΔEx14 (**Figure 1.5, Supplemental Figure 1.11**).

As an example of the differences between the two backgrounds, we focused on the JM- C-helix interface. This region displayed relatively high sensitivity to non-hydrophobic substitutions in TPR-MET (**Figure 1.3**), but it was more tolerant to mutations in the TPR-METΔEx14 background (**Figure 1.5, Supplemental Figure 1.11**). To test whether this JM and C-helix sensitivity difference translated to the full-length receptor, we introduced L1062D, a mutation at the JM interface, and S1122Q, an C-helix surface mutation, into the MET and METΔEx14 receptor backgrounds in HeLa cells lacking endogenous MET (**Figure 1.5**). Consistent with the results from the DMS screen, in unstimulated cells, we observed that a marker of MET activation, A-loop phosphorylation, was dramatically reduced in the MET receptor for L1062D, but less so in METΔEx14, relative to WT controls (**Figure 1.5**). Furthermore, upon HGF treatment, L1062D in the METΔEx14 background exhibited a high degree of activation, but L1062D MET did not. An additional marker of active MET signaling, phosphorylation on p44/42 MAPK (ERK), was similarly responsive (**Figure 1.5**). In contrast, S1122Q was expected to have a gain-of-function effect in the MET receptor and a loss-of-function effect in the METΔEx14 receptor. For this mutation we observed no difference relative to WT in A-loop phosphorylation at baseline or upon HGF stimulation (**Figure 1.5**).

These results suggest that the correlation between DMS fitness in TPR-MET and acute A-loop phosphorylation in the MET receptor is not absolute. Since KD activation at a single time point was the only parameter we explored with the membrane-associated receptor, other aspects such as sustained signaling, recruitment of specific signaling adapters, or changes in MET regulation may

be more consistent with the proliferative readout of the DMS. In addition, the inconsistency in the S1122Q result may be a specific feature of the dimerised, cytoplasmic TPR-MET signaling that is sensitive to interactions with the portion of the JM deleted by exon 14. Collectively, these results highlight that the JM- C-helix interface is sensitive to mutation and the presence or absence of exon 14 can alter this sensitivity. While the experimental parameters of this screen may limit how translatable some mutations are in a membrane-associated receptor or in non-proliferative conditions, the consistency of most residues between backgrounds provides increased confidence in the atlas of mutational effects on MET activation.

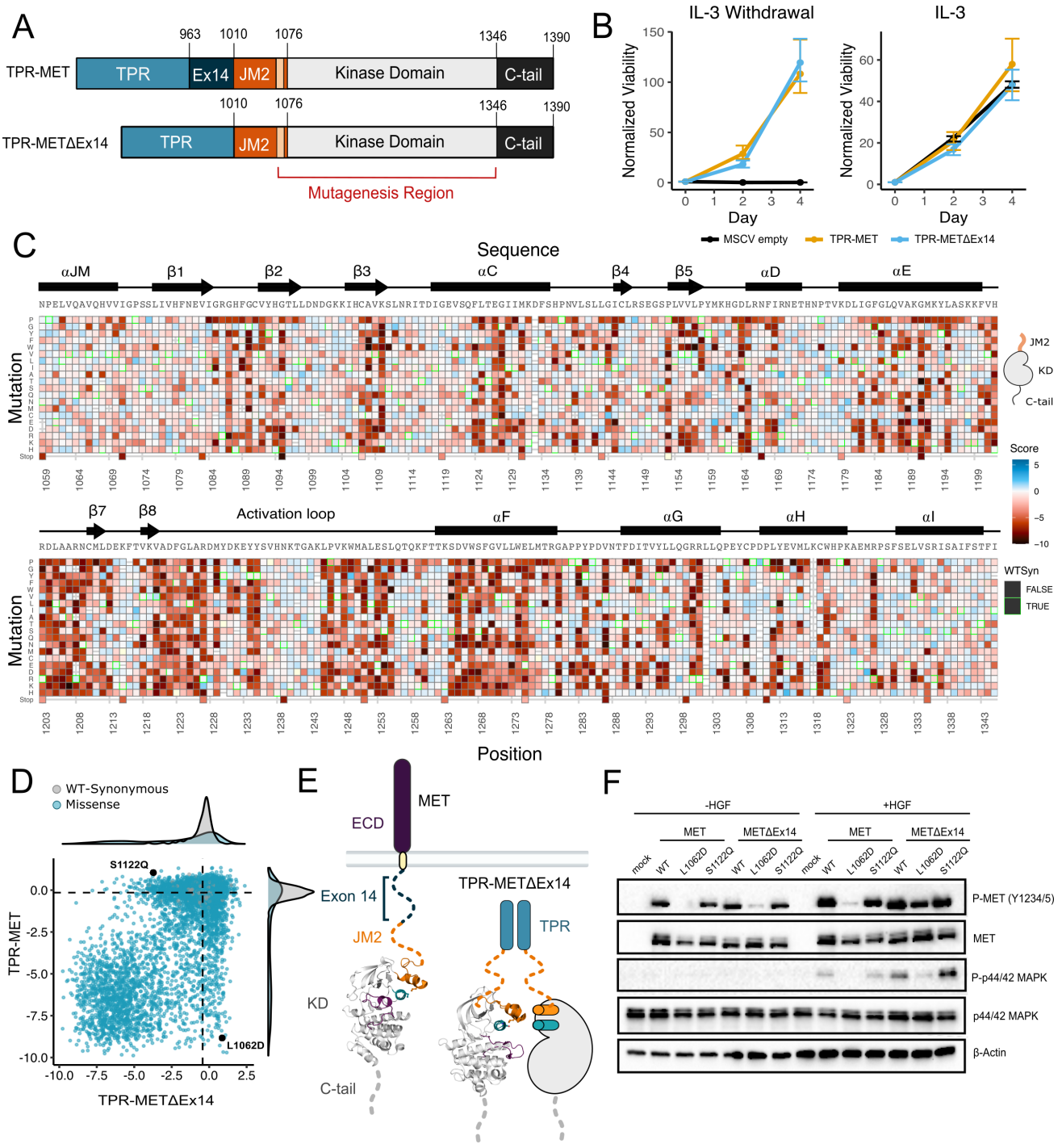

Figure 1.5. Comparative measurement of MET kinase domain variants across 287 amino acid positions in the absence (TPR-METΔEx14) and presence of exon 14 (TPR-MET). (A) Domain boundaries and schematics of the TPR-MET ICD and TPR-METΔEx14 ICD constructs. (Figure caption continued on the next page).

(Figure caption continued from the previous page). (B) Proliferation assay of parental TPR-MET, TPR-METΔEx14, and MSCV empty vectors expressed in Ba/F3 under IL-3 withdrawal and IL-3 conditions. Cell viability was normalized to day 0. (C) Activity score heatmap of METΔEx14 kinase domain variants. WT-synonymous substitutions are outlined in green. (D) Scatter plot of TPR-METΔEx14 versus TPR-MET activity scores for each variant with distributions displayed on the margins. Dashed lines represent the WT synonymous average score for METΔEx14 versus MET. (E) Schematic of the kinase domain (PDB 2G15, 3R7O) in a full-length receptor and TPR-METΔEx14 context. (F) Western blot of endogenous MET KO HeLa cells transiently transfected with L1062D and S112Q mutants in the MET and METΔEx14 receptor, with and without HGF stimulation (50ng/ml, 15 min stimulation, 37°C).

Analysis of cancer-associated and resistance mutations in MET and METΔEx14

To assess the ability of the DMS to classify driver, passenger, and resistance mutations, we first gathered all MET kinase domain mutations reported from clinical observations in cBioPortal (Cerami et al., 2012; Gao et al., 2013) (**Figure 1.6**). Relative to the distribution of all missense mutations, the distribution of clinically observed mutations is strongly shifted to higher fitness values for both TPR-MET and TPR-METΔEx14 screens (**Figure 1.6**). Most of these mutations have near WT-fitness levels, with a small number having GOF fitness effects (**Figure 1.6**). Next we further subdivided our observations based on annotations in cBioPortal as either "clinical, validated" or "clinical, not validated". Notably, mutations in the "clinical, not validated" category were outliers with lower fitness values, indicating that these are likely passenger mutations (**Figure 1.6**). These results validate that the DMS recapitulates known oncogenic MET kinase variants and suggest that the screen can be used to help classify driver vs. passenger mutations.

Interestingly, there are some missense mutations that are strong GOF variants in the DMS that have not been reported clinically, potentially indicative of novel activating mutations. We classify these mutations as "not clinically observed, GOF." We hypothesized that these variants are more difficult to observe clinically because of the constraints of the genetic code. To test this idea, we calculated the Hamming distance between the WT MET codon and mutant codon for each position within our dataset (**Figure 1.6**). We found that most "clinical, validated" mutations had Hamming distances of 1-2 nucleotide substitutions from WT (**Figure 1.6**). However, the most

common Hamming distances for "not clinically observed, GOF" codons shifted 2-3 changes away from WT (**Figure 1.6**). These GOF mutations are dispersed throughout the structure of MET kinase and have distinct patterns depending on the presence or absence of exon 14 (**Figure 1.6**). These results suggest that the DMS can identify GOF mutations that require a larger genetic "leap" than what is observed in natural populations. Furthermore, the relative paucity of "not clinically observed, GOF" mutations at Hamming distance of 1 suggests that clinical observations have nearly identified all possible activating MET mutations that require only a single nucleotide change. Collectively, this suggests that our atlas will be of particular use for deciding on driver status for rare mutations that require multiple nucleotide changes.

Finally, we assessed the distribution of fitness effects for clinically observed resistance mutations (Duplaquet et al., 2018; Fernandes et al., 2021; Saraon et al., 2021; Lu et al., 2017; Fujino et al., 2019). Resistance mutations, which are clustered around the active site, are also enriched towards higher fitness values than the background missense mutation distribution (**Figure 1.6**). This result suggests that most of these mutations can pre-exist in the population even in the absence of selective pressure from an inhibitor. GOF resistance mutations may indicate an effect on the equilibrium of kinase activation, whereas LOF resistance mutations likely affect inhibitor-protein interactions directly. For instance, Y1230C is a recurrent resistance mutation (Bardelli et al., 1998) that interrupts Pi interactions that stabilize inhibitors at the active site, but in the absence of an inhibitor is unfavorable in METΔEx14 (**Figure 1.6, Supplemental Figure 1.12**). These results indicate that DMS has potential to interpret the effects of resistance mutations, an area of active concern for patients being treated with MET inhibitors in the clinic.

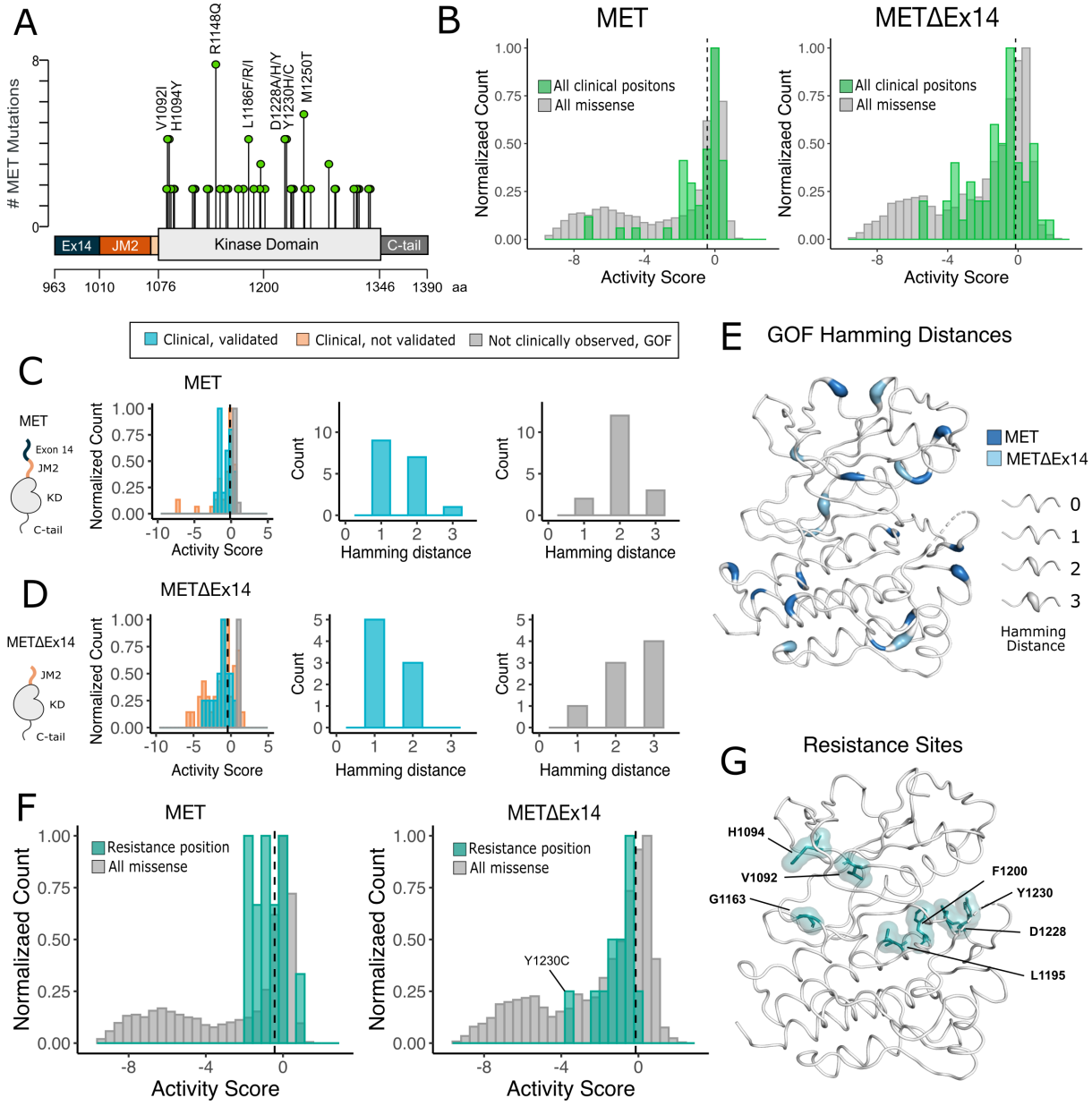

Figure 1.6. Mutations with greater proliferative effects than cancer-associated mutations, and differential sensitivities between MET and METΔEx14 identified.(A) Lollipop diagram of MET kinase domain mutations and frequencies annotated in cBioPortal. (B) Distributions of cancer-associated mutations overlaid with all missense mutations. Counts are normalized to the total mutations in each screen dataset. (Figure caption continued on the next page).

(Figure caption continued from the previous page). (C-D) Distributions of categorized cancer-associated mutations. Counts are normalized to the total mutations in each screen dataset. Hamming distance distributions of clinical, validated MET cancer mutations and clinically unobserved, GOF mutations detected in the screen for both ICD backgrounds. (E) Cancer-associated mutations mapped onto a MET kinase domain structure, colored according to MET and METΔEx14 backgrounds, with Hamming distance represented by the ribbon thickness at each position (PDB 3R7O). (F) Reported resistance mutation distributions for MET and METΔEx14, overlaid with their respective missense distributions. (G) Inhibitor resistance mutation positions shown on an active MET kinase domain structure in teal (PDB 3R7O).

Discussion

Our parallel DMS of the MET kinase domain has revealed how mutations affect the allosteric regulation of MET in two clinically relevant juxtamembrane backgrounds. Auto-regulation via juxtamembrane segments is a common feature of RTKs like the EGF, PDGF, EPH, and IR families (Hubbard et al 2004; Zhang et al., 2006; Jura et al., 2009). We propose that MET is similarly regulated based on the distinct sensitivity of the interface of JM and C helices to mutations between TPR-MET and TPR-METΔEx14. Given that exon 14 is directly upstream of this region, it is possible that the making and breaking of contacts between the JM and C helices during kinase activation observed in other families has a distinct structural analogue in MET. Rather than variable contacts between the JM and C-helix, as observed in other families, we hypothesize that the exon 14 region of the JM has activation-state dependent contacts with the JM- C unit. In this model JM- C-helix move in unison between active and inactive conformations, with the rest of the JM making contacts to JM that regulate the activation state. When exon 14 is skipped, these contacts are absent, tilting the equilibrium towards kinase activation. This model could augment known mechanisms of METΔEx14 activity, most notably a lack of Cbl-mediated downregulation, to enhance the oncogenic potential of this variant.

Conclusively addressing the question of how exon 14 skipping activates MET is difficult in the TPR-fusion system that we have employed here. While soluble, cytosolic oligomerization occurs for MET fusion proteins observed in some tumors, using the TPR-fusion may not accurately model all of the changes found in other types of MET lesions, such as METΔEx14. Therefore,

this strategy may underestimate the effects of regulatory mechanisms related to membrane engagement or ICD oligomerization. Nonetheless, the experimental parameters of this study based on cell proliferation allowed us to understand the mutational sensitivities of the kinase domain in a cytoplasmic and constitutively active environment..

Analyzing the mutational landscape with the TPR-MET fusion approach employed here has led to multiple new insights, some of which were also validated in the full-length MET receptor. For example, one of the most unexpected regions of mutational sensitivity was P1153 in the β4-β5 loop. Based on the observed proline sequence shift, β4-β5 loop conformational restraints, and conserved hydrophobic network around the β4-β5 loop position, we suggest that this proline residue is an evolutionary dead-end. In ancestral kinases, a proline could be adopted without a significant cost at the corresponding β4-β5 loop position due to this residue being positioned in proline-permissive Ramachandran space. After drift of the surrounding hydrophobic residues, the sequence for these residues has adapted to the unique structural properties of proline, rendering it impossible to substitute for an alternative amino acid. Interestingly, evolutionarily distant kinases that do not have proline at this position exhibit inhibitor resistance mutations at this site (Brenan et al., 2016; Persky et al., 2020; Lee and Shah, 2017). In some distant kinases such as PDK1, this β4-β5 and C-helix region is part of an allosteric binding site for inhibitors (the PIF pocket) (Rettenmaier et al 2014). Given that the proline pivot region is largely intolerant of mutations, this site could potentially be targeted for allosteric inhibitors to avoid the development of resistance mutations observed in the clinic for many other small molecule MET inhibitors..

In summary, our parallel DMS of MET and METΔEx14 has built an atlas of variant effects. Moreover, we identified a small number of unique sensitivities in each background, which provides hypotheses about the mechanism of exon 14 skipping in cancer. We also observed a number of strong GOF variants that have not been observed in the clinic. Strikingly, these variants are enriched in 2 and 3 nucleotide changes, suggesting that our DMS will be especially useful in classifying rare driver mutations and that the clinical population has essentially sampled

most of the single nucleotide changes. These results comprise a valuable resource for classifying driver, passenger, and resistance mutations for MET and other RTKs.

Methods

Mammalian cell culturing

Ba/F3 cells were purchased from DSMZ and maintained in 90% RPMI (Gibco), 10% HI-FBS (Gibco), 1% penicillin/streptomycin (Gibco), and 10ng/ml IL-3 (Fisher), and incubated at 37°C with 5% CO2. Ba/F3 cells were passaged at or below 1.0E6 cells/ml in order to avoid acquired IL-3 resistance, and regularly checked for IL-3 addiction by performing 3x PBS (Gibco) washes and outgrowth in the absence of IL-3 to confirm cell death in the parental, empty cell line.

Plat-E cells stably expressing retroviral envelope and packaging plasmids were originally gifted by Dr. Wendell Lim. Plat-E cells were maintained in 90% DMEM, HEPES (Gibco), 10% HI-FBS (Gibco), 1% penicillin/streptomycin (Gibco), 10ug/ml blasticidin, 1ug/ml puromycin, and incubated at 37°C with 5% CO2. Plat-E cells were maintained under blasticidin and puromycin antibiotic pressure unless being transfected.

HEK293 cells were maintained in DMEM (Gibco) supplemented with 10% FBS (Gibco) and 1% penicillin/streptomycin (Gibco) at 37°C in 5% CO2.

Human MET knockout HeLa cells were purchased from Abcam and maintained in 90% DMEM, HEPES (Gibco), 10% HI-FBS (Gibco), 1% penicillin/streptomycin (Gibco), and incubated at 37°C with 5% CO2

Cloning and retroviral vectors used

Both pUC19 (Cat. 50005) and MSCV (Cat. 68469) were ordered from Addgene. To ensure unique cut sites within the vectors for introduction and shuttling of the variant library, a new multiple cloning site was introduced into each plasmid. Wild type TPR-MET-IRES-mCherry and

TPR-METΔEx14-IRES-eGFP genes were cloned into pUC19 as the parental constructs for library generation and all site-directed mutagenesis. The full-length MET, METΔEx14, and RON receptor cDNAs were subcloned into pcDNA3.1 vector by Gibson assembly and incorporated a C-terminal single Flag tag sequence. All mutations were introduced by quick change mutagenesis.

MET kinase domain variant library generation and cloning

The MET kinase domain variant library was designed to span amino acid positions 1059-1345, which contained the full kinase domain (aa 1071-1345) and a portion of the juxtamembrane (aa 1059-1070). The library was synthesized by Twist Bioscience with one mammalian high-usage codon per amino acid to prevent over-representation of specific residues. The library was received in 96-well arrays of lyophilized DNA at 50 ng per well, where each well contained all variants (missense and WT-synonymous) per position of the kinase domain. The lyophilized library was resuspended in 100uL of 1X TE buffer, and 5ng of DNA from each well was amplified with low cycle PCR to increase the starting material using the following the NEB Q5 High-Fidelity recipe per well: 10μL 5X Q5 buffer, 5ng template DNA, 2.5μL 10μM forward primer, 2.5μL 10μM reverse primer, 1μL 10mM dNTPs (2.5μM each), 0.5μL Q5 Polymerase, nuclease free water to a final volume of 50μL. The following thermocycler parameters were then applied: initial denaturation at 98°C for 30s, followed by 10x cycles of denaturation at 98°C for 10s, annealing at 62°C for 30s, extension at 72°C for 1 min, and a final extension at 72°C for 5 min. A 1% agarose, 1X TBE diagnostic gel was run with 2μL of each sample to confirm amplification of all positions, then the samples were PCR cleaned using the Zymo 96-well DNA clean and concentrate kit, eluted in 10μL nuclease free water, pooled together in a low DNA-bind tube, and then DNA cleaned (Zymo) once more to further concentrate the pooled library.

The kinase domain variant library was digested with PstI-HF (NEB) and NdeI-HF (NEB) and cleaned up with the Zymo DNA clean and concentrate kit. Next, the two cloning vectors (pUC19_kozak-TPR-METΔEx14-IRES-eGFP and pUC19_kozak-TPR-MET-IRES-mCherry),

were digested with PstI-HF(NEB) and NdeI-HF (NEB), phosphatase treated with rSAP (NEB), gel extracted to isolate the backbone, and DNA cleaned (Zymo). The variant library was ligated into each vector with a 1:3 (insert: vector) T4 ligation at 16°C overnight (NEB). Ligations were DNA cleaned (Zymo), eluted in 10uL of nuclease free water, and electroporated into 50µL MegaX 10 beta cells (Invitrogen). Transformations were then recovered in 1mL of SOC for 1hr at 37°C. Post recovery, 10µL cells were collected, serial diluted, plated at varying dilutions (1:100, 1:1k, 1:10k, 1:100k, 1:1M) to evaluate transformation efficiencies. The remainder of the transformation then propagated in 50mL LB and Carbyinacillin at 37°C to an OD of 0.5, and then midi-prepped (Zymo).

Amino acid variants were successfully synthesized by Twist Biosciences for all positions with the exception of 1194 and 1278. In addition, premature stop codons were not included in the synthesized Twist library. To include these missing positions and early stop control, we generated a "fill-in" library. For positions 1194 and 1278, a forward primer for each amino acid mutation and a single reverse primer was designed for inverse PCR. An early stop codon "fill-in" library was also generated to introduce one stop codon every 33 bases, evenly spaced throughout the gene. This resulted in one stop codon every 11 positions, or 24 total premature stops. Again, a single forward and reverse primer was designed for each stop codon mutation using inverse PCR. Mutations were introduced into wild type pUC19_kozak-TPR-METΔEx14-IRES-eGFP and pUC19_kozak-TPR-MET-IRES-mCherry with the following NEB Q5 High-Fidelity conditions per reaction: 10µL 5X Q5 buffer, 5ng template DNA, 2.5µL 10µM forward primer, 2.5µL 10µM reverse primer, 1µL 10mM dNTPs (2.5µM each), 0.5µL Q5 Polymerase, nuclease free water to a final volume of 50µL. The following thermocycler parameters were then applied: initial denaturation at 98°C for 30s, 10x cycles of denaturation at 98°C for 10s, annealing at 62°C for 30s, extension at 72°C for 4.4 min, and a final extension at 72°C for 10 min. A 1% agarose diagnostic gel was run with 2µL of each reaction to conform amplification. Then all PCR samples were pooled, DNA cleaned (Zymo) and eluted in 50µL nuclease free water, DPN1 digested to remove template (NEB), DNA cleaned again and eluted in 12µL nuclease free water,

PNK treated (NEB), and blunt-end ligated at 16°C overnight with T4 ligase. Ligations were DNA cleaned the next morning (Zymo) and electroporated into MegaX 10 beta cells (Invitrogen). Transformations were recovered in 1mL of SOC for 1hr at 37°C, plated at varying dilutions to estimate transformation efficiencies, propagated in 50mL LB and Carbyinacillin at 37°C to an OD of 0.5, and then midi-prepped (Zymo). The Twist-synthesized library was then pooled together with the 1278, 1194, and premature stop "fill-in" libraries at equimolar concentrations to a total of 1ug of DNA.

7µg of each pooled library was restriction digested with MluI-HF (NEB) and MfeI-HF (NEB) to cut out variant libraries in the kozak-TPR-MET-IRES-mCherry and kozak-TPR-METΔEx14-IRES-eGFP backgrounds. Digests were gel extracted from pUC19 and DNA cleaned (Zymo). The empty, Puromycin resistant, retroviral expression vector MSCV (addgene) was also cut MluI-HF (NEB) and MfeI-HF (NEB), phosphatase treated with rSAP (NEB), and DNA cleaned. Isolated libraries were then ligated 1:1 (insert to vector) into the MSCV retroviral vector at 16°C overnight with T4 ligase. Ligations were then DNA cleaned (Zymo) and electroporated into ElectroMAX Stbl4 Competent Cells (Thermo Fisher). Transformations were recovered in 1mL of SOC for 1hr at 37°C and after recovery 10µL was serial diluted and plated to estimate transformation efficiencies, while the remainder was plated on bioassay dishes. Colonies were scraped from the bioassay dishes and midi-prepped for transfections (Zymo).

Variant library introduction into Ba/F3

The MSCV_kozak-TPR-MET-IRES-mCherry and MSCV_kozak-TPR-METΔEx14-IRES-eGFP variant libraries were transfected into Plat-E cells for retroviral packaging using Lipofectamine3000 (Invitrogen). Two T-175 flasks of Plat-E cells were prepared for each library in the absence of blasticidin and puromycin 24hr prior to transfection such that they would be at 70-80% confluency at the time of transfection. On the day of transfection, each flask of Plat-E cells was gently washed with PBS to remove the culturing media, and replaced with 35mL

Opti-MEM. For the transfection, Opti-MEM was brought to room temperature and two pairs of DNA Lo-bind 5mL tubes were prepared following manufacturer's instructions for Lipofectamine3000 scaled to a T-175 format. A total of 46µg DNA was used to transfect the libraries and package virus in parallel: MSCV_TPR-MET-IRES-eGFP, MSCV_TPR-METΔEx14-IRES-mCherry. Each flask was incubated with the transfection reagents for 5hr at 37°C, 5% CO2; the transfection media was then replaced with 50mL OptiMEM, 5% FBS, 1x GlutaMax, and 2% Sodium Pyruvate (Gibco) for viral packaging. After 48 hr post-transfection, the viral supernatant was harvested, passed through a 0.45 µm filter to remove cell debris, then precipitated overnight with 1:4 Retro-X concentrator (TakaraBio) at 4°C, then pelleted at 380xg for 45 min at 4C, and resuspended in 5mL of sterile, cold PBS and stored at 4°C in 1mL aliquots until transduced into Ba/F3 cells.

The concentrated virus was titiered in Ba/F3 cells in a 6-well plate format. Cells were seeded at 1.0E5 cells/ml with 10 ng/ml IL-3 and 8µg/ml polybrene (Sigma-Aldrich). Virus was added to wells at 0, 10x, 20x, 40x dilutions to determine the proper volume for a transduction MOI of 0.1-0.3. Cells were spinfected at 250xg for 60 minutes at room temperature, then incubated for 48 hr. The viral titer was calculated from the percent of fluorescent cells and viral dilution.

For the DMS viral transduction, 6 million cells were spinfected at an MOI of 0.1, in triplicate for a total of 3 biological replicates for each library, and incubated post spinfection in a 15cm dish with 30mL Ba/F3 media and 10ng/L IL-3 for 48hr. Infected cells were then selected with 1µg/ml puromycin for a total of 4 days with fluorescence and cell counts tracked each day.

DMS time point selection and sample preparation

After puromycin selection, all three biological replicates for both libraries, TPR-MET and TPR-METΔEx14, were washed free of puromycin and IL-3 with 3x PBS washes. A total of 6 million cells from each replicate was harvested and pelleted at 250xg to serve as the "time point 0" pre-selection sample (T0).

To begin selection of each replicate for each library, two sets of 15cm dishes were prepared with 2.0E5 cells/ml in 30mL 90% RPMI, 10% HI-FBS, 1% penicillin/streptomycin. One plate was kept free of IL-3 as the experimental IL-3 withdrawal condition, while the other plate was supplemented with 10ng/mL IL-3 to provide the control condition. Three time points post T0 were collected for each library replicate and condition for a total of four time points (T0, T1, T2, T3). Time points were harvested every 48hr across 7 days; 6 million cells were harvested for each condition and pelleted at 250xg for 5min; 2.0E5 cells/ml were split at every time point and maintained either in IL-3 or IL-3 withdrawal conditions.

The gDNA of each time point sample was isolated with the TakaraBio NucleoSpin Blood QuickPure kit the same day the cells were harvested. gDNA was eluted in a 50µl elution buffer using the high concentration and high yield elution manufacturer's protocol. Immediately after gDNA was isolated, 5µg of gDNA was used for PCR amplification of the target MET KD gene to achieve the proper variant coverage. A 150µl PCR master mix was prepared for each sample using the TakaraBio PrimeStar GXL system according to the following recipe: 30µl 5X PrimeStar GXL buffer, 4.5µl 10µM forward primer (0.3uM final), 4.5µl 10µM reverse primer (0.3uM final), 5µg gDNA, 12µl 10mM dNTPs (2.5mM each NTP), 6µl GXL polymerase, nuclease free water to a final reaction volume of 150uL. The PCR master mix was split into three PCR tubes with 50µl volumes and amplified with the following thermocycler parameters: initial denaturation at 98°C for 30 s, followed by 24x cycles of denaturation at 98°C for 10 s, annealing at 60°C for 15 s, extension at 68°C for 14 s, and a final extension at 68°C for 1 min.

Library preparation and deep sequencing

After all time points were selected, harvested, and PCR amplified, the target gene amplicon was isolated from gDNA by gel purification. The entire 150µl PCR reaction for each sample was mixed with 1X NEB Purple Loading Dye (6X stock) and run on a 0.8% agarose, 1X TBE gel, at 100 mA until there was clear ladder and band separation. The target amplicons were gel excised and purified with the Zymo Gel DNA Recovery kit. To remove excess agarose contamination,

each sample was then further cleaned using the Zymo DNA Clean and Concentrator-5 kit. Amplicon DNA concentrations were then determined by Qubit dsDNA HS assay (Invitrogen).

Libraries were then prepared for deep sequencing using the Nextera XT DNA Library Prep kit in a 96-well plate format (Illumina). Manufacturer's instructions were followed for each step: tagmentation, indexing and amplification, and clean up. Libraries were indexed using the IDT for Nextera Unique Dual Indexes Set C (Illumina). Then, indexed libraries were quantified using the Agilent TapeStation with HS D5000 screen tape (Agilent) and reagents (Agilent). DNA concentrations were further confirmed with a Qubit dsDNA HS assay. All samples were manually normalized and pooled at 10nM for MET and METΔEx14. The libraries were then paired-end sequenced (SP300) on two lanes of a NovaSeq6000.

MET kinase domain variant analysis and scoring

Demultiplexed paired-end reads were received from the sequencing core and processed further using a snakemake-based pipeline previously developed (Macdonald et al., 2022; Mölder et al., 2021). Initial QC was performed via FastQC (Andrews and Others, 2010), and continued via aggregation of intermediate output statistics with MultiQC (Ewels et al., 2016). First, any remaining adapter sequences or contaminant sequences were removed with BBDuk. Next, overlap-based error-correction was employed with BBMerge, before being mapped to the reference sequence with BBMap (Bushnell, 2014). Variant counts from each mapped BAM file were then made with the GATK AnalyzeSaturationMutagenesis tool (Van der Auwera and O'Connor, 2020). The output of this tool was processed using a script to remove variants that were not in our initial library design and to prepare output in a format for further processing with Enrich2 using weighted-least squares with wild type normalization (Rubin et al., 2017). It was noted that Enrich2 produces unexpected scores when some variants are unobserved across replicates or go to zero over a single time course: to avoid this, our script also detects this and removes them in advance.

MET and METΔEx14 mutational analysis

Raw Enrich2 scores were used for all comparative "activity score" measurements. gain-of-function and loss-of-function missense mutations were classified and calculated as ±2 SD from the mean activity score of the WT-synonymous distributions for MET and METΔEx14. For comparative analysis, propagation of error was calculated from the delta activity score and delta SE of each variant for MET and METΔEx14, and only variants with a SE difference lower than the activity score difference were used.

Validation of variants in the MET and METΔEx14 receptor by western blot

HEK293 cells were transiently transfected with Lipofectamine3000 (Invitrogen) according to the manufacturer's protocols. Cells were harvested 24 hours post transfection, lysed in buffer (50 mM Tris-HCl, pH 7.5, 150 mM NaCl, 2 mM EDTA, and 1% w/v Triton X-100 supplemented with protease inhibitor tablets (Roche), 1 mM sodium fluoride and 1 mM sodium vanadate). Clarified lysates were incubated with G1 affinity resin (Genscript) overnight at 4°C. Resin was washed with lysis buffer (without inhibitors) and proteins eluted by addition of Laemmli sample reducing buffer. Proteins were separated by SDS-PAGE on a 4-15% gradient gel (BioRad) and transferred to PVDF membrane (Millipore). Membranes were probed with Flag (2368), MET pY1234/5 (3077) (Cell Signaling Technologies).

Human MET knockout HeLa cells were transiently transfected with Lipofectamine3000 (Invitrogen) according to the manufacturer's protocols in a 6-well plate format. Post transfection (24hr), cells were washed with PBS (Gibco) (3x washes) to remove serum and transfection media, and replaced with DMEM (Gibco) in the absence of any additives. Cells were serum starved for 4 hr, then stimulated with 50 ng/ml HGF (PeproTech) for 15 min at 37°C, then immediately washed with cold PBS (3x washes), and maintained on ice. Cells were then lysed in buffer (50 mM Tris-HCl, pH 7.5, 150 mM NaCl, 2 mM EDTA, and 1% w/v Triton X-100 supplemented with protease inhibitor tablets (Roche), 1 mM sodium fluoride, and 1 mM sodium

vanadate) on ice. Clarified whole cell lysates were run on a 8-16% SDS-PAGE gel (BioRad) and transferred to a nitrocellulose membrane (BioRad). Membranes were probed with MET pY1234/5 (Cat 3077), Met (8198), P-p44/42 MAPK Erk1/2 (T202/Y204) (4376), p44/42 MAPK Erk1/2 (4695), and β-Actin (4970) (Cell Signaling Technologies).

Ba/F3 proliferation assay

Ba/F3 cells stably expressing TPR-MET, TPR-METΔEx14, and empty MSCV constructs were seeded at 2.5E4 cells/ml in triplicate in a 94-well, round bottom plate for each time point in the presence and absence of 10ng/ml IL-3. CellTiter-Glo reagent (Promega) was mixed at a 1:1 ratio with cells and luminescence was measured on a Veritas luminometer at 0, 48, and 96 hrs post-seeding. In this study, we use a modified nomenclature, where we refer to TPR-MET as the TPR-fusion of MET with the full-length juxtamembrane sequence and TPR-METΔEx14 as the TPR-fusion lacking exon 14. Cell numbers were determined from a Ba/F3 cell and ATP standard curve generated according to the manufacturer's instructions. Data are presented as cell viability normalized to the fold change from the 0hr time point.

For IL-3 titrations, Ba/F3 cells stably expressing TPR-MET, TPR-METΔEx14, and empty MSCV constructs were 3x PBS washed and 5000 cells were seeded in a 94-well, round bottom plate. IL-3 was added to wells at 0-10ng/ml (0, 0.078, 0.16, 0.31, 1.3, 2.5, 5, 10 ng/ml). CellTiter-Glo reagent (Promega) was mixed at a 1:1 ratio with cells and luminescence was measured on a Veritas luminometer at 0, 24, and 48 hrs after seeding and IL-3 addition.

Cell numbers for all proliferation assays were determined from a Ba/F3 and ATP CellTiter-Glo standard curve generated according to the manufacturer's instructions. Data are presented as cell viability normalized to the fold change from the 0hr time point.

MET kinase domain structural ensemble and RTK structural comparisons

Structural visualization, mapping, and analysis was completed using PyMOL unless otherwise stated. All human MET (UniProtKB accession: P08581) kinase domain crystal structures currently available were downloaded from the PDB. All PDB structures were loaded and globally aligned to generate the kinase domain ensemble. Residue distances were calculated from alpha-carbon x,y,z coordinates and computationally analyzed. Raw PDB files were used to categorize structure features: resolution, construct boundaries, conformation, sequence features, mutations, and apo/holo states.

To choose representative active and inactive structures for score mapping and visualization, we generated an ensemble of 88 human MET kinase domain structures currently deposited in the PDB, and classified activity states based on alpha-carbon distances between catalytic site residues K1110, E1127, and F1223 (Modi and Dunbrack, 2019), with the majority of the MET KD structures in a "BLBplus" or "SRC-like" inactive conformation (Modi and Dunbrack, 2019). In study we refer to 3R7O, 3Q6W, 4IWD as as our representative "active" structures because they display classical active confirmation hallmarks (C-helix-in, K1110-E1127 salt bridge, DFG-in, solvent exposed A-loop despite being inhibited. Within the ensemble, there is only one ATP-bound structure (PDB 3DKC), which harbors A-loop Y1234F and Y1235D stabilizing mutations, and also displays an inactive conformation. Within the group of inactive structures, there are two main conformational species based on DFG/ C-helix positioning and A-loop conformation: "BLBplus" and "BBAminus" (PDB 2G15 and PDB 5HTI represent the two species) (Modi and Dunbrack, 2019).

RTK structural analysis and comparisons

Crystal structures of active and inactive human IR (PDB 4XLV, 4IBM), KIT (PDB 1PKG, 1T45), EPHA3 (PDB 2QO9), RET (PDB 2IVT, 2IVS), MET (PDB 3R7O, 2G15), and AXL (PDB 5UAB) were obtained through the PDB. RMSD was calculated and plotted with the Bio3D

package in R for each kinase using the inactive structure as the reference.

For β5 positional comparison and Ramachandran analysis, PDB files were obtained for each kinase, and analyzed with the Bio3D package in R to attain the Phi and Psi angles of each residue. The general and proline contour data was obtained from Lovell et al., 2003 and plotted as an overlay with the specific kinase β5 residues aforementioned.

Cancer and resistance mutation analysis

Cancer-associated missense mutations for the MET kinase domain was obtained from cBioPortal (NCBI ID: NM_000245). Resistance mutations were obtained from literature references (Duplaquet et al., 2018; Fernandes et al 2021; Saraon et al., 2021; Lu et al., 2017; Fujino et al., 2019).

Sequence alignments

All human RTK protein sequences used in alignments were acquired from UniProt. Unless otherwise stated, alignments were done with MuscleWS using default parameters through JalView, and amino acids were colored according to physicochemical properties, or percent sequence identity where noted.

Acknowledgements

Sequencing was performed at the UCSF CAT, supported by UCSF PBBR, RRP IMIA, and NIH 1S10OD028511-01 grants. This work was supported by NIH CA239604 to EAC, NJ, JSF; HHMI Hanna Gray Fellowship and UCSF QBI Fellow program to WCM; and the UCSF Program for Breakthrough Biomedical Research, funded in part by the Sandler Foundation, to JSF.

Competing Interests

JSF is a consultant for, has equity in, and receives research support from Relay Therapeutics. N.J. is a founder of Rezo Therapeutics and a shareholder of Rezo Therapeutics, Sudo Therapeutics, and Type6 Therapeutics. N.J. is a SAB member of Sudo Therapeutics, Type6 Therapeutic and NIBR Oncology. The Jura laboratory has received sponsored research support from Genentech, Rezo Therapeutics and Type6 Therapeutics. E.A.C. is a consultant at IHP Therapeutics, Valar Labs, Tatara Therapeutics and Pear Diagnostics, reports receiving commercial research grants from Pfizer, and has stock ownership in Tatara Therapeutics, HDT Bio, Clara Health, Aqtual, and Guardant Health.

Code and data availability

The sequencing data has been deposited at the NCBI SRA (bioproject PRJNA993160). Original data files and analysis source code is available at
`https://github.com/fraser-lab/MET\_KinaseDomain\_DMS`

Supplemental Figures

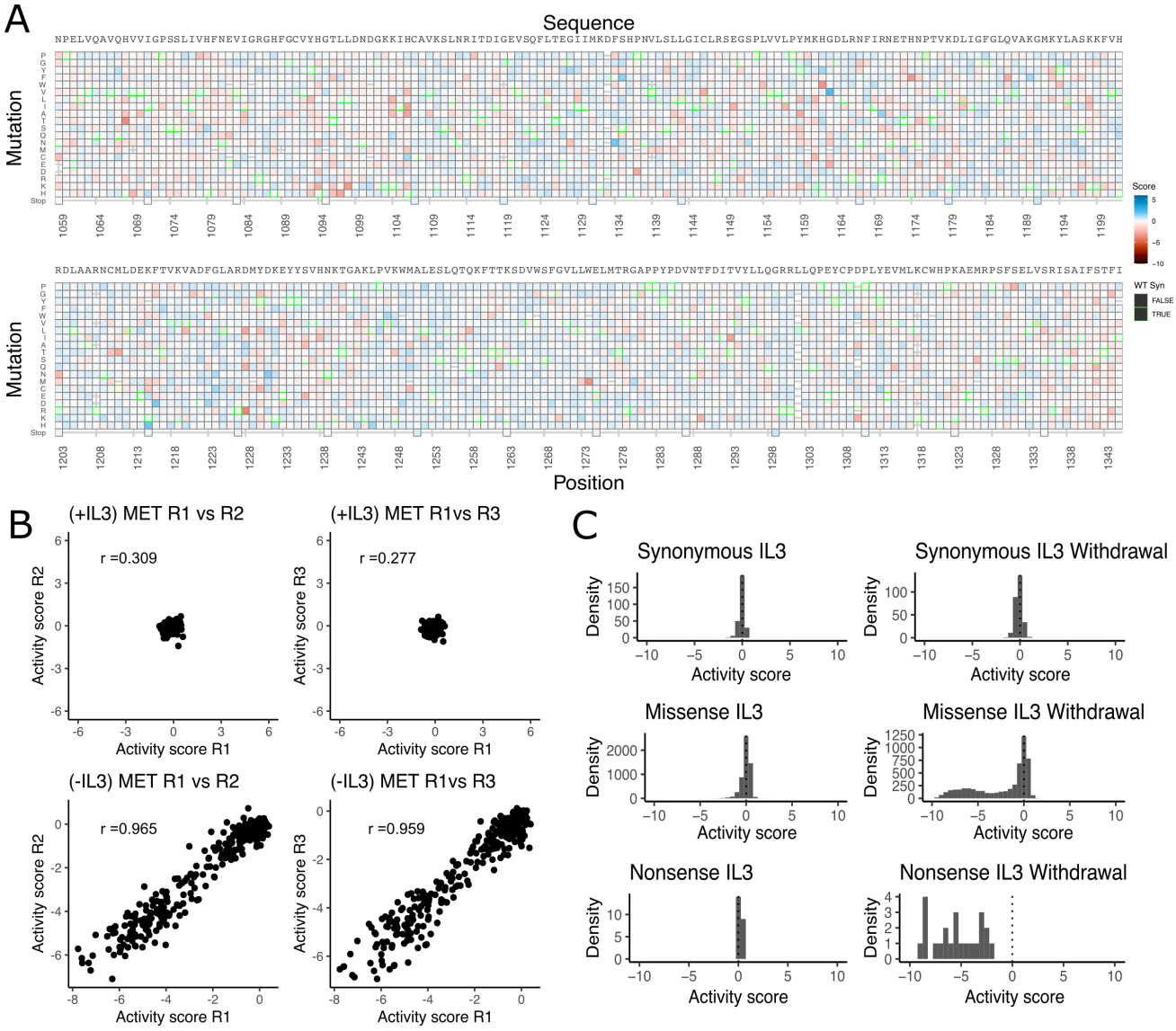

Supplemental Figure 1.7. Validation of the MET kinase domain saturation mutagenesis library in IL-3 and IL-3 withdrawal selections. (A) Heatmap of MET kinase domain variants in the full-length juxtamembrane background for the IL-3 control condition that was run in parallel to the IL-3 withdrawal selection. (B) Replicate correlation analysis for both IL-3 and IL-3 withdrawal conditions, where the mean score for each position was plotted against the replicate value. The Pearson's correlation score is reported in each respective graph. (C) Distributions of synonymous, missense, and nonsense mutations for IL-3 and IL-3 withdrawal conditions.

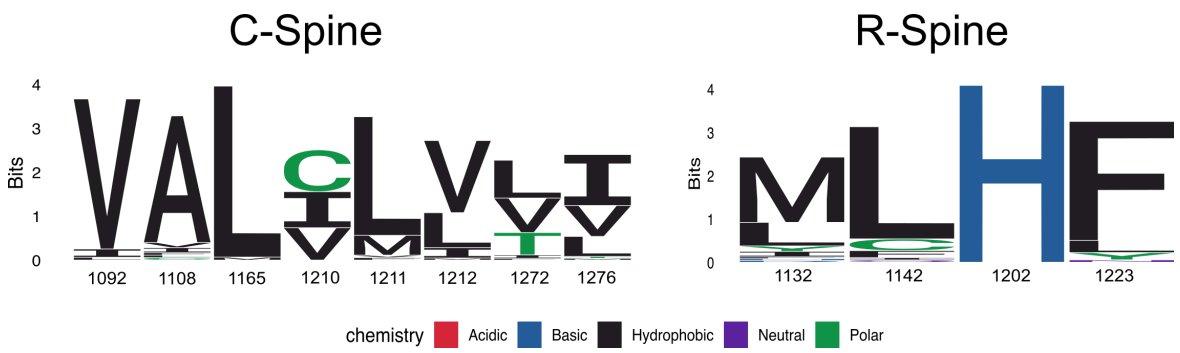

Supplemental Figure 1.8. Analysis of RTK R- and C-spine protein sequence conservation. Logo diagram representing the amino acid conservation of the C- and R-spine accross all RTK kinase domain protein sequences.

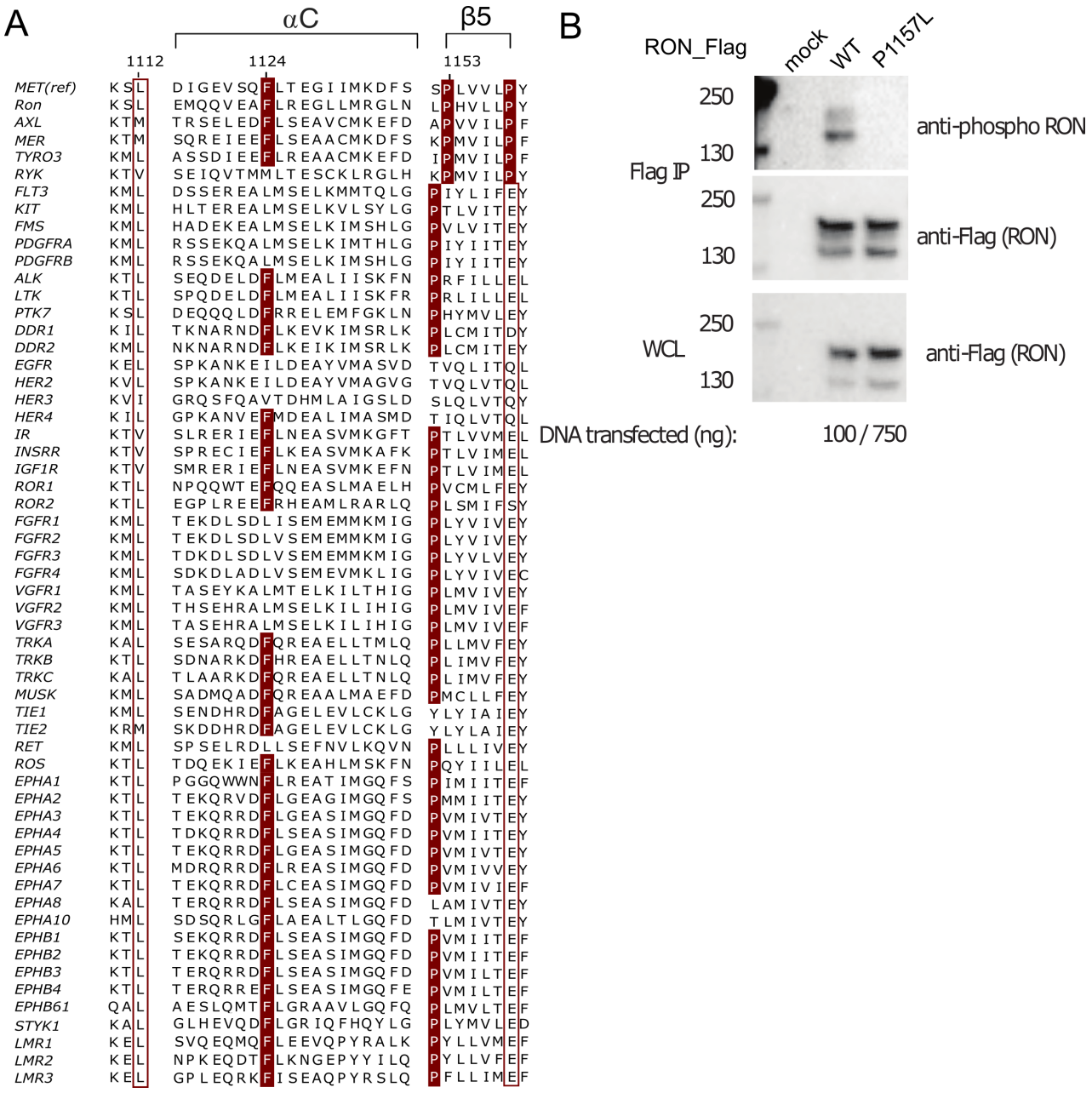

Supplemental Figure 1.9. RTK β5-turn site sequence analysis and validation in RON (A) Protein sequence alignment of human RTK kinase domains with conservation highlighted for residues corresponding to MET positions 1112, 1124, 1153, and 1158. (B) FLAG-IP Western blot of RON with a P1157L mutation at the corresponding β5-turn site in MET expressed for 24hr in HEK293 cells with input transfection DNA concentrations for wild type RON and P1157L constructs.

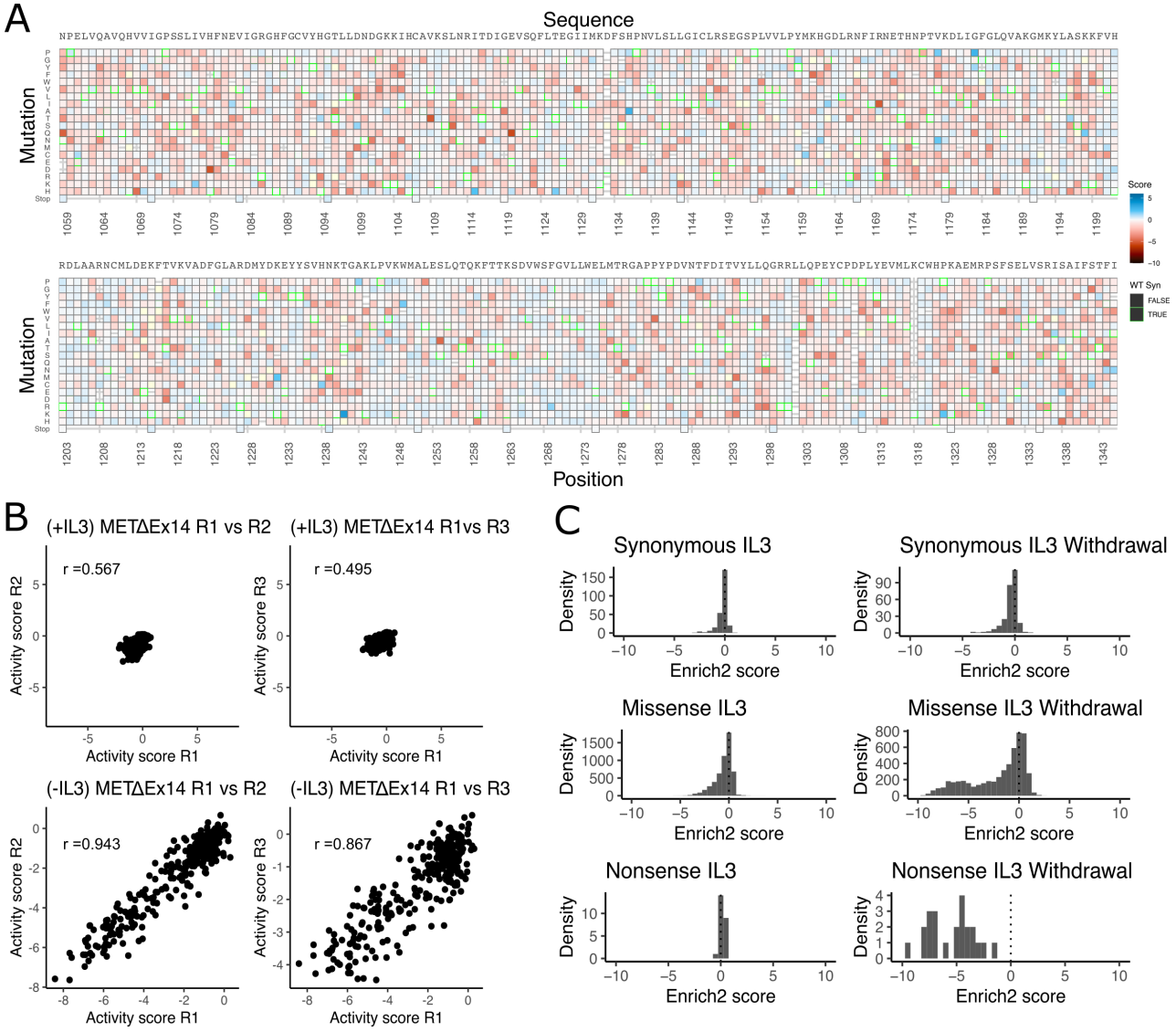

Supplemental Figure 1.10. Validation of the METΔEx14 saturation mutagenesis library in IL-3 and IL-3 withdrawal selections. (A) Heatmap of METΔEx14 kinase domain variants in the IL-3 control condition that was run in parallel to the IL-3 withdrawal selection. (B) Replicate correlation analysis for both IL-3 and IL-3 withdrawal, where the mean score for each position was plotted against the replicate value. The Pearson's correlation score is reported in each respective graph. (C) Distributions of synonymous, missense, and nonsense mutations for IL-3 and IL-3 withdrawal conditions.

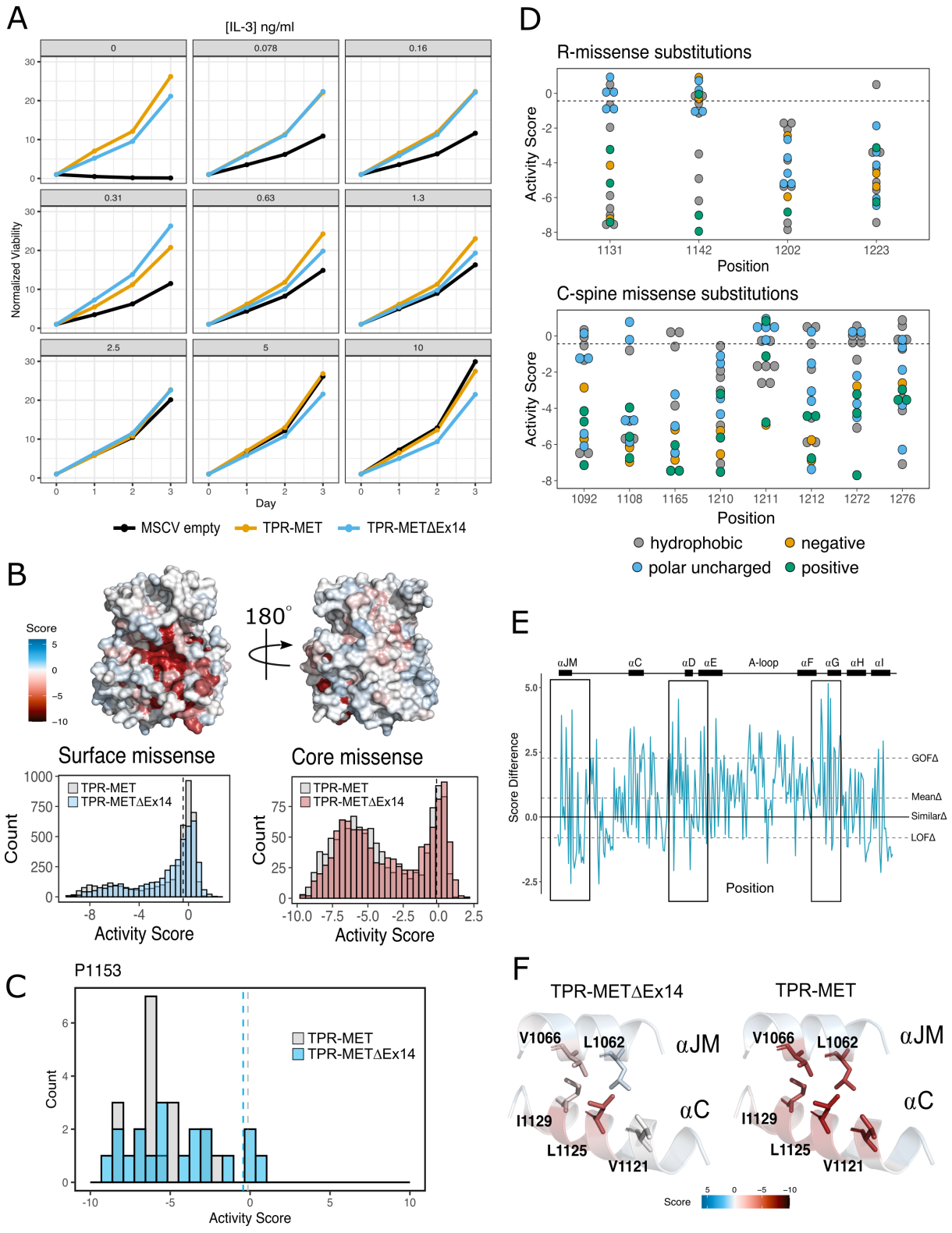

Supplemental Figure 1.11. Comparative analysis of the TPR-METΔEx14 and TPR-MET mutational landscapes. (Figure caption continued on the next page).

(Figure caption continued from the previous page). (A) IL-3 titration proliferation assay comparing Ba/F3 cells stably expressing TPR-MET, TPR-METΔEx14, and MSCV empty constructs over the course of 3 days at an IL-3 concentration range of 0, 0.078, 0.16, 0.31, 1.3, 2.5, 5, 10 ng/ml. Cell viability was normalized to day 0 for each condition. (B) Surface representation of TPR-METΔEx14 average activity scores mapped on a TPR-MET kinase domain structure (PDB 3R7O). Synonymous and nonsense mutations were left out of the averaging and surface representation. Residues at the N- and C-term that were not screened, but modeled in the crystal structure are in white and not considered in the averaging and mapping. Comparison of surface and core residues activity score distributions for TPR-METΔEx14, overlayed with the distributions for TPR-MET. A vertical dashed line in both graphs represents the mean score of WT-synonymous mutations. (C) Mutational distributions of P1153 variants for TPR-METΔEx14 (blue) and MET (gray). Dashed lines represent the mean of the WT-synonymous distribution for each library. (D) Activity scores and physiochemistry of variants shown for each residue position of the R- and C-spine of TPR-METΔEx14. (E) Mean difference plot for TPR-METΔEx14 and TPR-MET at each screened position. (E) Average score of mutations at the hydrophobic interface of JM and C for both TPR-METΔEx14 and TPR-MET.

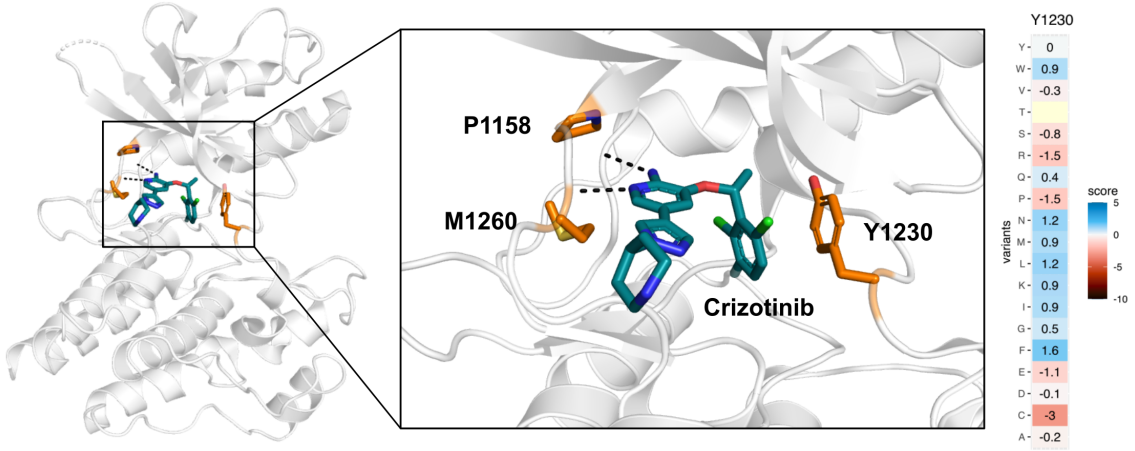

Supplemental Figure 1.12. Inhibitor-protein interactions mapped for Y1230 and crizotinib within the active site. Crizotinib-bound MET kinase domain (2WGJ) illustrating the inhibitor-protein interactions at the active site with the loss-of-function Y1230 position annotated. Heatmap for Y1230 in METΔEx14 showing missense scores subtracted from WT synonymous.

References

Abella, J. V., Peschard, P., Naujokas, M. A., Lin, T., Saucier, C., Urbé, S., & Park, M. (2005). Met/Hepatocyte Growth Factor Receptor Ubiquitination Suppresses Transformation and Is Required for Hrs Phosphorylation. Molecular and Cellular Biology, 25(21), 9632–9645. https://doi.org/10.1128/MCB.25.21.9632-9645.2005

Ahler, E., Register, A. C., Chakraborty, S., Fang, L., Dieter, E. M., Sitko, K. A., Vidadala, R. S. R., Trevillian, B. M., Golkowski, M., Gelman, H., Stephany, J. J., Rubin, A. F., Merritt, E. A., Fowler, D. M., & Maly, D. J. (2019). A Combined Approach Reveals a Regulatory Mechanism Coupling Src's Kinase Activity, Localization, and Phosphotransferase-Independent Functions. Molecular Cell, 74(2), 393-408.e20. https://doi.org/10.1016/j.molcel.2019.02.003

Andrews, S., & Others. (2010). "FastQC: A Quality Control Tool for High Throughput Sequence Data." Babraham Bioinformatics, Babraham Institute, Cambridge, United Kingdom.https://www.bioinformatics.babraham.ac.uk/projects/fastqc/

Azam, M., Seeliger, M. A., Gray, N. S., Kuriyan, J., & Daley, G. Q. (2008). Activation of tyrosine kinases by mutation of the gatekeeper threonine. Nature Structural & Molecular Biology, 15(10), 1109–1118. https://doi.org/10.1038/nsmb.1486

Bardelli, A., Longati, P., Gramaglia, D., Basilico, C., Tamagnone, L., Giordano, S., Ballinari, D., Michieli, P., & Comoglio, P. M. (1998). Uncoupling signal transducers from oncogenic MET mutants abrogates cell transformation and inhibits invasive growth. Proceedings of the National Academy of Sciences, 95(24), 14379–14383. https://doi.org/10.1073/pnas.95.24.14379

Birchmeier, C., Birchmeier, W., Gherardi, E., & Vande Woude, G. F. (2003). Met, metastasis, motility and more. Nature Reviews Molecular Cell Biology, 4(12), 915–925.

https://doi.org/10.1038/nrm1261

Brenan, L., Andreev, A., Cohen, O., Pantel, S., Kamburov, A., Cacchiarelli, D., Persky, N. S., Zhu, C., Bagul, M., Goetz, E. M., Burgin, A. B., Garraway, L. A., Getz, G., Mikkelsen, T. S., Piccioni, F., Root, D. E., & Johannessen, C. M. (2016). Phenotypic Characterization of a Comprehensive Set of MAPK1/ERK2 Missense Mutants. Cell Reports, 17(4), 1171–1183. https://doi.org/10.1016/j.celrep.2016.09.061

Bushnell, B. 2014. "BBTools Software Package."

Cabail, M. Z., Li, S., Lemmon, E., Bowen, M. E., Hubbard, S. R., & Miller, W. T. (2015). The insulin and IGF1 receptor kinase domains are functional dimers in the activated state. Nature Communications, 6(1), 6406. https://doi.org/10.1038/ncomms7406

Cerami, E., Gao, J., Dogrusoz, U., Gross, B. E., Sumer, S. O., Aksoy, B. A., Jacobsen, A., Byrne, C. J., Heuer, M. L., Larsson, E., Antipin, Y., Reva, B., Goldberg, A. P., Sander, C., & Schultz, N. (2012). The cBio Cancer Genomics Portal: An Open Platform for Exploring Multidimensional Cancer Genomics Data. Cancer Discovery, 2(5), 401–404. https://doi.org/10.1158/2159-8290.CD-12-0095

Chakraborty, S., Ahler, E., Simon, J. J., Fang, L., Potter, Z. E., Sitko, K. A., Stephany, J. J., Guttman, M., Fowler, D. M., & Maly, D. J. (2021). Profiling of the drug resistance of thousands of Src tyrosine kinase mutants uncovers a regulatory network that couples autoinhibition to the dynamics of the catalytic domain [Preprint]. Biochemistry. https://doi.org/10.1101/2021.12.05.471322

Chen, H., Ma, J., Li, W., Eliseenkova, A. V., Xu, C., Neubert, T. A., Miller, W. T., & Mohammadi, M. (2007). A Molecular Brake in the Kinase Hinge Region Regulates the Activity of Receptor Tyrosine Kinases. Molecular Cell, 27(5), 717–730. https://doi.org/10.1016/j.molcel.2007.06.028

Chen, L., Marsiglia, W. M., Chen, H., Katigbak, J., Erdjument-Bromage, H., Kemble, D. J., Fu, L., Ma, J., Sun, G., Zhang, Y., Liang, G., Neubert, T. A., Li, X., Traaseth, N. J., & Mohammadi, M. (2020). Molecular basis for receptor tyrosine kinase A-loop tyrosine transphosphorylation. Nature Chemical Biology, 16(3), Article 3. https://doi.org/10.1038/s41589-019-0455-7

Chiara, F., Michieli, P., Pugliese, L., & Comoglio, P. M. (2003). Mutations in the met Oncogene Unveil a "Dual Switch" Mechanism Controlling Tyrosine Kinase Activity. Journal of Biological Chemistry, 278(31), 29352–29358. https://doi.org/10.1074/jbc.M302404200

Cooper, C. S., Park, M., Blair, D. G., Tainsky, M. A., Huebner, K., Croce, C. M., & Vande Woude, G. F. (1984). Molecular cloning of a new transforming gene from a chemically transformed human cell line. Nature, 311(5981), 29–33. https://doi.org/10.1038/311029a0

Comoglio, P. M., Trusolino, L., & Boccaccio, C. (2018). Known and novel roles of the MET oncogene in cancer: A coherent approach to targeted therapy. Nature Reviews Cancer, 18(6), Article 6. https://doi.org/10.1038/s41568-018-0002-y

Daley, G. Q., & Baltimore, D. (1988). Transformation of an interleukin 3-dependent hematopoietic cell line by the chronic myelogenous leukemia-specific P210bcr/abl protein. Proceedings of the National Academy of Sciences, 85(23), 9312–9316. https://doi.org/10.1073/pnas.85.23.9312

Dar, A. C., & Shokat, K. M. (2011). The Evolution of Protein Kinase Inhibitors from Antagonists to Agonists of Cellular Signaling. Annual Review of Biochemistry, 80(1), 769–795. https://doi.org/10.1146/annurev-biochem-090308-173656

Duplaquet, L., Kherrouche, Z., Baldacci, S., Jamme, P., Cortot, A. B., Copin, M.-C., & Tulasne,

D. (2018). The multiple paths towards MET receptor addiction in cancer. Oncogene, 37(24), 3200–3215. https://doi.org/10.1038/s41388-018-0185-4

Elizabeth A. Tovar, & Graveel, C. R. (2017). MET in human cancer: Germline and somatic mutations. Annals of Translational Medicine, 5(10), Article 10. https://doi.org/10.21037/atm.2017.03.64

Ewels, P., Magnusson, M., Lundin, S., & Käller, M. (2016). MultiQC: Summarize analysis results for multiple tools and samples in a single report. Bioinformatics, 32(19), 3047–3048. https://doi.org/10.1093/bioinformatics/btw354

Fernandes, M., Hoggard, B., Jamme, P., Paget, S., Truong, M.-J., Grégoire, V., Vinchent, A., Descarpentries, C., Morabito, A., Stanislovas, J., Farage, E., Meneboo, J.-P., Sebda, S., Bouchekioua-Bouzaghou, K., Nollet, M., Humez, S., Perera, T., Fromme, P., Grumolato, L., … Kherrouche, Z. (2023). MET exon 14 skipping mutation is a hepatocyte growth factor (HGF)-dependent oncogenic driver in vitro and in humanized HGF knock-in mice. Molecular Oncology. https://doi.org/10.1002/1878-0261.13397

Fernandes, M., Jamme, P., Cortot, A. B., Kherrouche, Z., & Tulasne, D. (2021). When the MET receptor kicks in to resist targeted therapies. Oncogene, 40(24), 4061–4078. https://doi.org/10.1038/s41388-021-01835-0

Ferracini, R., Longati, P., Naldini, L., Vigna, E., & Comoglio, P. M. (1991). Identification of the major autophosphorylation site of the Met/hepatocyte growth factor receptor tyrosine kinase. Journal of Biological Chemistry, 266(29), 19558–19564. https://doi.org/10.1016/S0021-9258(18)55031-6

Fowler, D. M., & Fields, S. (2014). Deep mutational scanning: A new style of protein science. Nature Methods, 11(8), 801–807. https://doi.org/10.1038/nmeth.3027

Frampton, G. M., Ali, S. M., Rosenzweig, M., Chmielecki, J., Lu, X., Bauer, T. M., Akimov, M.,

Bufill, J. A., Lee, C., Jentz, D., Hoover, R., Ou, S.-H. I., Salgia, R., Brennan, T., Chalmers, Z. R., Jaeger, S., Huang, A., Elvin, J. A., Erlich, R., … Miller, V. A. (2015). Activation of MET via Diverse Exon 14 Splicing Alterations Occurs in Multiple Tumor Types and Confers Clinical Sensitivity to MET Inhibitors. Cancer Discovery, 5(8), 850–859. https://doi.org/10.1158/2159-8290.CD-15-0285

Fujino, T., Kobayashi, Y., Suda, K., Koga, T., Nishino, M., Ohara, S., Chiba, M., Shimoji, M., Tomizawa, K., Takemoto, T., & Mitsudomi, T. (2019). Sensitivity and Resistance of MET Exon 14 Mutations in Lung Cancer to Eight MET Tyrosine Kinase Inhibitors In Vitro. Journal of Thoracic Oncology, 14(10), 1753–1765. https://doi.org/10.1016/j.jtho.2019.06.023

Gajiwala, K. S., Grodsky, N., Bolaños, B., Feng, J., Ferre, R., Timofeevski, S., Xu, M., Murray, B. W., Johnson, T. W., & Stewart, A. (2017). The Axl kinase domain in complex with a macrocyclic inhibitor offers first structural insights into an active TAM receptor kinase. Journal of Biological Chemistry, 292(38), 15705–15716. https://doi.org/10.1074/jbc.M116.771485

Gao, J., Aksoy, B. A., Dogrusoz, U., Dresdner, G., Gross, B., Sumer, S. O., Sun, Y., Jacobsen, A., Sinha, R., Larsson, E., Cerami, E., Sander, C., & Schultz, N. (2013). Integrative Analysis of Complex Cancer Genomics and Clinical Profiles Using the cBioPortal. Science Signaling, 6(269), pl1–pl1. https://doi.org/10.1126/scisignal.2004088

Gherardi, E., Sandin, S., Petoukhov, M. V., Finch, J., Youles, M. E., Öfverstedt, L.-G., Miguel, R. N., Blundell, T. L., Vande Woude, G. F., Skoglund, U., & Svergun, D. I. (2006). Structural basis of hepatocyte growth factor/scatter factor and MET signalling. Proceedings of the National Academy of Sciences, 103(11), 4046–4051. https://doi.org/10.1073/pnas.0509040103

Gherardi, E., Youles, M. E., Miguel, R. N., Blundell, T. L., Iamele, L., Gough, J.,

Bandyopadhyay, A., Hartmann, G., & Butler, P. J. G. (2003). Functional map and domain structure of MET, the product of the c-met protooncogene and receptor for hepatocyte growth factor/scatter factor. Proceedings of the National Academy of Sciences, 100(21), 12039–12044. https://doi.org/10.1073/pnas.2034936100

Graziani, A., Gramaglia, D., Cantley, L. C., & Comoglio, P. M. (1991). The tyrosine-phosphorylated hepatocyte growth factor/scatter factor receptor associates with phosphatidylinositol 3-kinase. Journal of Biological Chemistry, 266(33), 22087–22090. https://doi.org/10.1016/S0021-9258(18)54536-1

Griffith, J., Black, J., Faerman, C., Swenson, L., Wynn, M., Lu, F., Lippke, J., & Saxena, K. (2004). The Structural Basis for Autoinhibition of FLT3 by the Juxtamembrane Domain. Molecular Cell, 13(2), 169–178. https://doi.org/10.1016/S1097-2765(03)00505-7

Haling, J. R., Sudhamsu, J., Yen, I., Sideris, S., Sandoval, W., Phung, W., Bravo, B. J., Giannetti, A. M., Peck, A., Masselot, A., Morales, T., Smith, D., Brandhuber, B. J., Hymowitz, S. G., & Malek, S. (2014). Structure of the BRAF-MEK Complex Reveals a Kinase Activity Independent Role for BRAF in MAPK Signaling. Cancer Cell, 26(3), 402–413. https://doi.org/10.1016/j.ccr.2014.07.007

Hedger, G., Sansom, M. S. P., & Koldsø, H. (2015). The juxtamembrane regions of human receptor tyrosine kinases exhibit conserved interaction sites with anionic lipids. Scientific Reports, 5(1), Article 1. https://doi.org/10.1038/srep09198

Hobbs, H. T., Shah, N. H., Shoemaker, S. R., Amacher, J. F., Marqusee, S., & Kuriyan, J. (2022). Saturation mutagenesis of a predicted ancestral Syk-family kinase (p. 2022.04.24.489292). bioRxiv. https://doi.org/10.1101/2022.04.24.489292

Hu, J., Ahuja, L. G., Meharena, H. S., Kannan, N., Kornev, A. P., Taylor, S. S., & Shaw, A. S. (2015). Kinase Regulation by Hydrophobic Spine Assembly in Cancer. Molecular and

Cellular Biology, 35(1), 264–276. https://doi.org/10.1128/MCB.00943-14

Hubbard, S. R. (2004). Juxtamembrane autoinhibition in receptor tyrosine kinases. Nature Reviews Molecular Cell Biology, 5(6), 464–471. https://doi.org/10.1038/nrm1399

Huse, M., & Kuriyan, J. (2002). The Conformational Plasticity of Protein Kinases. Cell, 109(3), 275–282. https://doi.org/10.1016/S0092-8674(02)00741-9

Jura, N., Endres, N. F., Engel, K., Deindl, S., Das, R., Lamers, M. H., Wemmer, D. E., Zhang, X., & Kuriyan, J. (2009). Mechanism for Activation of the EGF Receptor Catalytic Domain by the Juxtamembrane Segment. Cell, 137(7), 1293–1307. https://doi.org/10.1016/j.cell.2009.04.025

Kang, J., Deng, Q.-M., Feng, W., Chen, Z.-H., Su, J.-W., Chen, H.-J., Wang, W., Zhang, S., Wang, Q., Chen, Z., Zhong, W.-Z., Xu, C., & Yang, J.-J. (2023). Response and acquired resistance to MET inhibitors in de novo MET fusion-positive advanced non-small cell lung cancer. Lung Cancer, 178, 66–74. https://doi.org/10.1016/j.lungcan.2023.01.017

Kato, T. (2017). Biological roles of hepatocyte growth factor-Met signaling from genetically modified animals (Review). Biomedical Reports, 7(6), 495–503. https://doi.org/10.3892/br.2017.1001

Knowles, P. P., Murray-Rust, J., Kjær, S., Scott, R. P., Hanrahan, S., Santoro, M., Ibáñez, C. F., & McDonald, N. Q. (2006). Structure and Chemical Inhibition of the RET Tyrosine Kinase Domain. Journal of Biological Chemistry, 281(44), 33577–33587. https://doi.org/10.1074/jbc.M605604200

Koga, T., Suda, K., & Mitsudomi, T. (2022). Utility of the Ba/F3 cell system for exploring on-target mechanisms of resistance to targeted therapies for lung cancer. Cancer Science, 113(3), 815–827. https://doi.org/10.1111/cas.15263

Kong-Beltran, M., Seshagiri, S., Zha, J., Zhu, W., Bhawe, K., Mendoza, N., Holcomb, T., Pujara, K., Stinson, J., Fu, L., Severin, C., Rangell, L., Schwall, R., Amler, L., Wickramasinghe, D., & Yauch, R. (2006). Somatic Mutations Lead to an Oncogenic Deletion of Met in Lung Cancer. Cancer Research, 66(1), 283–289. https://doi.org/10.1158/0008-5472.CAN-05-2749

Kornev, A. P., Haste, N. M., Taylor, S. S., & Ten Eyck, L. F. (2006). Surface comparison of active and inactive protein kinases identifies a conserved activation mechanism. Proceedings of the National Academy of Sciences, 103(47), 17783–17788. https://doi.org/10.1073/pnas.0607656103

Kornev, A. P., Taylor, S. S., & Ten Eyck, L. F. (2008). A helix scaffold for the assembly of active protein kinases. Proceedings of the National Academy of Sciences, 105(38), 14377–14382. https://doi.org/10.1073/pnas.0807988105

Lee, B. J., & Shah, N. P. (2017). Identification and characterization of activating ABL1 1b kinase mutations: Impact on sensitivity to ATP-competitive and allosteric ABL1 inhibitors. Leukemia, 31(5), 1096–1107. https://doi.org/10.1038/leu.2016.353

Lemmon, M. A., & Schlessinger, J. (2010). Cell Signaling by Receptor Tyrosine Kinases. Cell, 141(7), 1117–1134. https://doi.org/10.1016/j.cell.2010.06.011

Levina, A., Fleming, K. D., Burke, J. E., & Leonard, T. A. (2022). Activation of the essential kinase PDK1 by phosphoinositide-driven trans-autophosphorylation. Nature Communications, 13(1), 1874. https://doi.org/10.1038/s41467-022-29368-4

Li, S., Covino, N. D., Stein, E. G., Till, J. H., & Hubbard, S. R. (2003). Structural and Biochemical Evidence for an Autoinhibitory Role for Tyrosine 984 in the Juxtamembrane Region of the Insulin Receptor. Journal of Biological Chemistry, 278(28), 26007–26014. https://doi.org/10.1074/jbc.M302425200

Linossi, E. M., Estevam, G. O., Oshima, M., Fraser, J. S., Collisson, E. A., & Jura, N. (2021). State of the structure address on MET receptor activation by HGF. Biochemical Society Transactions, 49(2), 645–661. https://doi.org/10.1042/BST20200394

Liu, J., Shen, L., Qian, Y., Liu, Y., Su, M., & Yi, L. (2022). Durable response to crizotinib in an advanced lung adenocarcinoma patient harboring rare CD47-MET fusion: A case report. Translational Cancer Research, 11(8). https://doi.org/10.21037/tcr-22-141

Longati, P., Bardelli, A., Ponzetto, C., Naldini, L., & Comoglio, P. M. (1994). Tyrosines1234-1235 are critical for activation of the tyrosine kinase encoded by the MET proto-oncogene (HGF receptor). Oncogene, 9(1), 49–57.

Lovell, S. C., Davis, I. W., Arendall III, W. B., de Bakker, P. I. W., Word, J. M., Prisant, M. G., Richardson, J. S., & Richardson, D. C. (2003). Structure validation by Cα geometry: ϕ,ψ and Cβ deviation. Proteins: Structure, Function, and Bioinformatics, 50(3), 437–450. https://doi.org/10.1002/prot.10286

Lu, X., Peled, N., Greer, J., Wu, W., Choi, P., Berger, A. H., Wong, S., Jen, K.-Y., Seo, Y., Hann, B., Brooks, A., Meyerson, M., & Collisson, E. A. (2017). MET Exon 14 Mutation Encodes an Actionable Therapeutic Target in Lung Adenocarcinoma. Cancer Research, 77(16), 4498–4505. https://doi.org/10.1158/0008-5472.CAN-16-1944

Ma, P. C., Kijima, T., Maulik, G., Fox, E. A., Sattler, M., Griffin, J. D., Johnson, B. E., & Salgia, R. (2003). c-MET Mutational Analysis in Small Cell Lung Cancer: Novel Juxtamembrane Domain Mutations Regulating Cytoskeletal Functions1. Cancer Research, 63(19), 6272–6281.

Macdonald, C. B., Nedrud, D., Grimes, P. R., Trinidad, D., Fraser, J. S., & Coyote-Maestas, W. (2023). DIMPLE: Deep insertion, deletion, and missense mutation libraries for exploring protein variation in evolution, disease, and biology. Genome Biology, 24(1), 36.

https://doi.org/10.1186/s13059-023-02880-6

Mak, H. H. L., Peschard, P., Lin, T., Naujokas, M. A., Zuo, D., & Park, M. (2007). Oncogenic activation of the Met receptor tyrosine kinase fusion protein, Tpr–Met, involves exclusion from the endocytic degradative pathway. Oncogene, 26(51), 7213–7221. https://doi.org/10.1038/sj.onc.1210522

McClendon, C. L., Kornev, A. P., Gilson, M. K., & Taylor, S. S. (2014). Dynamic architecture of a protein kinase. Proceedings of the National Academy of Sciences, 111(43), E4623–E4631. https://doi.org/10.1073/pnas.1418402111

Meharena, H. S., Chang, P., Keshwani, M. M., Oruganty, K., Nene, A. K., Kannan, N., Taylor, S. S., & Kornev, A. P. (2013). Deciphering the Structural Basis of Eukaryotic Protein Kinase Regulation. PLoS Biology, 11(10), e1001680. https://doi.org/10.1371/journal.pbio.1001680

Melnick, J. S., Janes, J., Kim, S., Chang, J. Y., Sipes, D. G., Gunderson, D., Jarnes, L., Matzen, J. T., Garcia, M. E., Hood, T. L., Beigi, R., Xia, G., Harig, R. A., Asatryan, H., Yan, S. F., Zhou, Y., Gu, X.-J., Saadat, A., Zhou, V., … Caldwell, J. S. (2006). An efficient rapid system for profiling the cellular activities of molecular libraries. Proceedings of the National Academy of Sciences, 103(9), 3153–3158. https://doi.org/10.1073/pnas.0511292103

Modi, V., & Dunbrack, R. L. (2019). Defining a new nomenclature for the structures of active and inactive kinases. Proceedings of the National Academy of Sciences, 116(14), 6818–6827. https://doi.org/10.1073/pnas.1814279116

Mölder, F., Jablonski, K. P., Letcher, B., Hall, M. B., Tomkins-Tinch, C. H., Sochat, V., Forster, J., Lee, S., Twardziok, S. O., Kanitz, A., Wilm, A., Holtgrewe, M., Rahmann, S., Nahnsen, S., & Köster, J. (2021). Sustainable data analysis with Snakemake. F1000Research, 10, 33. https://doi.org/10.12688/f1000research.29032.2

Naldini, L., Vigna, E., Ferracini, R., Longati, P., Gandino, L., Prat, M., & Comoglio, P. M. (1991). The tyrosine kinase encoded by the MET proto-oncogene is activated by autophosphorylation. Molecular and Cellular Biology, 11(4), 1793–1803. https://doi.org/10.1128/mcb.11.4.1793-1803.1991

Pal, K., Bandyopadhyay, A., Zhou, X. E., Xu, Q., Marciano, D. P., Brunzelle, J. S., Yerrum, S., Griffin, P. R., Vande Woude, G., Melcher, K., & Xu, H. E. (2017). Structural Basis of TPR-Mediated Oligomerization and Activation of Oncogenic Fusion Kinases. Structure, 25(6), 867-877.e3. https://doi.org/10.1016/j.str.2017.04.015

Park, M., Dean, M., Cooper, C. S., Schmidt, M., O'Brien, S. J., Blair, D. G., & Vande Woude, G. F. (1986). Mechanism of met oncogene activation. Cell, 45(6), 895–904. https://doi.org/10.1016/0092-8674(86)90564-7

Persky, N. S., Hernandez, D., Do Carmo, M., Brenan, L., Cohen, O., Kitajima, S., Nayar, U., Walker, A., Pantel, S., Lee, Y., Cordova, J., Sathappa, M., Zhu, C., Hayes, T. K., Ram, P., Pancholi, P., Mikkelsen, T. S., Barbie, D. A., Yang, X., … Johannessen, C. M. (2020). Defining the landscape of ATP-competitive inhibitor resistance residues in protein kinases. Nature Structural & Molecular Biology, 27(1), 92–104. https://doi.org/10.1038/s41594-019-0358-z

Peschard, P., Fournier, T. M., Lamorte, L., Naujokas, M. A., Band, H., Langdon, W. Y., & Park, M. (2001). Mutation of the c-Cbl TKB Domain Binding Site on the Met Receptor Tyrosine Kinase Converts It into a Transforming Protein. Molecular Cell, 8(5), 995–1004. https://doi.org/10.1016/S1097-2765(01)00378-1

Petrelli, A., Gilestro, G. F., Lanzardo, S., Comoglio, P. M., Migone, N., & Giordano, S. (2002). The endophilin–CIN85–Cbl complex mediates ligand-dependent downregulation of c-Met. Nature, 416(6877), 187–190. https://doi.org/10.1038/416187a

Petrini, I. (2015). Biology of MET: A double life between normal tissue repair and tumor progression. Annals of Translational Medicine, 3(6), Article 6. https://doi.org/10.3978/j.issn.2305-5839.2015.03.58

Ponzetto, C., Bardelli, A., Zhen, Z., Maina, F., dalla Zonca, P., Giordano, S., Graziani, A., Panayotou, G., & Comoglio, P. M. (1994). A multifunctional docking site mediates signaling and transformation by the hepatocyte growth factor/scatter factor receptor family. Cell, 77(2), 261–271. https://doi.org/10.1016/0092-8674(94)90318-2

Rettenmaier, T. J., Sadowsky, J. D., Thomsen, N. D., Chen, S. C., Doak, A. K., Arkin, M. R., & Wells, J. A. (2014). A small-molecule mimic of a peptide docking motif inhibits the protein kinase PDK1. Proceedings of the National Academy of Sciences, 111(52), 18590–18595. https://doi.org/10.1073/pnas.1415365112

Rodrigues, G. A., & Park, M. (1993). Dimerization mediated through a leucine zipper activates the oncogenic potential of the met receptor tyrosine kinase. Molecular and Cellular Biology, 13(11), 6711–6722.

Rubin, A. F., Gelman, H., Lucas, N., Bajjalieh, S. M., Papenfuss, A. T., Speed, T. P., & Fowler, D. M. (2017). A statistical framework for analyzing deep mutational scanning data. Genome Biology, 18(1), 150. https://doi.org/10.1186/s13059-017-1272-5

Saraon, P., Pathmanathan, S., Snider, J., Lyakisheva, A., Wong, V., & Stagljar, I. (2021). Receptor tyrosine kinases and cancer: Oncogenic mechanisms and therapeutic approaches. Oncogene, 40(24), 4079–4093. https://doi.org/10.1038/s41388-021-01841-2

Schiering, N., Knapp, S., Marconi, M., Flocco, M. M., Cui, J., Perego, R., Rusconi, L., & Cristiani, C. (2003). Crystal structure of the tyrosine kinase domain of the hepatocyte growth factor receptor c-Met and its complex with the microbial alkaloid K-252a. Proceedings of the National Academy of Sciences, 100(22), 12654–12659.

https://doi.org/10.1073/pnas.1734128100

Sun, D., Wu, W., Wang, L., Qu, J., Han, Q., Wang, H., Song, S., Liu, N., Wang, Y., & Hou, H. (2023). Identification of MET fusions as novel therapeutic targets sensitive to MET inhibitors in lung cancer. Journal of Translational Medicine, 21(1), 150. https://doi.org/10.1186/s12967-023-03999-7

Taylor, S. S., & Kornev, A. P. (2011). Protein kinases: Evolution of dynamic regulatory proteins. Trends in Biochemical Sciences, 36(2), 65–77. https://doi.org/10.1016/j.tibs.2010.09.006

Till, J. H., Becerra, M., Watty, A., Lu, Y., Ma, Y., Neubert, T. A., Burden, S. J., & Hubbard, S. R. (2002). Crystal Structure of the MuSK Tyrosine Kinase: Insights into Receptor Autoregulation. Structure, 10(9), 1187–1196. https://doi.org/10.1016/S0969-2126(02)00814-6

Trusolino, L., Bertotti, A., & Comoglio, P. M. (2010). MET signalling: Principles and functions in development, organ regeneration and cancer. Nature Reviews Molecular Cell Biology, 11(12), Article 12. https://doi.org/10.1038/nrm3012

Ung, P. M.-U., Rahman, R., & Schlessinger, A. (2018). Redefining the Protein Kinase Conformational Space with Machine Learning. Cell Chemical Biology, 25(7), 916-924.e2. https://doi.org/10.1016/j.chembiol.2018.05.002

Van der Auwera, G. A., & O'Connor, B. D. (2020). Genomics in the cloud: using Docker, GATK, and WDL in Terra. O'Reilly Media.

Vigna, E., Gramaglia, D., Longati, P., Bardelli, A., & Comoglio, P. M. (1999). Loss of the exon encoding the juxtamembrane domain is essential for the oncogenic activation of TPR-MET. Oncogene, 18(29), 4275–4281. https://doi.org/10.1038/sj.onc.1202791

Wang, W., Marimuthu, A., Tsai, J., Kumar, A., Krupka, H. I., Zhang, C., Powell, B., Suzuki, Y., Nguyen, H., Tabrizizad, M., Luu, C., & West, B. L. (2006). Structural characterization of autoinhibited c-Met kinase produced by coexpression in bacteria with phosphatase. Proceedings of the National Academy of Sciences, 103(10), 3563–3568. https://doi.org/10.1073/pnas.0600048103

Warmuth, M., Kim, S., Gu, X., Xia, G., & Adrián, F. (2007). Ba/F3 cells and their use in kinase drug discovery. Current Opinion in Oncology, 19(1), 55–60. https://doi.org/10.1097/CCO.0b013e328011a25f

Weidner, K. M., Di Cesare, S., Sachs, M., Brinkmann, V., Behrens, J., & Birchmeier, W. (1996). Interaction between Gab1 and the c-Met receptor tyrosine kinase is responsible for epithelial morphogenesis. Nature, 384(6605), Article 6605. https://doi.org/10.1038/384173a0

Weingartner, K. A., Tran, T., Tripp, K. W., & Kavran, J. M. (2023). Dimerization and autophosphorylation of the MST family of kinases are controlled by the same set of residues. bioRxiv. https://doi.org/10.1101/2023.03.09.531926

Wiesner, S., Wybenga-Groot, L. E., Warner, N., Lin, H., Pawson, T., Forman-Kay, J. D., & Sicheri, F. (2006). A change in conformational dynamics underlies the activation of Eph receptor tyrosine kinases. The EMBO Journal, 25(19), 4686–4696. https://doi.org/10.1038/sj.emboj.7601315

Wybenga-Groot, L. E., Baskin, B., Ong, S. H., Tong, J., Pawson, T., & Sicheri, F. (2001). Structural Basis for Autoinhibition of the EphB2 Receptor Tyrosine Kinase by the Unphosphorylated Juxtamembrane Region. Cell, 106(6), 745–757. https://doi.org/10.1016/S0092-8674(01)00496-2

Yeung, W., Ruan, Z., & Kannan, N. (2020). Emerging roles of the αC-β4 loop in protein kinase structure, function, evolution, and disease. IUBMB Life, 72(6), 1189–1202.

https://doi.org/10.1002/iub.2253

Zhang, X., Gureasko, J., Shen, K., Cole, P. A., & Kuriyan, J. (2006). An Allosteric Mechanism for Activation of the Kinase Domain of Epidermal Growth Factor Receptor. Cell, 125(6), 1137–1149. https://doi.org/10.1016/j.cell.2006.05.013

Chapter 2: Resistance mechanisms and differential sensitivities of the MET receptor tyrosine kinase domain to inhibitors mapped through deep mutational scanning

Contributing authors

Gabriella O. Estevam[1,2], Edmond M. Linossi[3,4], Jingyou Rao[8], Christian B. Macdonald[1], Ashraya Ravikumar[1], Karson Chrispens[11], Willow Coyote-Maestas[1,7], Harold Pimentel[8,9,10], Eric A. Collisson[5,6], Natalia Jura[5,6], James S. Fraser[1,7,*]

Affiliations

1. Department of Bioengineering and Therapeutic Sciences, University of California, San Francisco, San Francisco, United States
2. Tetrad Graduate Program, University of California San Francisco, San Francisco, United States
3. Cardiovascular Research Institute, University of California San Francisco, San Francisco, United States
4. Department of Cellular and Molecular Pharmacology, University of California San Francisco, United States
5. Helen Diller Family Comprehensive Cancer Center, University of California, San Francisco, United States
6. Department of Medicine/Hematology and Oncology, University of California, San Francisco, United States
7. Quantitative Biosciences Institute, University of California, San Francisco, United States
8. Department of Computer Science, University of California, Los Angeles, United States
9. Department of Computational Medicine, David Geffen School of Medicine, University of California, Los Angeles, United States
10. Department of Human Genetics, David Geffen School of Medicine, University of California,

Los Angeles, United States

11. Biophysics Graduate Program, University of California San Francisco, San Francisco, United States

* - jfraser@fraserlab.com

Introduction

Tyrosine kinases (TKs) are critical signaling molecules which activate and regulate cellular pathways (Attwood et al., 2021). Small molecule inhibitors are designed to selectively disrupt aberrant signaling cascades associated with oncogenesis, as exemplified by imatinib's remarkable selectivity for Abl (Cohen et al., 2021; Attwood et al., 2021). With the growing potential for ATP-competitive drugs in durable treatment outcomes, the landscape of tyrosine kinase inhibitors (TKIs) and TK targets has also expanded, including transmembrane receptor tyrosine kinases (RTKs) (Cohen et al., 2021; Attwood et al., 2021). However, resistance mutations that arise from TKI selective pressure poses a challenge in drug efficacy and second line therapy deployment, especially for rare and novel mutations which have limited to no treatment reference.

MET is an RTK and proto-oncogene that has been implicated in the pathogenesis of gastric, renal, colorectal, and lung cancers, with non-small cell lung cancer (NSCLC) being linked to the exon14 skipped MET splice variant (METΔEx14) (Frampton et al., 2015; Duplaquet et al., 2018; Wood et al., 2021; Lu et al., 2017). Molecular profiling and next-generation sequencing of tumor samples has provided insight on cancer-associated MET variants, and continues to serve as a primary reference for treatment (Frampton et al., 2015; Bahcall et al., 2021).

The challenge of acquired resistance following MET inhibitor therapy has been approached with strategies like sequential treatment of type I and type II TKIs (Bahcall et al., 2016; Recondo et al., 2020), and combination therapy with type I and type II TKIs - both which have demonstrated promise in preventing resistance (Bahcall et al., 2022; Fernandes et al., 2021). Nevertheless, the efficacy of these strategies is still limited to the potential development of secondary and tertiary

resistance mutations. Clinical reports following post-treatment outcomes have annotated commonly occurring resistance mutations at positions such as D1228, Y1230, G1163, L1195, H1094 for MET (Fernandes et al., 2021; Lu et al., 2017; Recondo et al., 2020), and experimentally Fujino et al., 2019 provided an initial path towards identifying likely secondary resistance mutations in an exon 14 skipped context against a panel of inhibitors (Fujino et al., 2019). However, without extensive documentation of both potential mutational resistance and sensitivity to MET TKIs, there is still a barrier towards leveraging non-cross-resistant mutations in therapy, optimizing inhibitor pairings, and informing rational drug design.

Deep mutational scanning (DMS) of the MET kinase domain in wild-type and METΔEx14 intracellular background contributed to the identification of conserved regulatory motifs, interactions involving the juxtamembrane and C-helix, a critical β5 motif, clinically documented cancer mutations, and classification of variants of unknown significance (Estevam et al., 2023). Beyond defining phenotypic landscapes, inhibitor-based DMS studies have elucidated the landscape of ATP-competitive resistance across various kinases such as ERK, CDK4/6, Src, EGFR and others (Brenan et al., 2016; Persky et al., 2020; Chakraborty et al., 2023; An et al., 2023).

Here, we further explore the landscape of TKI resistance with the MET kinase domain, utilizing the murine Ba/F3 cell line in a constitutively active, TPR fusion background to again investigate mutational responses in two intracellular domain isoforms: MET and METΔEx14 (Estevam et al., 2023). Against a panel of 11 MET inhibitors, we have identified novel resistance mutations and uncovered common MET resistance mechanisms across inhibitor types. Additionally, we adopt Rosace as a growth-based, Bayesian fitness scoring framework, which shows reduced false discovery rates and allows for post-processing normalization of inhibitor treatments (Rao et al., 2023). With our dataset, we have analyzed differential sensitivities to inhibitor pairs and provided a framework for assessing inhibitor efficacy based on mutational sensitivity and likelihood.

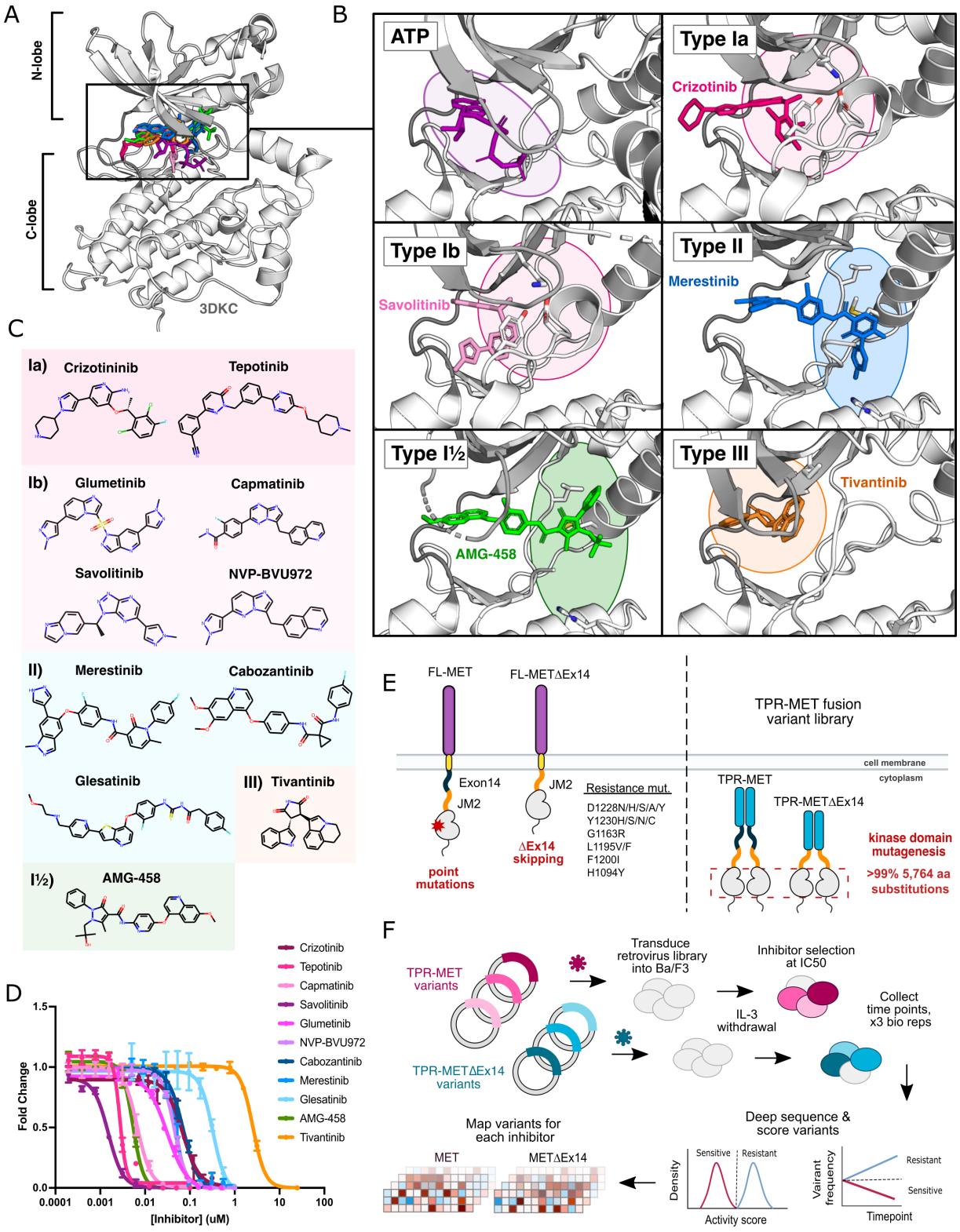

Figure 2.1. MET kinase inhibitor types and resistance mutations screened against a nearly comprehensive library of kinase domain substitutions. (Figure caption continued on the next page).

(Figure caption continued from the previous page). (A) Crystal structure of the ATP-bound MET kinase domain (3DKC) overlaid with type Ia (crizotinib, 2WGJ), type Ib (savolitinib, 6SDE), type II (merestinib, 4EEV), type I½ (AMG-458, 5T3Q), and type III inhibitors (tivantinib, 3RHK). (B) Pocket view of ATP and each inhibitor type bound to the active site of the MET kinase domain with the respective inhibitor and crystal structures from panel A. (C) 2D chemical structures of each inhibitor screened against the site saturation mutagenesis library of the MET kinase domain, with each experimentally determined IC50 values displayed for the selection system used within this study. (D) Dose-response curves for each inhibitor against the wild type MET intracellular domain expressed in a TPR-fusion in the Ba/F3 cell line. (E) Schematics of the full length and exon14 skipped MET receptor alongside the TPR-fusion constructs with the full length and exon14 skipped intracellular domain, displaying four mechanisms of oncogenic activity: point mutations, exon14 skipping, constitutive activity through domain fusions, and inhibitor resistance mutations. (F) Experimental workflow for defining the mutational landscape of the wild type TPR-MET and exon14 skipped TPR-METΔEx14 intracellular domain against 11 ATP-competitive inhibitors in Ba/F3, interleukin-3 (IL-3) withdrawn pooled competition assay.

Results

Measuring the mutational fitness of 5,764 MET kinase domain variants against ATP-competitive inhibitors

Thousands of compounds have been screened against the MET kinase domain, and while several have undergone clinical trials, currently, four MET inhibitors have received FDA approval: crizotinib, cabozantinib, tepotinib, and capmatinib (Santarpia et al., 2021; Wang and Lu, 2023). Resistance mutations have been commonly identified at drug-binding residues, but to understand the full landscape of mutational sensitivity and resistance of MET to various drugs, a panel of 11 inhibitors were selected to profile against a nearly comprehensive library of kinase domain variants in the MET and METΔEx14 intracellular domain. To explore a range of properties, inhibitors were chosen based on clinical usage, chemistries, and "type" classifications.

Small-molecule kinase inhibitors fall into four distinct groups, characterized by their binding modality to the ATP pocket and conformational preferences (Arter et al., 2022; Attwood et al., 2021). Among these groups, three are ATP-competitive: type I, type II, and type I½ (**Figure 2.1**). Type I inhibitors occupy the adenosine binding pocket, form hydrogen bonds with "hinge" region

residues, and favor an active, DFG ”in” conformation. This conformational preference is crucial for the switch from an active to an inactive state, involving the movement of the C-helix to an ”in” position, creating a salt bridge between E1127 and K1110. Type I inhibitors leverage pi-stacking interactions with Y1230 and salt-bridge formation between D1228 and K1110, facilitating inactivation. In MET, type I inhibitors are further classified as type 1a or 1b based on their interaction with solvent front residue G1163 (**Figure 2.1**) (Cui 2014; Fujino et al., 2019; Wang et al., 2023). Type II inhibitors also occupy the adenosine pocket but extend into an opening in the R-spine, typical of an inactive, DFG ”out” conformation. This opening is usually occupied by the DFG-motif Phe in an active conformation (Arter et al., 2022) (**Figure 2.1**). Type I½ inhibitors combine features from both type I and type II inhibitors, engaging with both the adenosine pocket and the R-spine pocket while binding to a DFG ”in” and C-helix ”out” conformation (Arter et al., 2022) (**Figure 2.1**). Finally, type-III inhibitors are allosteric, non-ATP competitive inhibitors, often binding adjacent to, but non-overlapping with ATP (Arter et al., 2022) (**Figure 2.1**).

Within our panel, we included six type I inhibitors (crizotinib, capmatinib, tepotinib, glumetinib, savolitinib, and NVP-BVU972), three type II inhibitors (cabozantinib, glesatinib, merestinib), and the proposed type III inhibitor available to us at the time, tivantinib (**Figure 2.1**). To assess inhibitor potencies and determine equi-potent concentrations to apply during DMS selections and growth rate normalization, we generated dose responses for each inhibitor against our parental strain of wild type TPR-MET (wild type intracellular domain) and TPR-METΔEx14 (exon 14 skipped intracellular domain) constructs, stably expressed in Ba/F3s, to obtain working IC50 values (**Figure 2.1**).

To understand the resistance landscape MET against these inhibitors, we utilized our previously published library harboring >99% of all possible 5,764 kinase domain (1059-1345aa) variants expressed in a TPR-fusion background carrying either a wild type MET or exon 14 skipped intracellular domain (**Figure 2.1**) (Estevam et al., 2023). While TPR fusions afford cytoplasmic

expression, constitutive oligomerization, and HGF-independent activation, membrane-proximal effects are lost (Cooper et al., 1984; Park et al., 1986; Peschard et al., 2001; Rodrigues and Park, 1993; Vigna et al., 1999; Mak et al., 2007; Pal et al., 2017; Lu et al., 2017; Fujino et al., 2019). Again, we employed the Ba/F3 cell line as our selection system due to its undetectable expression of endogenous RTKs and addiction to exogenous interleukin-3 (IL-3), allowing for transgenic kinase addiction and proliferation in the absence of IL-3 (Daley and Baltimore, 1988; Warmuth et al., 2007; Koga et al., 2022). Libraries were grown in a dual selection system, with both IL-3 withdrawal and drug inhibition, with the expectation that gain-of-function mutations would be enriched over time. Time points were selected every two doubling over the course of four time points, and cells were split and maintained in the absence of IL-3 and drug at IC50 for each condition, including a DMSO control. All samples, across all timepoints and replicates, were prepared for NGS and deep sequenced in parallel, on the same Illumina NovaSeq6000 run to identify variant frequencies (**Figure 2.1**). We then measured variant fitness scores using Rosace (Rao et al., 2023) for each selection condition (**Figure 2.1, Supplemental Figure 2.7**).

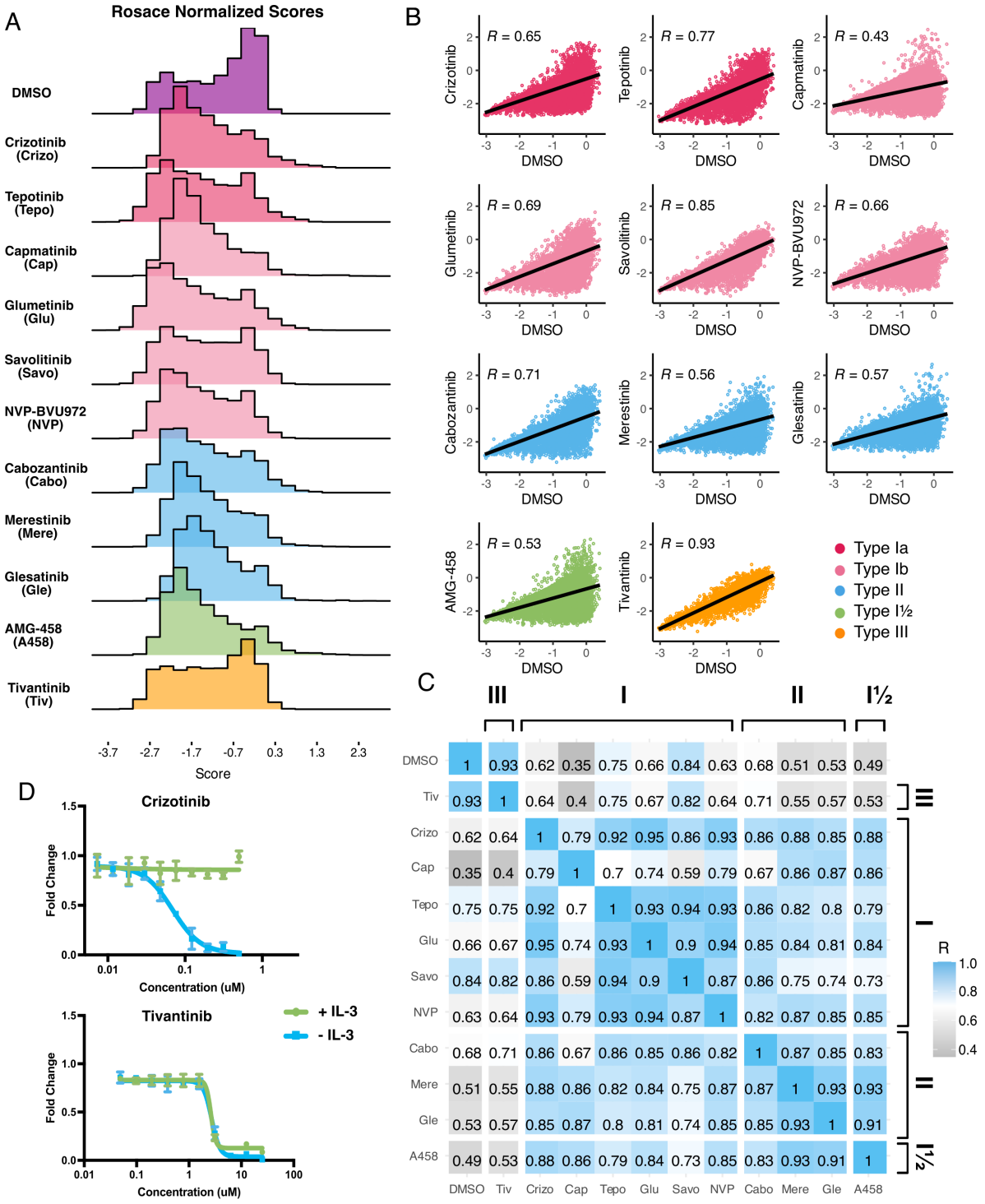

Figure 2.2. Mutational landscape of the MET kinase domain under 11 ATP-competitive inhibitor selection.(A) Distributions of all variants (wild type synonymous, early stop, and missense) for each condition, scored with Rosace and normalized to the growth rate of the DMSO control population. (Figure caption continued on the next page).

(Figure caption continued from the previous page). (B) Correlation plots for all mutational fitness scores for each drug against DMSO, fitted with a linear regression and Pearson's R value displayed. (C) Heatmap showing the Pearson's R correlation for each condition against each other, annotated by condition and inhibitor type. Correlations are colored according to a scale bar from gray to blue (low to high correlation). (D) Dose-responses of crizotinib and tivantinib tested against stable Ba/F3 cells expressing the wild type intracellular domain of MET fused to TPR, tested in the presence and absence of interleukin-3 (IL-3).

Defining the mutational landscape of resistant and sensitizing mutations for the MET kinase domain

Despite tyrosine kinase inhibitors belonging to generalizable groups, individually, each inhibitor occupies a broad chemical space and harbors unique chemical signatures (**Figure 2.1**). Mutations are expected to affect the kinase by either impairing structure (stability, folding, expression) or function (activity, conformation, resistance). At baseline, regardless of inhibitor selection there are mutations that will have shared effects, primarily those pertaining to structure. However, in comparing the fitness landscape of inhibitors, they can be further refined in regard to their group and overarching effect on kinase activity.

Each screened condition has a distinct mutational distribution (**Figure 2.2**). While cellular growth rates were attempted to be controlled through using equi-potent concentration of drugs during cellular selection, there was no direct way to validate this post-processing. Therefore to generate meaningful comparisons between inhibitor scores and conditions and perform downstream subtractions, we normalized cell growth rates for each inhibitor to the growth rate observed for the DMSO population. As expected, the DMSO the control population displayed a bimodal distribution with mutations exhibiting wild type fitness centering around 0, with a wider distribution of mutations that exhibited loss or gain-of-function effects (**Figure 2.2**). Also as expected, inhibitor-treated populations displayed distributions with a loss-of-function peak, representative of mutations that are sensitive to the inhibitor. Unlike DMSO, inhibitor populations were right-skewed, showing greater enrichment of gain-of-function scores at the positive tail of distributions (**Figure 2.2**). These population differences were exemplified by the

low correlation between each inhibitor and DMSO, with capmatinib showing the greatest difference from DMSO with a Pearson's R of 0.45, and tivantinib standing as an outlier with a Pearson's R of 0.93 (**Figure 2.2**).

In comparing all conditions to each other, we were able to further capture differences between and within inhibitor types, where there was a greater expectation for likeness. Type II inhibitors displayed the greatest similarities to one another, with merestinib and glesatinib having the highest correlation (r = 0.93) and cabozantinib and glesatinib showing the lowest (r = 0.87) (**Figure 2.2**). While type I inhibitors were also highly correlated, capmatinib stood out as an outlier, showing the lowest correlation with savolitinib (r = 0.59) and the highest with crizotinib and NVP-BVU972 (r = 0.79 for both)(**Figure 2.2**). While there was only one type I½ inhibitor, AMG-458, it displayed a wide range of correlations, showing the higher similarity with type II inhibitors than type I, likely due to it's similar type II back pocket interactions with the R-spine (**Figure 2.1, 2.2**). Nevertheless, AMG-458 was most distinct from cabozantinib (r = 0.83) and also type I inhibitors tepotinib (r = 0.79) and savolitinib (r = 0.73) (**Figure 2.2**). Between type I and type II groups, with the exception of capmatinib, tepotinib and savolitinib showed the lowest correlation with merestinib and glesatinib (**Figure 2.2**).

However, tivantinib continuously stood out as an outlier, showing strong correlation with the DMSO control (r = 0.93) and low correlation with all other inhibitors, similar to DMSO, suggesting the negative growth effect observed was not due to direct MET selection. Until recently (Michaelides et al, 2023), tivantinb was considered the only type III MET-inhibitor and showed promising early clinical trial results (Eathiraj et al., 2011; Wang et al., 2022). In vitro assays on the purified MET kinase domain have shown that tivantinib has the potential to hinders catalytic activity (Munshi et al., 2010) and structural studies have suggested that its tricyclic aromatic ring can occupy the ATP-binding site without competing with ATP (Eathiraj et al., 2011). Yet in contradiction, comparative MET-dependent and MET-independent cell-based studies on tivantinib, have also shown nondiscriminatory anti-tumor activity, posing that

tivantinib may have alternative inhibitory mechanism than a MET-selective one (Michieli and Di Nicolantonio, 2013; Basilico et al., 2013; Katayama et al., 2013; Fujino et al, 2019).

Therefore, to further test the hypothesis that tivantinib is not MET-selective, we compared the dose response of tivantinib to crizotinib in IL-3 and IL-3 withdrawal conditions for TPR-MET and TPR-METΔEx14 in Ba/F3 cells (**Figure 2.2**). While the expectation was that both crizotinib and tivantinib would display inhibition in the absence of IL-3, if there was also selection in the presence of IL-3, that would suggest a non-MET-selective effect given that the cells are not "MET-addicted." Indeed, in comparing the dose responses, while crizotinib only displayed an inhibitory effect under IL-3 withdrawal conditions, tivantinib displayed equivalent inhibiton regardless of IL-3 and MET-dependence (**Figure 2.2**), further supporting not only that tivantinib may have cytotoxicity effects unrelated to METinhibition, but also underscoring the sensitivity of the DMS in identifying direct protein-drug effects.

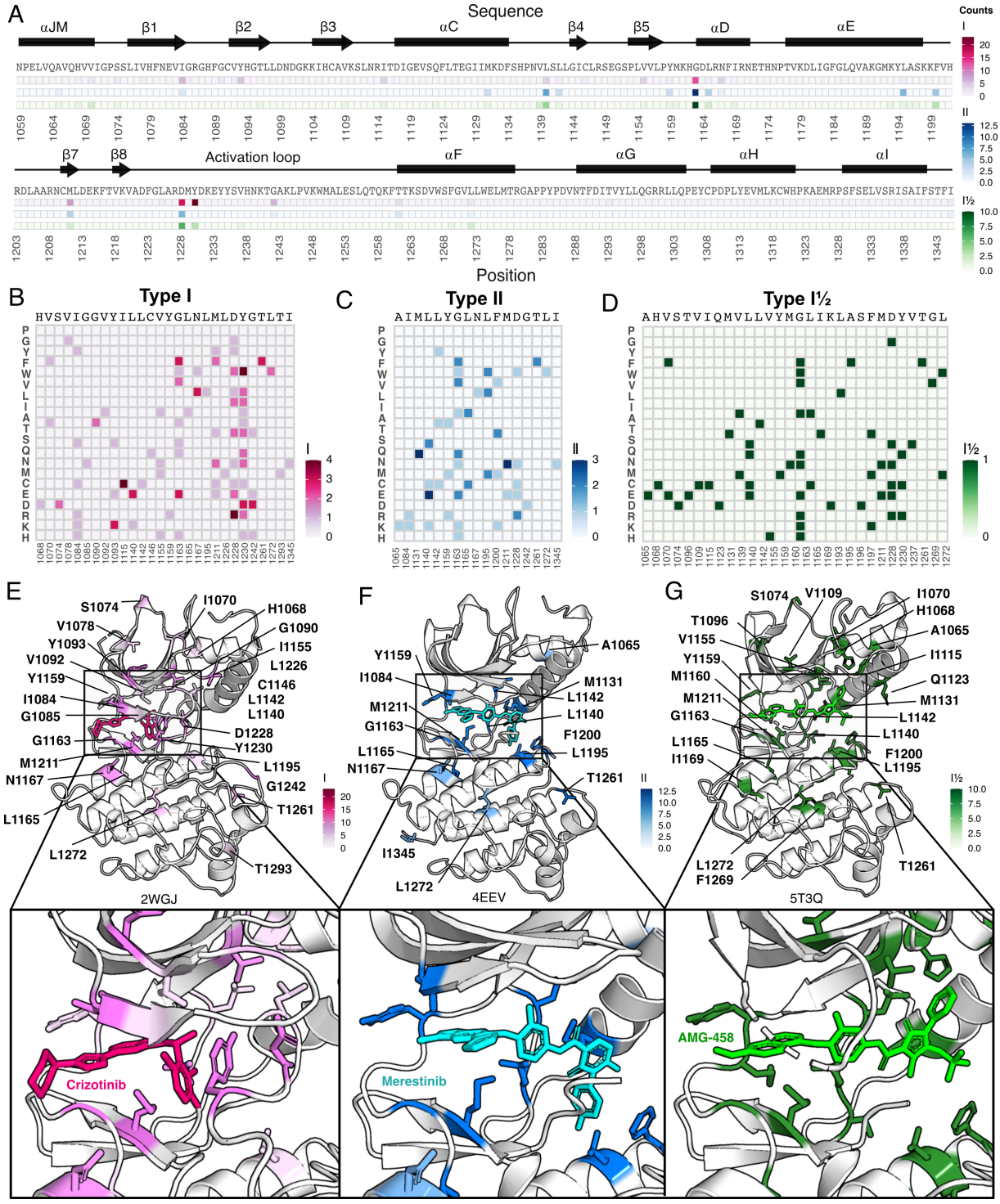

Figure 2.3. Novel resistance mutations and "hotspots" identified for MET inhibitors types. (A) Collapsed heatmap of common resistance positions along the kinase domain, with the wild type protein sequence and secondary structure annotated. Each tile represents a sum of counts for statistically filtered resistance mutations across all inhibitors for type I (pink), type II (blue), and the type I½ inhibitor AMG-458 (green). (Figure caption continued on the next page)

(Figure caption continued from the previous page). (B-D) Expanded heatmap showing each resistance position and the counts for each specific resistance mutation across all inhibitor types type I (pink), type II (blue), and the type I½ inhibitor AMG-458 (green). Wild type sequence and variant change are annotated. (E-F) Average frequency of resistance mutations for each mapped on to a representative type I (crizotinib, 2WGJ) and type II (merestinib, 4EEV) crystal structure, alongside the type I ½, AMG-458 structure (5T3Q), with associated scale bars. Individual positions are annotated on each structure, with a zoom-in of the bound-inhibitor and surrounding resistance sites.

Novel resistance mutations identified for type I, type II, and type I ½ inhibitors

ATP-competitive inhibitors are grouped into "types" based on their binding modality and conformational preference of the kinase domain (Arter et al, 2021; Cui 2014). While each inhibitor is chemically unique, and will have associated idiosyncratic resistance mutations, with the general structural space each type samples, there are also expected shared resistance mutations and positions, or "hotspots," that promiscuously confer resistance. By identifying commonalities not only within an inhibitor type, but also across inhibitor types, we can better understand residues and regions of the kinase to both avoid and exploit in drug design and treatment.

Mutations were considered resistant if the fitness score was significantly above wild type. To best apply this filtering to identify inhibitor-related resistance mutations, the fitness scores of each variant in each inhibitor condition was first subtracted from DMSO - eliminating baseline gain-of-function and loss-of-function mutations. Next we statistically filtered resistance mutation by their score and p-value (**Supplemental Figure 2.7**). For each inhibitor, the frequency of a specific resistance mutation was counted, then further summarized within the inhibitor type (I, II, I ½) to generate a heatmap of shared resistance frequencies. Finally, the heatmap of all resistance frequencies was collapsed into a single dimension heatmap that plotted the total frequency of resistance mutations at a position (**Figure 2.3**).

In this condensed heatmap, several common resistance positions emerged within an inhibitor type and across inhibitor types, providing a broad view of "hotspots." Two positions stood out with the

highest frequency of resistance, G1163 and D1228 (**Figure 2.3**) and physicochemical tolerance (**Figure 2.3**), unsurprisingly due to their inhibitor interactions - G1163 being at the solvent front entrance of the active site and D1228 stabilizing an inactive conformation of the A-loop with an inhibitor bound (Cui 2014; Recondo et al., 2020; Fernandes et al., 2021). Y1230 was another unsurprising hotspot, given that it stabilizes inhibitors at the active site through pi-stacking interactions (Cui 2014), particularly for type I inhibitors. Interestingly, there was also a discernible difference between inhibitor types in Y1230 mutational frequencies, where in type I and I ½ Y1230 appears as a resistance hotspot, and type II, where it does not (**Figure 2.3**). Other common resistance positions that are discernable between inhibitor types are F1200 and L1195 (Recondo et al., 2020), both which appear as hotspots within our analysis for type II but not type I (**Figure 2.3**). At the base of the active site, M1211 is a previously documented resistance site (Tidet et al., 2011) and also a C-spine residue (Estevam et al., 2023), which harbors resistance mutations for all inhibitor types within our analysis (**Figure 2.3**).

Outside of common and expected resistance hotspots, positions I1084, L1140, L1142, T1261, and L1272 carried resistance mutations for each inhibitor group (**Figure 2.3**). I1084 is located at the solvent front of the phosphate-loop (P-loop) of the kinase N-lobe (**Figure 2.1**) which is responsible for stabilization of the ATP phosphate groups. I1084 also takes part in a hydrophobic "subpocket" of the ATP binding site where inhibitors can bind (Peach et al., 2009; Rickert et al., 2011; Wang and Lu, 2023). Interestingly, an I1084T mutation has been identified in hereditary papillary renal cell carcinomas, and experimentally has shown sensitivity to crizotinib, capmatinib, and merestinib (Guérin et al., 2023). Within the physiochemical breakdown of resistance in our analysis, while I1084T indeed does not emerge as a resistance mutation, substitution to I1084R/K are resistant in both type I and II inhibitors, but not in the type I ½ AMG-458 (**Figure 2.3**), showing a potential for I1084 resistance development if mutated to a positively charged residue. L1140 and L1142, unlike I1084, are buried with the kinase domain core, with L1142 being an R-spine residue and L1140 forming the back of the ATP-binding pocket (**Figure 2.3**), with substitutions that add charge (but do not hinder ATP-binding)

displaying the largest resistance frequencies for L1140 (L1140C/E/K) (**Figure 2.3**). T1261 and L1272 are the most distal resistance positions within our analysis, located within the C-lobe's F-helix (**Figure 2.3**), and are only classified as resistant when mutated to T1261F and L1272W (**Figure 2.3**). Structurally, it is unobvious how these two mutations could confer resistance, but we speculate their proximity to the A-loop may play a role in disrupting an inhibitor-induced inactive conformation.

While generalizing resistance positional hotspots reveals commonalities across inhibitor types, within one inhibitor type not all variants are necessarily shared for a position. Therefore, an additional opportunity exists to strategize inhibitors based on mutation identity within the same or different inhibitor type. From the hotspot analysis, specific mutations were grouped based on their appearance across specific drugs (**Supplemental Figure 2.9**). Mutations like Y1230F, D1228R and I1115C were the most common amongst type I inhibitors, compared to M1211N, M1131Q, L1140E being the most common amongst type II inhibitors (**Supplemental Figure 2.9**), underscoring how variants, occurrence, an structural locations of shared mutations that can be categorized.

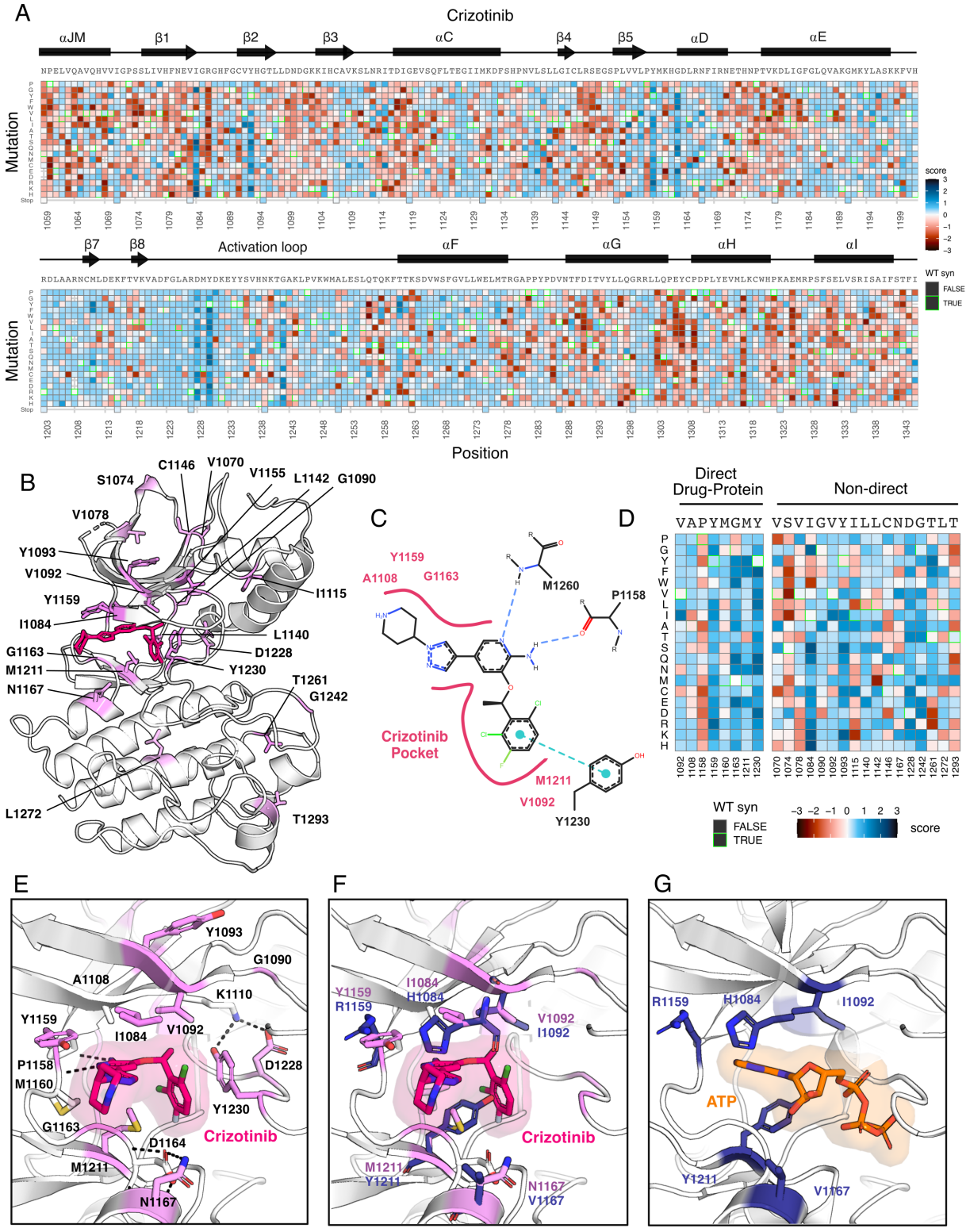

Figure 2.4. Novel resistance mutations identified and mapped for crizotinib. (Figure caption continued on the next page).

(Figure caption continued from the previous page). (A) Heatmap of crizotinib fitness scores subtracted from the corresponding mutation in DMSO, scaled from loss-of-function (red) to gain-of-function (blue), with the wild type protein sequence, secondary structure, kinase domain residue position, and mutational substitution annotated. Wild type synonymous substitutions are outlined in green. (B) Resistance positions mapped onto the crizotinib crystal structure (PDB 2WGJ). Positions are labeled and colors are scaled according to the average score for the resistance mutations at each site. (C) 2D protein-drug interactions between crizotinib and the MET kinase domain (PDB 2WGJ) with pocket residues and polar and pi interactions annotated. Schematic generated through https://proteins.plus/. (D) Condensed crizotinib heatmap displaying direct drug-protein interacting and non-direct resistance position. (E-F) Crizotinib binding site and pocket residues displayed and overlaid with ATP from PDB 3DKC, and mutations for I1084H, V1092I, Y1159R, M1211Y, and N1167V structurally modeled.

Analysis of MET kinase domain variant sensitivity and resistance for unique inhibitors

Although inhibitor types share resistance hotspots, individual inhibitors, regardless of type, will carry distinguishing, idiosyncratic resistance and sensitivity patterns. Understanding the mutational fitness of structural regions to unique inhibitors, coupled with a reference of potential resistance mutations, can serve as a framework for evaluating drugs relative to cancer-associated mutations.

Crizotinib is a one of four FDA approved inhibitors for MET and is a multitarget TKI (Cui et al., 2011; Wang and Lu, 2023; Santarpia et al., 2021), which we use as an example to study the fitness landscape of a unique inhibitor. As before, to identify mutations that show gain-of-function and loss-of-function above baseline, all fitness scores were subtracted from DMSO (**Figure 2.4**), with the expectation that most mutations related to fold, expression, stability, and would be canceled, while mutations with drug sensitivity or resistance would be enhanced. Indeed, the highest frequency of gain-of-function mutations occurred at positions like D1228, Y1230, and G1163, in agreement with our hotspot analysis and clinical reports (Fernandes et al., 2021). However, regions with high sensitivity occurred throughout the kinase, primarily in loop-regions which have the greatest mutational tolerance in DMSO, but do not provide a growth advantage in the presence of an inhibitor (**Supplemental Figure 2.9, 2.10**), therefore showing the largest differential in sensitivity but not necessarily because of direct

inhibitor sensitivity. Nevertheless, regulatory motifs like the juxtamembrane helix (JM-helix), P-loop, and C-helix also displayed patterns of sensitivity (**Figure 2.4**). Instead, mutations with strong loss-of-function fitness within the inhibitor binding site or regulatory motifs, may point to true drug sensitivity.

In mapping filtered resistance positions to the crizotinib crystal structure (PDB 2WGJ), our DMS results further emphasize the emergence of resistance mutations at the ATP-binding site and direct-protein drug interacting residues (**Figure 2.4**), with the exception of P1158, located at the cusp of 5 and hinge region and showing the highest sensitivity towards mutations despite primarily supporting crizotinib binding through backbone H-bonding (**Figure 2.4**). Positions like M1211, Y1159, V1092 also hinge and C-spine residues which support the ATP-binding site, and mutations that introduce charge or change the confirmation of the pocket to clash with crizotinib but not ATP, confer resistance (**Figure 2.4**).

Outside of direct drug-protein interactions, positions I1084, T1261, Y1093, and, G1242 were displayed the largest mutability and resistance (**Figure 2.4**). I1084 and Y1093 are proximal to the P-loop, with substitutions that clash with the inhibitor coinciding with I1084 resistance 1, while mutations that introduce charge to Y1093 may conformationally change the the ATP-binding pocket. Distal mutations like N1167 or G1242 likely confer resistance though alternative mechanisms, by destabilizing interactions with neighboring residues, such as the displacement of a salt bridge between N1167 and D1164, or potentially reducing A-loop flexibility in the case of G1242 mutations (**Figure 2.4**).

In broadening our resistance analysis to all inhibitors that passed statistical filters, unique resistance mutations continue to be enriched at the ATP-binding site, but with discernable differences in enrichment between type I and II inhibitors R-spine and C-helix regions (**Figure 2.5**). Mapping inhibitor-specific positions and mutational scores, not only provides a mutation-level breakdown of inhibitor contributions to common resistance mutations, but also highlights differences in structural resistance enrichment and across inhibitors (**Figure 2.5**).

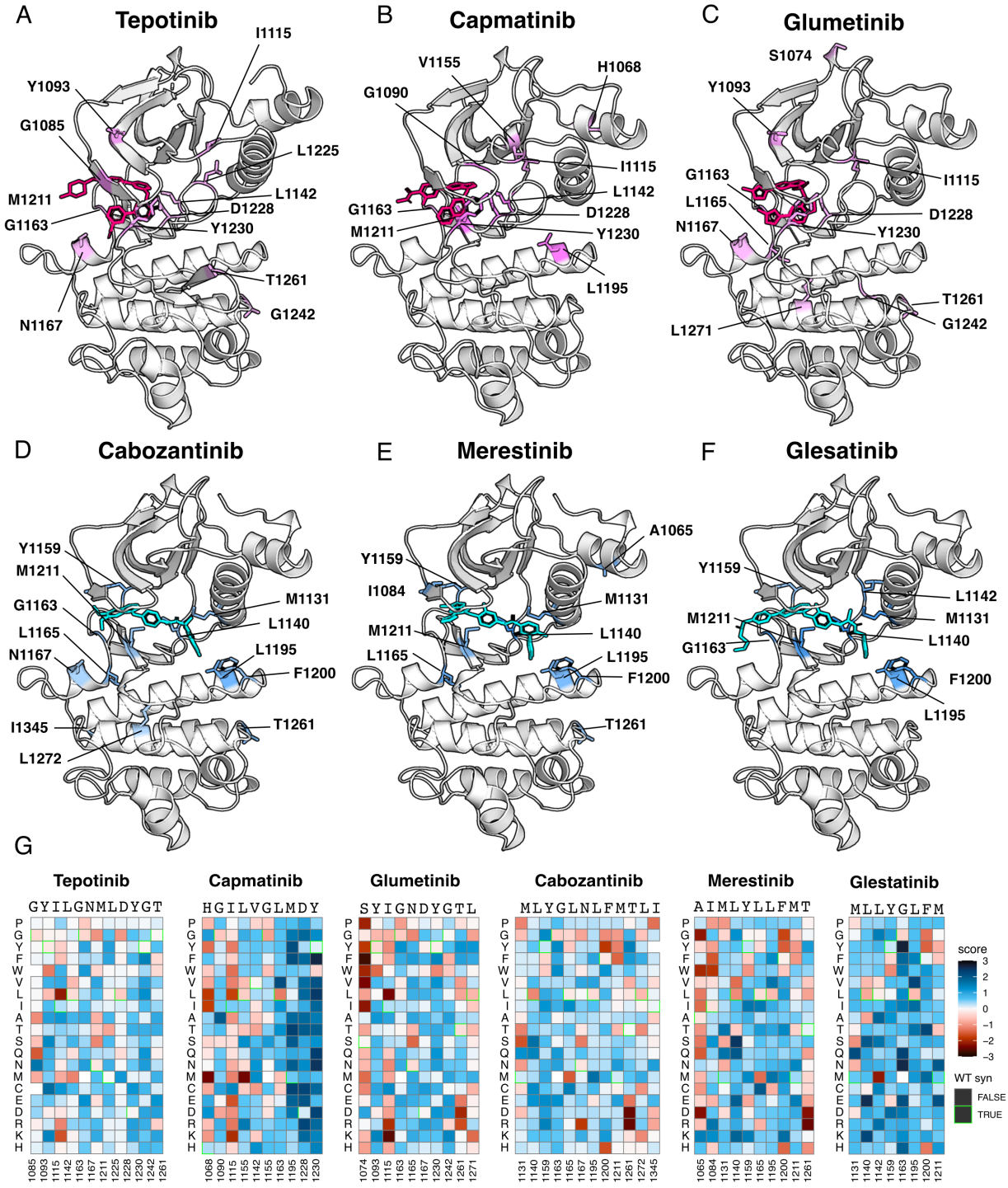

Figure 2.5. Resistance mutations mapped onto experimental and docked kinase domain structures for type I and type II inhibitors. (Figure caption continued on the next page).

(Figure caption continued from the previous page). (A-F) Resistance positions and average resistance mutational score mapped onto representative crystal structures and labeled (type I: pink, type II: blue). (G) Heatmaps of each resistance position for each drug with fitness scores scaled from loss-of-function (red) to gain-of-function (blue). Wild type synonymous substitutions are outlined in green.

Differential sensitivities of the MET kinase domain to type I and type II inhibitors

Acquired resistance following TKI treatment can substantially narrow second-line therapy options. Strategies aimed at preventing resistance, such as sequential or combination dosing of type I and type II inhibitors, have been explored and offer promise in preventing resistance (Bahcall et al., 2016; Recondo et al., 2020; Bahcall et al., 2022; Fernandes et al., 2021). However, the efficacy of these strategies is limited to the emergence of secondary resistance mutations, and specific inhibitor pairings are further limited to case examples of disparate effects.

To identify residue mutations and regions of nonoverlapping sensitivities that can inform inhibitor pairs, we applied cross-comparison analysis of all type I and type II inhibitor fitnesses. As before, by performing linear regression, inhibitor effect likeness was evaluated broadly based on correlations (**Figure 2.2**), which we repeated with DMSO subtracted fitness scores (**Figure 2.6**). Type I and type II pairs with the highest correlations included capmatinib and glesatinib (r = 0.92), which may have the largest overlapping fitness profile compared to pairs with the lowest correlations, like savolitinib and merestinib (r = 0.7) (**Figure 2.6**). Overall, cabozantinib showed the lowest average correlation with all type I inhibitors, making it the most divergent type II inhibitor within our screen, and potentially offering the least overlap in resistance (**Figure 2.6**).

We narrowed our characterization on two type I and II pairings based on clinical precedence, comparing crizotinib to cabozantinib, and capmatinib to glesatinib (Bahcall et al., 2022) (**Figure 2.6**). Mutations were filtered on whether they are gain-of-function in one inhibitor, but loss-of-function in the other (**Figure 2.6**). In structurally mapping the average score of differential mutations for each residue position, as expected, enrichment was observed in the

typical direct protein-drug interacting positions like Y1230 for type I and M1131 For type II inhibitors (**Figure 2.6**). However, regions of sensitivity or resistance outside of these direct drug-protein interacting residues provide an opportunity to strategize inhibitors based on identified cancer-associated mutations. Speculatively, cabozantinib could be a beneficial second-line option for a M1211Y resistance mutation post TKI treatment with crizotinib, but not for an M1211E resistance mutation, which has a wild type to gain-of-function profile across all inhibitors screened. Nevertheless, such a sequential approach would require experimental validation of differential effects.

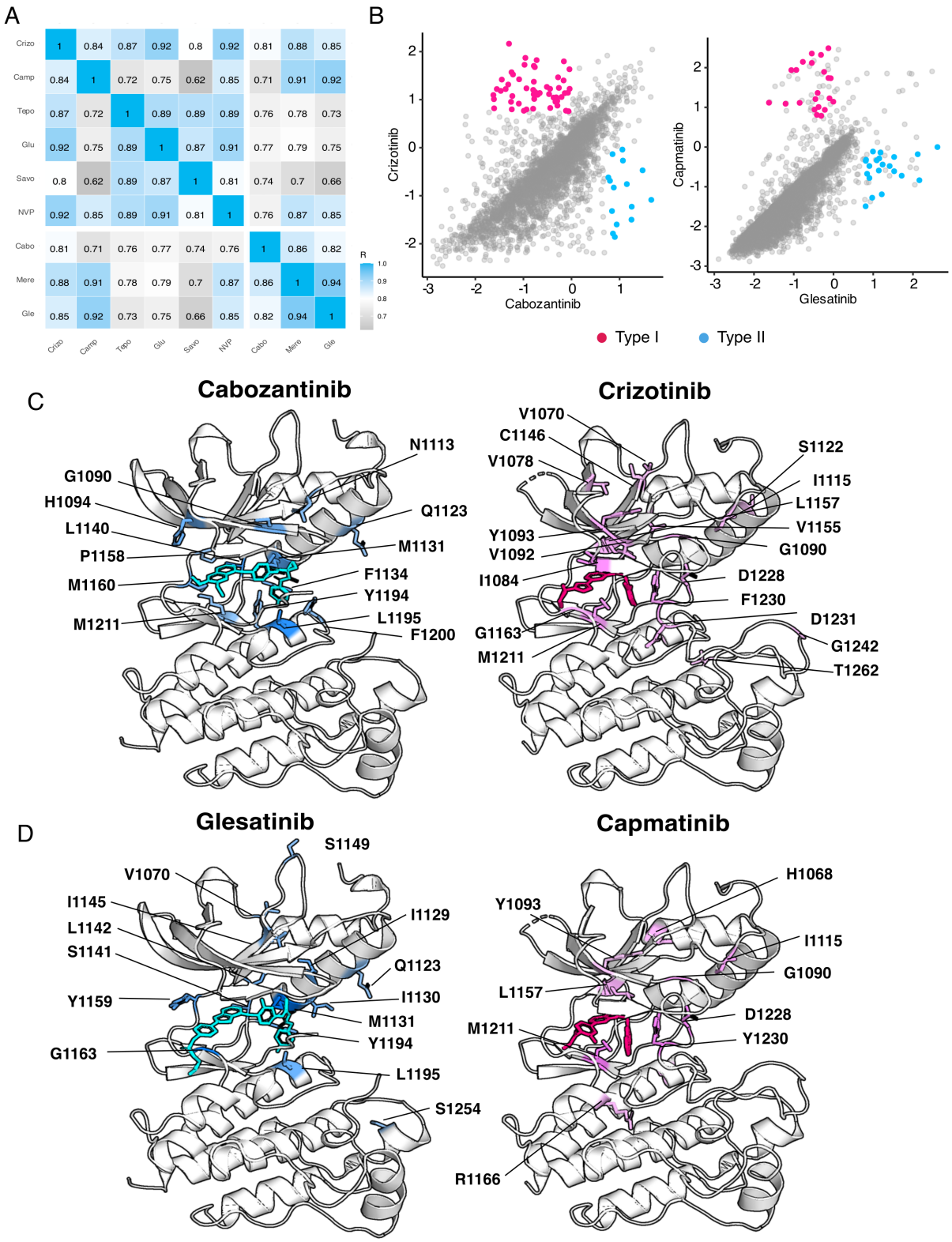

Figure 2.6. MET kinase domain differential sensitivities revealed for type I and type II inhibitors. (A) Heatmap showing Pearson's correlation values for all combinations of screened type I and type II inhibitors. (Figure caption continued on the next page).

(Figure caption continued from the previous page). Correlations were determined from DMSO subtracted fitness scores. (B) Correlation plot correlation plot of DMSO subtracted fitness scores for crizotinib, cabozantinib and glesatinib, capmatinib. Mutations with differential scores are highlighted for type I (pink) and type II (blue). (C-D) Average scores of mutations with differential sensitivities within inhibitor pairs mapped and annotated in respective crystal structures (crizotinib, 2WGJ; cabozantinib, docked into 4EEV; glesatinib, docked into 4EEV; capmatinib, docked into 2WGJ). Positions that are gain-of-function for type I but loss-of-function in type II are highlighted in pink, whereas positions that are gain-of-function for type II but loss-of-function in type I are highlighted in blue.

Discussion

ATP-competitive tyrosine kinase inhibitors offer increasing promise in the treatment of disease, but also face several challenges which negatively impact efficacy and outcomes, including resistance development and optimal combination or sequence of treatments (Attwood et al., 2021; Recondo et al., 2020). Our DMS of the MET receptor tyrosine kinase domain against a panel of inhibitors offers a framework for experimentally identifying resistance mutations, both unique and shared amongst drugs, in an activated kinase context.

By massively screening the effect of a nearly comprehensive library of amino acid substitutions in the MET kinase domain against 11 inhibitors, generalizable patterns for inhibitor types emerged. In accordance with the binding modality of both type I and II inhibitors, residues that commonly confer resistance, or act as "hotspots," were mapped to previously reported sites like D1228, Y1230, M1211, G1163, and novel sites like I1084, L1140, L1142, T1261, and L1272. While residues neighboring the ATP-binding pocket are predicted to acquire resistance, annotation of hotspot differences between inhibitor types also offers an opportunity to leverage inhibitor types, like in the case of I1084 which is a resistance hotspot for type I and II inhibitors, but not the screened type I½ inhibitor, AMG-458. Understanding hotspots that are distal from the ATP-binding site also offer a design opportunity for allosteric inhibitors that can target cancer-associated and resistance-associated regions within the C-lobe (Mingione et al., 2023). Cross-correlating fitness landscapes also allows for the evaluation of inhibitor effect "likeness" at a population level, providing a reference for inhibitor combination or sequence usage.

Beyond annotating generalizable patterns, our DMS can serve as a reference for rare and novel mutations bespoke to an inhibitor which again can be leveraged in the case of personalized treatment approaches and respective to secondary resistance mutations, dual resistance mutations, or evaluating inhibitor overlap. Finally, at the scale of mutational effects and inhibitor types screened, these fitness scores can serve as a training dataset for machine learning algorithms to virtually screen inhibitors outside of this study and generate predictions that can inform the design of novel inhibitors or inhibitor choices.

Methods

Mammalian cell culturing Ba/F3 cells (DSMZ) and maintained in 90% RPMI (Gibco), 10% HI-FBS (Gibco), 1% penicillin/streptomycin (Gibco), and 10ng/ml IL-3 (Fisher), and incubated at 37°C with 5% CO2. Cells were passaged at or below 1.0E6 cells/ml to avoid acquired IL-3 resistance, and regularly checked for IL-3 dependence by performing 3x PBS (Gibco) washes and outgrowth in the absence of IL-3.

Plat-E cells stably expressing retroviral envelope and packaging plasmids were originally gifted by Dr. Wendell Lim, and maintained in 90% DMEM,HEPES (Gibco), 10% HI-FBS (Gibco), 1% penicillin/streptomycin (Gibco), 10ug/ml blasticidin, 1ug/ml puromycin. Cells were cultured at 37°C with 5% CO2 and maintained under blasticidin and puromycin antibiotic pressure unless being transfected.

Dose response and IC50 determination

Ba/F3 cells stably expressing TPR-MET and TPR-METΔEx14 were washed with DPBS (Gibico) 3x times to remove IL-3 and puromycin. Cells were resuspended in 90% RPMI and 10% FBS, and were seeded in the wells of a 96-well, round-bottom plate at a density of 2.5e4 cells/ml in 200ul. Cells were incubated for 24hr to allow kinase-driven signaling. The next day, inhibitors were added to triplicate rows of cells at a concentration range of 0 to 10uM (2-fold dilutions), and

allowed to incubate for 72hr post TKI addition. CellTiter-Glo reagent (Promega) was mixed at a 1:1 ratio with cells and luminescence was measured on a Veritas luminometer. Cell numbers were determined from a Ba/F3 cell and ATP standard curve generated according to the manufacturer's instructions. Dose response curves were fit using Prism's log(inhibitor) vs. response, variable slope function. Data are presented as cell viability normalized to the fold change from the TKI free control.

MET kinase domain variant library generation, cloning, and library introduction into Ba/F3

In this study, we repurposed cell lines transduced with TPR-MET and TPR-METΔEx14 kinase domain variant libraries, previously validated (Estevam et al., 2023).

DMS time point selection and sample preparation

For each biological replicate, a stock of 4.0e6 cells transduced with TPR-MET and TPR-METΔEx14 kinase domain variants were thawed and expanded for 48 hrs in the presence of IL-3 and puromycin to prevent pre-TKI selection. Each batch of cells were grown to a density of 72 million cells to be split into 12 dishes for each selection condition. Cells were first washed with DPBS (Gibco) 3x times to remove IL-3 and antibiotics. Cells were resuspended in 90% RPMI and 10% FBS, counted, and split across 12 dishes (15cm) at 30mL. A total of 6 million cells from each replicate was harvested and pelleted at 250xg to serve as the "time point 0" pre-selection sample (T0). This was performed for both libraries in parallel.

To begin selection of each replicate for each library, 0.01% DMSO was added to the control plate while the appropriate IC50 concentration of inhibitor was added to each respective plate. Three time points post T0 were collected for each library replicate and condition for a total of four time points (T0, T1, T2, T3). Time points were harvested every two doublings (72hr) across 12 days; 6 million cells were harvested for each condition and pelleted at 250xg for 5min; 2.0E5 cells/ml were split at every time point and maintained either in DMSO or TKI.

The gDNA of each time point sample was isolated with the TakaraBio NucleoSpin Blood QuickPure kit the same day the cells were harvested. gDNA was eluted in a 50µl elution buffer using the high concentration and high yield elution manufacturer's protocol. Immediately after gDNA was isolated, 5µg of gDNA was used for PCR amplification of the target MET KD gene to achieve the proper variant coverage. A 150µl PCR master mix was prepared for each sample using the TakaraBio PrimeStar GXL system according to the following recipe: 30µl 5X PrimeStar GXL buffer, 4.5µl 10µM forward primer (0.3uM final), 4.5µl 10µM reverse primer (0.3uM final), 5µg gDNA, 12µl 10mM dNTPs (2.5mM each NTP), 6µl GXL polymerase, nuclease free water to a final reaction volume of 150uL. The PCR master mix was split into three PCR tubes with 50µl volumes and amplified with the following thermocycler parameters: initial denaturation at 98°C for 30 s, followed by 24x cycles of denaturation at 98°C for 10 s, annealing at 60°C for 15 s, extension at 68°C for 14 s, and a final extension at 68°C for 1 min.

Library preparation and deep sequencing

After all time points were selected, harvested, and PCR amplified, the target gene amplicon was isolated from gDNA by gel purification. The entire 150µl PCR reaction for each sample was mixed with 1X NEB Purple Loading Dye (6X stock) and run on a 0.8% agarose, 1X TBE gel, at 100 mA until there was clear ladder and band separation. The target amplicons were gel excised and purified with the Zymo Gel DNA Recovery kit. To remove excess agarose contamination, each sample was then further cleaned using the Zymo DNA Clean and Concentrator-5 kit. Amplicon DNA concentrations were then determined by Qubit dsDNA HS assay (Invitrogen).

Libraries were then prepared for deep sequencing using the Nextera XT DNA Library Prep kit in a 96-well plate format (Illumina). Manufacturer's instructions were followed for each step: tagmentation, indexing and amplification, and clean up. Libraries were indexed using the IDT for Nextera Unique Dual Indexes Set C (Illumina). Then, indexed libraries were quantified using the Agilent TapeStation with HS D5000 screen tape (Agilent) and reagents (Agilent). DNA concentrations were further confirmed with a Qubit dsDNA HS assay. All samples were manually

normalized and pooled at 10nM for MET and METΔEx14. The libraries were then paired-end sequenced (SP300) on two lanes of a NovaSeq6000.

MET kinase domain variant analysis and scoring

Raw Rosace fitness scores were used for all comparative measurements. Fitness scores for each inhibitor condition were normalized post-processing to the growth rate of the DMSO control population, to allow for DMSO subtraction of variants and direct variant comparison.
Gain-of-function and resistance mutations were classified as (1) DMSO subtracted variant score >= 0 (2) raw variant score >= 0 (3) a low p-value (p <= 0.1) (4) corresponding variant score in DMSO is <=0 .

Kinase domain structural analysis

Unless otherwise stated, all structural analysis was performed on PyMol. Inhibitors that lacked an experimental crystal structure were docked into a representative type I (2WGJ) or type II (4EEV) structure with AutoDock Vina (https://vina.scripps.edu/).

Acknowledgements

Sequencing was performed at the UCSF CAT, supported by UCSF PBBR, RRP IMIA, and NIH 1S10OD028511-01 grants. This work was supported by NIH CA239604 to EAC, NJ, JSF; HHMI Hanna Gray Fellowship and UCSF QBI Fellow program to WCM; and the UCSF Program for Breakthrough Biomedical Research, funded in part by the Sandler Foundation, to JSF.

Competing Interests

JSF is a consultant for, has equity in, and receives research support from Relay Therapeutics. N.J. is a founder of Rezo Therapeutics and a shareholder of Rezo Therapeutics, Sudo Therapeutics, and Type6 Therapeutics. N.J. is a SAB member of Sudo Therapeutics, Type6 Therapeutic and NIBR Oncology. The Jura laboratory has received sponsored research support from Genentech, Rezo Therapeutics and Type6 Therapeutics. E.A.C. is a consultant at IHP Therapeutics, Valar Labs, Tatara Therapeutics and Pear Diagnostics, reports receiving commercial research grants from Pfizer, and has stock ownership in Tatara Therapeutics, HDT Bio, Clara Health, Aqtual, and Guardant Health.

Supplemental Figures

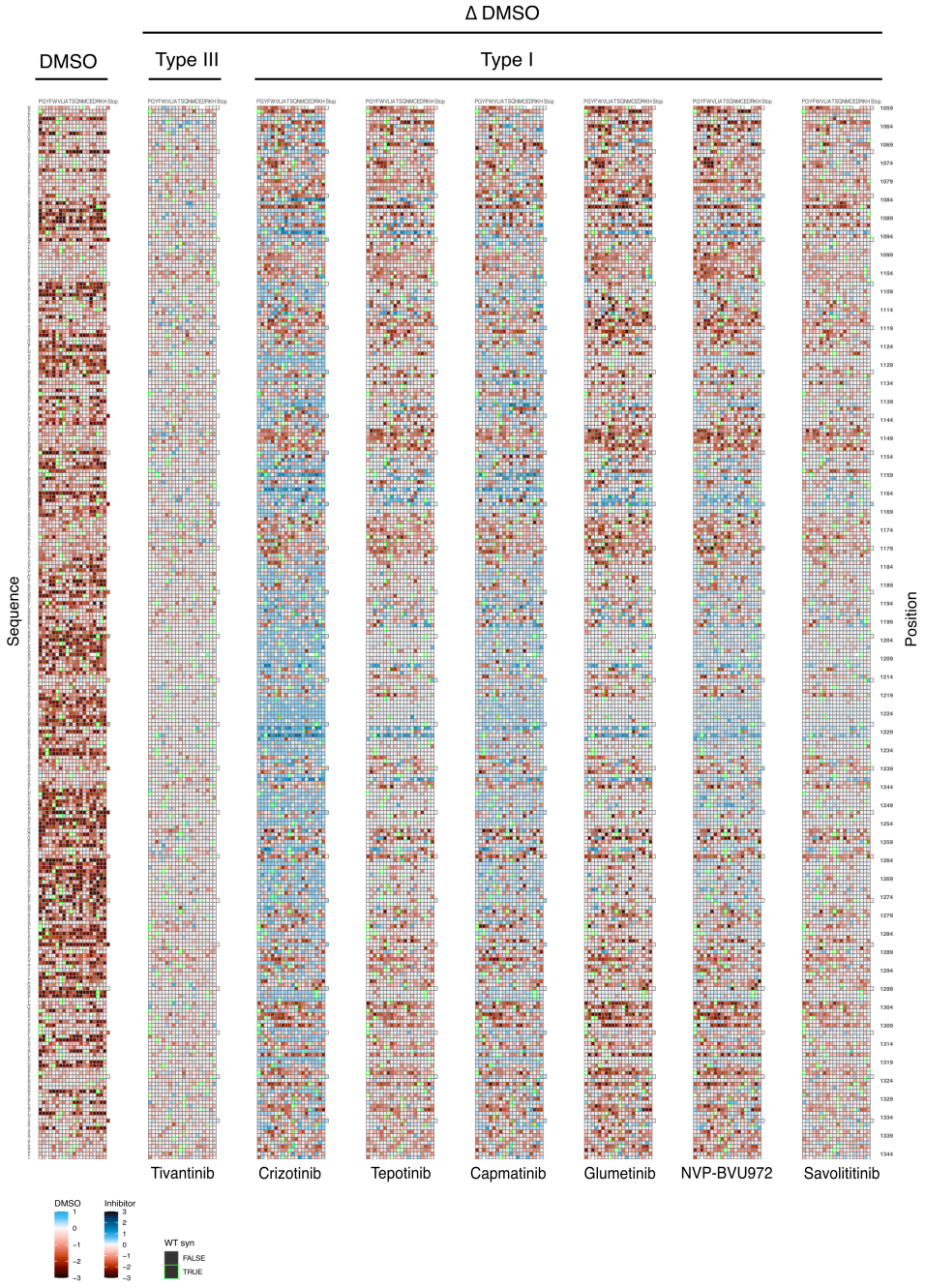

Supplemental Figure 2.7. Fitness landscapes the MET kinase domain screened against type I and III inhibitors. Heatmaps of DMSO and DMSO subtracted fitness scores for the MET kinase domain for tivantinib, crizotinib, capmatinib, tepotinib, glumetinib, savolitinib, and NVP-BVU972. Fitness scores are scaled from negative (red) to positive (blue). Wild type fitness scores are white, and wild type synonymous mutations are outlined in green.

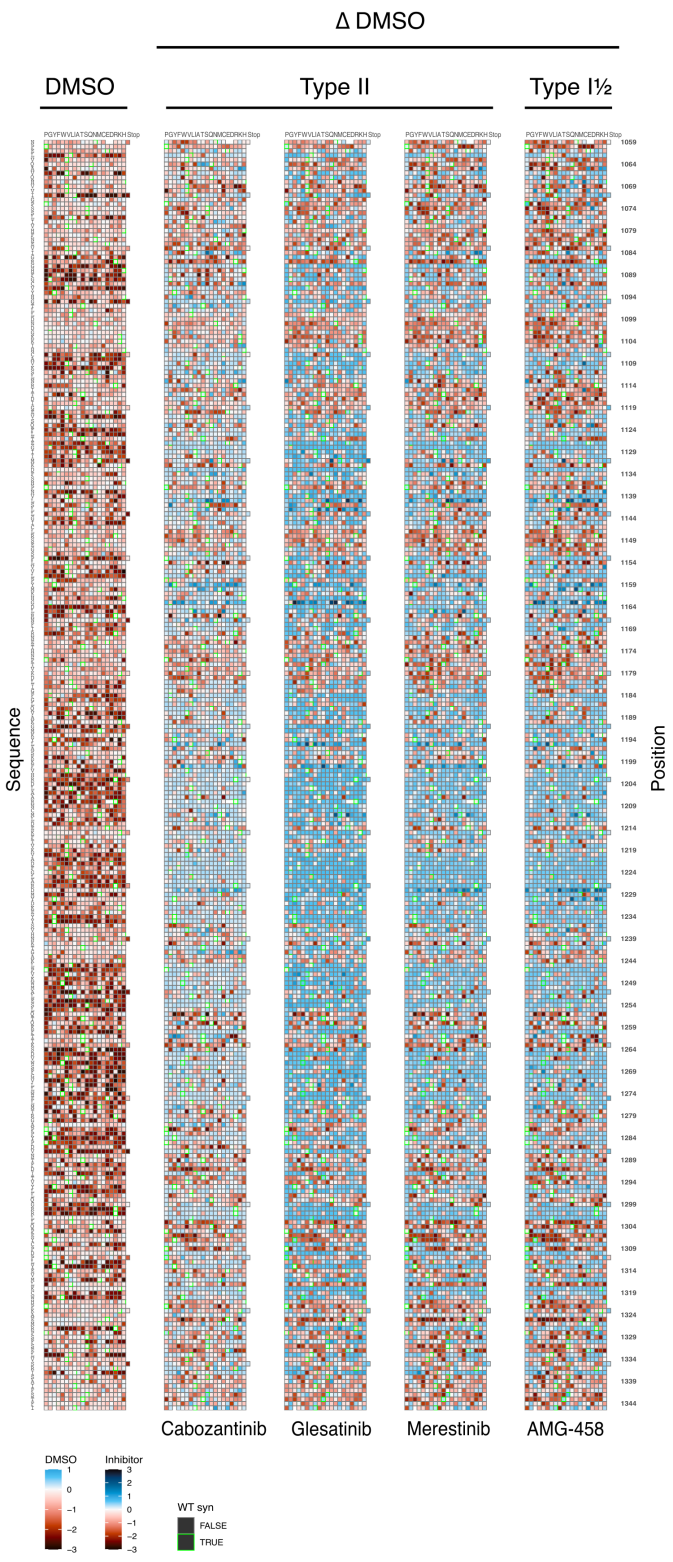

Supplemental Figure 2.8. Fitness landscapes the MET kinase domain screened against type II inhibitors. Heatmaps of DMSO and DMSO subtracted fitness scores for the MET kinase domain for cabozantinib, merestinib, and glesatinib. Fitness scores are scaled from negative (red) to positive (blue). Wild type fitness scores are white, and wild type synonymous mutations are outlined in green.

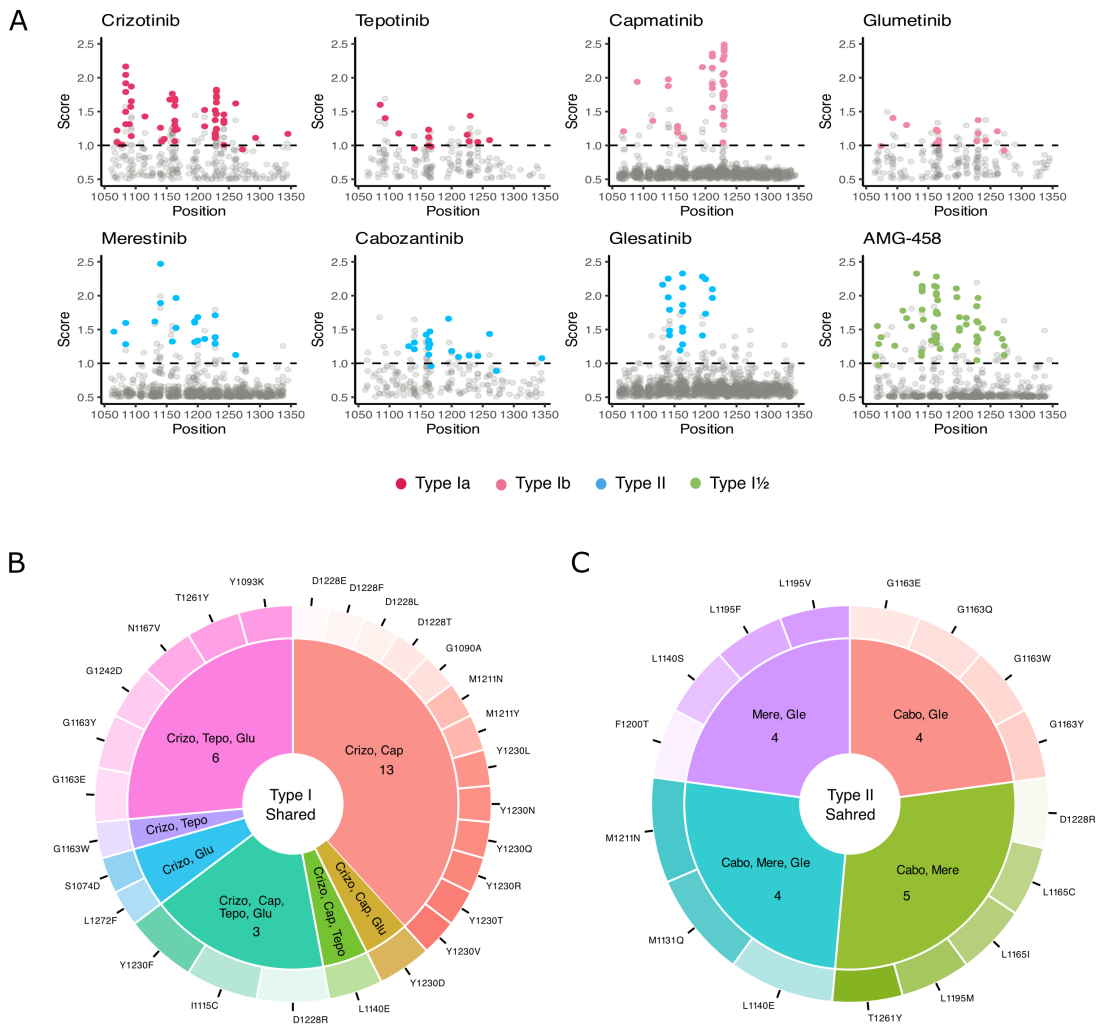

Supplemental Figure 2.9. Statistically filtered resistance mutations for individual inhibitors and shared mutations amongst type I and type II inhibitors. (A) Fitness scores for all variants above a score of 0.5 plotted for each kinase domain position. Individual mutations that pass score and statistical thresholds for resistance classification are highlighted (type Ia, hot pink; type Ib, light pink; type II, blue; type I1/2, green). Horizontal reference line on each graph is set to a score of 1. (B-C) Pie-doughnut charts showing the breakdown of shared resistance mutations across inhibitors of the same type, with the specific variants annotated.

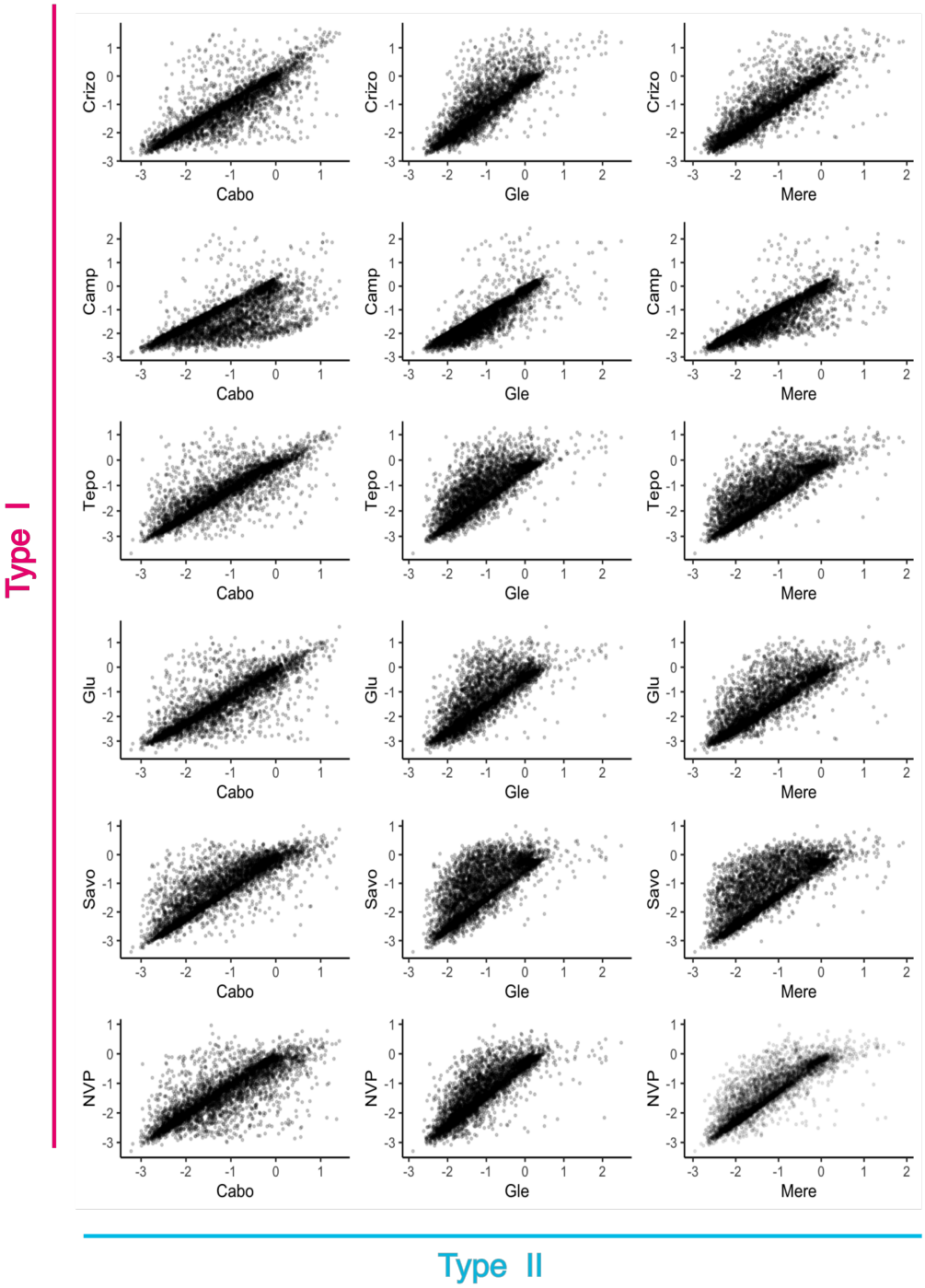

Supplemental Figure 2.10. Type I and type II inhibitor fitness score correlations. Correlation plots of DMSO subtracted fitness scores for all type I and type II inhibitor pairs.

References

An, L., Wang, Y., Wu, G., Wang, Z., Shi, Z., Liu, C., Wang, C., Yi, M., Niu, C., Duan, S., Li, X., Tang, W., Wu, K., Chen, S., & Xu, H. (2023). Defining the sensitivity landscape of EGFR variants to tyrosine kinase inhibitors. Translational Research, 255, 14–25. https://doi.org/10.1016/j.trsl.2022.11.002

Arter, C., Trask, L., Ward, S., Yeoh, S., & Bayliss, R. (2022). Structural features of the protein kinase domain and targeted binding by small-molecule inhibitors. Journal of Biological Chemistry, 298(8), 102247. https://doi.org/10.1016/j.jbc.2022.102247

Attwood, M. M., Fabbro, D., Sokolov, A. V., Knapp, S., & Schiöth, H. B. (2021). Trends in kinase drug discovery: Targets, indications and inhibitor design. Nature Reviews Drug Discovery, 20(11), Article 11. https://doi.org/10.1038/s41573-021-00252-y

Awad, M. M., Oxnard, G. R., Jackman, D. M., Savukoski, D. O., Hall, D., Shivdasani, P., Heng, J. C., Dahlberg, S. E., Jänne, P. A., Verma, S., Christensen, J., Hammerman, P. S., & Sholl, L. M. (2016). MET Exon 14 Mutations in Non-Small-Cell Lung Cancer Are Associated With Advanced Age and Stage-Dependent MET Genomic Amplification and c-Met Overexpression. Journal of Clinical Oncology: Official Journal of the American Society of Clinical Oncology, 34(7), 721–730. https://doi.org/10.1200/JCO.2015.63.4600

Bahcall, M., Paweletz, C. P., Kuang, Y., Taus, L. J., Sim, T., Kim, N. D., Dholakia, K. H., Lau, C. J., Gokhale, P. C., Chopade, P. R., Hong, F., Wei, Z., Köhler, J., Kirschmeier, P. T., Guo, J., Guo, S., Wang, S., & Jänne, P. A. (2022). Combination of Type I and Type II MET Tyrosine Kinase Inhibitors as Therapeutic Approach to Prevent Resistance. Molecular Cancer Therapeutics, 21(2), 322–335. https://doi.org/10.1158/1535-7163.MCT-21-0344

Bahcall, M., Sim, T., Paweletz, C. P., Patel, J. D., Alden, R. S., Kuang, Y., Sacher, A. G., Kim, N. D., Lydon, C. A., Awad, M. M., Jaklitsch, M. T., Sholl, L. M., Jänne, P. A., & Oxnard, G. R.

(2016). Acquired MET D1228V Mutation and Resistance to MET Inhibition in Lung Cancer. Cancer Discovery, 6(12), 1334–1341.
https://doi.org/10.1158/2159-8290.CD-16-0686

Basilico, C., Pennacchietti, S., Vigna, E., Chiriaco, C., Arena, S., Bardelli, A., Valdembri, D., Serini, G., & Michieli, P. (2013). Tivantinib (ARQ197) Displays Cytotoxic Activity That Is Independent of Its Ability to Bind MET. Clinical Cancer Research, 19(9), 2381–2392.
https://doi.org/10.1158/1078-0432.CCR-12-3459

Bouysset, C., & Fiorucci, S. (2021). ProLIF: A library to encode molecular interactions as fingerprints. Journal of Cheminformatics, 13(1), 72.
https://doi.org/10.1186/s13321-021-00548-6

Brenan, L., Andreev, A., Cohen, O., Pantel, S., Kamburov, A., Cacchiarelli, D., Persky, N. S., Zhu, C., Bagul, M., Goetz, E. M., Burgin, A. B., Garraway, L. A., Getz, G., Mikkelsen, T. S., Piccioni, F., Root, D. E., & Johannessen, C. M. (2016). Phenotypic Characterization of a Comprehensive Set of MAPK1/ERK2 Missense Mutants. Cell Reports, 17(4), 1171–1183.
https://doi.org/10.1016/j.celrep.2016.09.061

Cai, B., Li, X., Huang, X., Ma, T., Qu, B., Yu, W., Yang, W., Zhang, P., Chen, J., & Liu, F. (2021). Case Report: Sequential Combination Targeted Therapy With Type I and II MET Inhibitors in a Metastatic EGFR-Mutated, MET-Amplified NSCLC Patient With Acquired MET Y1230H Mutation. Frontiers in Oncology, 11.
https://www.frontiersin.org/articles/10.3389/fonc.2021.738832

Chakraborty, S., Ahler, E., Simon, J. J., Fang, L., Potter, Z. E., Sitko, K. A., Stephany, J. J., Guttman, M., Fowler, D. M., & Maly, D. J. (2023). Profiling of drug resistance in Src kinase at scale uncovers a regulatory network coupling autoinhibition and catalytic domain dynamics. Cell Chemical Biology.
https://doi.org/10.1016/j.chembiol.2023.08.005

Chardon, F. M., Suiter, C. C., Daza, R. M., Smith, N. T., Parrish, P., McDiarmid, T., Lalanne, J.-B., Martin, B., Calderon, D., Ellison, A., Berger, A. H., Shendure, J., & Starita, L. M. (2023). A multiplex, prime editing framework for identifying drug resistance variants at scale (p. 2023.07.27.550902). bioRxiv. https://doi.org/10.1101/2023.07.27.550902

Cohen, P., Cross, D., & Jänne, P. A. (2021). Kinase drug discovery 20 years after imatinib: Progress and future directions. Nature Reviews Drug Discovery, 20(7), Article 7. https://doi.org/10.1038/s41573-021-00195-4

Cui, J. J. (2014). Targeting Receptor Tyrosine Kinase MET in Cancer: Small Molecule Inhibitors and Clinical Progress. Journal of Medicinal Chemistry, 57(11), 4427–4453. https://doi.org/10.1021/jm401427c

Cui, J. J., Tran-Dubé, M., Shen, H., Nambu, M., Kung, P.-P., Pairish, M., Jia, L., Meng, J., Funk, L., Botrous, I., McTigue, M., Grodsky, N., Ryan, K., Padrique, E., Alton, G., Timofeevski, S., Yamazaki, S., Li, Q., Zou, H., … Edwards, M. P. (2011). Structure Based Drug Design of Crizotinib (PF-02341066), a Potent and Selective Dual Inhibitor of Mesenchymal–Epithelial Transition Factor (c-MET) Kinase and Anaplastic Lymphoma Kinase (ALK). Journal of Medicinal Chemistry, 54(18), 6342–6363. https://doi.org/10.1021/jm2007613

Dar, A. C., & Shokat, K. M. (2011). The Evolution of Protein Kinase Inhibitors from Antagonists to Agonists of Cellular Signaling. Annual Review of Biochemistry, 80(1), 769–795. https://doi.org/10.1146/annurev-biochem-090308-173656

Diedrich, K., Krause, B., Berg, O., & Rarey, M. (2023). PoseEdit: Enhanced ligand binding mode communication by interactive 2D diagrams. Journal of Computer-Aided Molecular Design, 37(10), 491–503. https://doi.org/10.1007/s10822-023-00522-4

Du, Z., & Lovly, C. M. (2018). Mechanisms of receptor tyrosine kinase activation in cancer. Molecular Cancer, 17(1), 58. https://doi.org/10.1186/s12943-018-0782-4

Duplaquet, L., Kherrouche, Z., Baldacci, S., Jamme, P., Cortot, A. B., Copin, M.-C., & Tulasne, D. (2018). The multiple paths towards MET receptor addiction in cancer. Oncogene, 37(24), 3200–3215. https://doi.org/10.1038/s41388-018-0185-4

Eathiraj, S., Palma, R., Volckova, E., Hirschi, M., France, D. S., Ashwell, M. A., & Chan, T. C. K. (2011). Discovery of a Novel Mode of Protein Kinase Inhibition Characterized by the Mechanism of Inhibition of Human Mesenchymal-epithelial Transition Factor (c-Met) Protein Autophosphorylation by ARQ 197. Journal of Biological Chemistry, 286(23), 20666–20676. https://doi.org/10.1074/jbc.M110.213801

Eberhardt, J., Santos-Martins, D., Tillack, A. F., & Forli, S. (2021). AutoDock Vina 1.2.0: New Docking Methods, Expanded Force Field, and Python Bindings. Journal of Chemical Information and Modeling, 61(8), 3891–3898. https://doi.org/10.1021/acs.jcim.1c00203

Elizabeth A. Tovar, & Graveel, C. R. (2017). MET in human cancer: Germline and somatic mutations. Annals of Translational Medicine, 5(10), Article 10. https://doi.org/10.21037/atm.2017.03.64

Engstrom, L. D., Aranda, R., Lee, M., Tovar, E. A., Essenburg, C. J., Madaj, Z., Chiang, H., Briere, D., Hallin, J., Lopez-Casas, P. P., Baños, N., Menendez, C., Hidalgo, M., Tassell, V., Chao, R., Chudova, D. I., Lanman, R. B., Olson, P., Bazhenova, L., … Christensen, J. G. (2017). Glesatinib Exhibits Antitumor Activity in Lung Cancer Models and Patients Harboring MET Exon 14 Mutations and Overcomes Mutation-mediated Resistance to Type I MET Inhibitors in Nonclinical Models. Clinical Cancer Research, 23(21), 6661–6672. https://doi.org/10.1158/1078-0432.CCR-17-1192

Escorcia, F. E., Houghton, J. L., Abdel-Atti, D., Pereira, P. R., Cho, A., Gutsche, N. T., Baidoo, K. E., & Lewis, J. S. (2020). ImmunoPET Predicts Response to Met-targeted Radioligand Therapy in Models of Pancreatic Cancer Resistant to Met Kinase Inhibitors. Theranostics,

10(1), 151–165. https://doi.org/10.7150/thno.37098

Evolutionary Modeling of Combination Treatment Strategies To Overcome Resistance to Tyrosine Kinase Inhibitors in Non-Small Cell Lung Cancer. (n.d.). https://doi.org/10.1021/mp200270v

Fernandes, M., Jamme, P., Cortot, A. B., Kherrouche, Z., & Tulasne, D. (2021). When the MET receptor kicks in to resist targeted therapies. Oncogene, 40(24), 4061–4078. https://doi.org/10.1038/s41388-021-01835-0

Flynn, J. M., Huang, Q. Y. J., Zvornicanin, S. N., Schneider-Nachum, G., Shaqra, A. M., Yilmaz, N. K., Moquin, S. A., Dovala, D., Schiffer, C. A., & Bolon, D. N. A. (2023). Systematic Analyses of the Resistance Potential of Drugs Targeting SARS-CoV-2 Main Protease. ACS Infectious Diseases. https://doi.org/10.1021/acsinfecdis.3c00125

Frampton, G. M., Ali, S. M., Rosenzweig, M., Chmielecki, J., Lu, X., Bauer, T. M., Akimov, M., Bufill, J. A., Lee, C., Jentz, D., Hoover, R., Ou, S.-H. I., Salgia, R., Brennan, T., Chalmers, Z. R., Jaeger, S., Huang, A., Elvin, J. A., Erlich, R., … Miller, V. A. (2015). Activation of MET via Diverse Exon 14 Splicing Alterations Occurs in Multiple Tumor Types and Confers Clinical Sensitivity to MET Inhibitors. Cancer Discovery, 5(8), 850–859. https://doi.org/10.1158/2159-8290.CD-15-0285

Fujino, T., Kobayashi, Y., Suda, K., Koga, T., Nishino, M., Ohara, S., Chiba, M., Shimoji, M., Tomizawa, K., Takemoto, T., & Mitsudomi, T. (2019). Sensitivity and Resistance of MET Exon 14 Mutations in Lung Cancer to Eight MET Tyrosine Kinase Inhibitors In Vitro. Journal of Thoracic Oncology, 14(10), 1753–1765. https://doi.org/10.1016/j.jtho.2019.06.023

Fujino, T., Suda, K., & Mitsudomi, T. (2021). Lung Cancer with MET exon 14 Skipping Mutation: Genetic Feature, Current Treatments, and Future Challenges. Lung Cancer: Targets

and Therapy, 12, 35–50. https://doi.org/10.2147/LCTT.S269307

Guérin, C. M., Vinchent, A., Fernandes, M., Damour, I., Laratte, A., Tellier, R., Estevam, G. O., Meneboo, J.-P., Villenet, C., Descarpentries, C., Fraser, J. S., Figeac, M., Cortot, A. B., Rouleau, E., & Tulasne, D. (2023). MET variants with activating N-lobe mutations identified in hereditary papillary renal cell carcinomas still require ligand stimulation (p. 2023.11.03.565283). bioRxiv. https://doi.org/10.1101/2023.11.03.565283

Hanson, S. M., Georghiou, G., Thakur, M. K., Miller, W. T., Rest, J. S., Chodera, J. D., & Seeliger, M. A. (2019). What Makes a Kinase Promiscuous for Inhibitors? Cell Chemical Biology, 26(3), 390-399.e5. https://doi.org/10.1016/j.chembiol.2018.11.005

Hoemberger, M., Pitsawong, W., & Kern, D. (2020). Cumulative mechanism of several major imatinib-resistant mutations in Abl kinase. Proceedings of the National Academy of Sciences, 117(32), 19221–19227. https://doi.org/10.1073/pnas.1919221117

Katayama, R., Aoyama, A., Yamori, T., Qi, J., Oh-hara, T., Song, Y., Engelman, J. A., & Fujita, N. (2013). Cytotoxic Activity of Tivantinib (ARQ 197) Is Not Due Solely to c-MET Inhibition. Cancer Research, 73(10), 3087–3096. https://doi.org/10.1158/0008-5472.CAN-12-3256

Kim, S.-M., Kim, H., Yun, M. R., Kang, H. N., Pyo, K.-H., Park, H. J., Lee, J. M., Choi, H. M., Ellinghaus, P., Ocker, M., Paik, S., Kim, H. R., & Cho, B. C. (2016). Activation of the Met kinase confers acquired drug resistance in FGFR-targeted lung cancer therapy. Oncogenesis, 5(7), Article 7. https://doi.org/10.1038/oncsis.2016.48

Li, A., Yang, J., Zhang, X., Zhang, Z., Su, J., Gou, L., Bai, Y., Zhou, Q., Yang, Z., Han-Zhang, H., Zhong, W.-Z., Chuai, S., Zhang, Q., Xie, Z., Gao, H., Chen, H., Wang, Z., Wang, Z., Yang, X., … Wu, Y. (2017). Acquired MET Y1248H and D1246N Mutations Mediate Resistance to MET Inhibitors in Non–Small Cell Lung Cancer. Clinical Cancer Research,

23(16), 4929–4937. https://doi.org/10.1158/1078-0432.CCR-16-3273

Lu, X., Peled, N., Greer, J., Wu, W., Choi, P., Berger, A. H., Wong, S., Jen, K.-Y., Seo, Y., Hann, B., Brooks, A., Meyerson, M., & Collisson, E. A. (2017). MET Exon 14 Mutation Encodes an Actionable Therapeutic Target in Lung Adenocarcinoma. Cancer Research, 77(16), 4498–4505. https://doi.org/10.1158/0008-5472.CAN-16-1944

McDermott, U., Sharma, S. V., Dowell, L., Greninger, P., Montagut, C., Lamb, J., Archibald, H., Raudales, R., Tam, A., Lee, D., Rothenberg, S. M., Supko, J. G., Sordella, R., Ulkus, L. E., Iafrate, A. J., Maheswaran, S., Njauw, C. N., Tsao, H., Drew, L., … Settleman, J. (2007). Identification of genotype-correlated sensitivity to selective kinase inhibitors by using high-throughput tumor cell line profiling. Proceedings of the National Academy of Sciences, 104(50), 19936–19941. https://doi.org/10.1073/pnas.0707498104

Michaelides, I. N., Collie, G. W., Börjesson, U., Vasalou, C., Alkhatib, O., Barlind, L., Cheung, T., Dale, I. L., Embrey, K. J., Hennessy, E. J., Khurana, P., Koh, C. M., Lamb, M. L., Liu, J., Moss, T. A., O'Neill, D. J., Phillips, C., Shaw, J., Snijder, A., … Yang, W. (2023). Discovery and Optimization of the First ATP Competitive Type-III c-MET Inhibitor. Journal of Medicinal Chemistry, 66(13), 8782–8807. https://doi.org/10.1021/acs.jmedchem.3c00401

Michieli, P., & Di Nicolantonio, F. (2013). Tivantinib—A cytotoxic drug in MET inhibitor's clothes? Nature Reviews Clinical Oncology, 10(7), Article 7. https://doi.org/10.1038/nrclinonc.2013.86

Mingione, V. R., Paung, Y., Outhwaite, I. R., & Seeliger, M. A. (2023). Allosteric regulation and inhibition of protein kinases. Biochemical Society Transactions, 51(1), 373–385. https://doi.org/10.1042/BST20220940

Munshi, N., Jeay, S., Li, Y., Chen, C.-R., France, D. S., Ashwell, M. A., Hill, J., Moussa, M. M.,

Leggett, D. S., & Li, C. J. (2010). ARQ 197, a Novel and Selective Inhibitor of the Human c-Met Receptor Tyrosine Kinase with Antitumor Activity. Molecular Cancer Therapeutics, 9(6), 1544–1553. https://doi.org/10.1158/1535-7163.MCT-09-1173

Paik, P. K., Drilon, A., Fan, P.-D., Yu, H., Rekhtman, N., Ginsberg, M. S., Borsu, L., Schultz, N., Berger, M. F., Rudin, C. M., & Ladanyi, M. (2015). Response to MET Inhibitors in Patients with Stage IV Lung Adenocarcinomas Harboring MET Mutations Causing Exon 14 Skipping. Cancer Discovery, 5(8), 842–849. https://doi.org/10.1158/2159-8290.CD-14-1467

Peach, M. L., Tan, N., Choyke, S. J., Giubellino, A., Athauda, G., Burke, T. R. Jr., Nicklaus, M. C., & Bottaro, D. P. (2009). Directed Discovery of Agents Targeting the Met Tyrosine Kinase Domain by Virtual Screening. Journal of Medicinal Chemistry, 52(4), 943–951. https://doi.org/10.1021/jm800791f

Persky, N. S., Hernandez, D., Do Carmo, M., Brenan, L., Cohen, O., Kitajima, S., Nayar, U., Walker, A., Pantel, S., Lee, Y., Cordova, J., Sathappa, M., Zhu, C., Hayes, T. K., Ram, P., Pancholi, P., Mikkelsen, T. S., Barbie, D. A., Yang, X., … Johannessen, C. M. (2020). Defining the landscape of ATP-competitive inhibitor resistance residues in protein kinases. Nature Structural & Molecular Biology, 27(1), 92–104. https://doi.org/10.1038/s41594-019-0358-z

Puccini, A., Marín-Ramos, N. I., Bergamo, F., Schirripa, M., Lonardi, S., Lenz, H.-J., Loupakis, F., & Battaglin, F. (2019). Safety and Tolerability of c-MET Inhibitors in Cancer. Drug Safety, 42(2), 211–233. https://doi.org/10.1007/s40264-018-0780-x

Rao, J., Xin, R., Macdonald, C., Howard, M., Estevam, G. O., Yee, S. W., Wang, M., Fraser, J. S., Coyote-Maestas, W., & Pimentel, H. (2023). Rosace: A robust deep mutational scanning analysis framework employing position and mean-variance shrinkage (p. 2023.10.24.562292). bioRxiv. https://doi.org/10.1101/2023.10.24.562292

Recondo, G., Bahcall, M., Spurr, L. F., Che, J., Ricciuti, B., Leonardi, G. C., Lo, Y.-C., Li, Y. Y., Lamberti, G., Nguyen, T., Milan, M. S. D., Venkatraman, D., Umeton, R., Paweletz, C. P., Albayrak, A., Cherniack, A. D., Price, K. S., Fairclough, S. R., Nishino, M., … Awad, M. M. (2020). Molecular Mechanisms of Acquired Resistance to MET Tyrosine Kinase Inhibitors in Patients with MET Exon 14–Mutant NSCLC. Clinical Cancer Research, 26(11), 2615–2625. https://doi.org/10.1158/1078-0432.CCR-19-3608

Recondo, G., Che, J., Jänne, P. A., & Awad, M. M. (2020). Targeting MET Dysregulation in Cancer. Cancer Discovery, 10(7), 922–934. https://doi.org/10.1158/2159-8290.CD-19-1446

Reungwetwattana, T., Liang, Y., Zhu, V., & Ou, S.-H. I. (2017). The race to target MET exon 14 skipping alterations in non-small cell lung cancer: The Why, the How, the Who, the Unknown, and the Inevitable. Lung Cancer, 103, 27–37. https://doi.org/10.1016/j.lungcan.2016.11.011

Rickert, K. W., Patel, S. B., Allison, T. J., Byrne, N. J., Darke, P. L., Ford, R. E., Guerin, D. J., Hall, D. L., Kornienko, M., Lu, J., Munshi, S. K., Reid, J. C., Shipman, J. M., Stanton, E. F., Wilson, K. J., Young, J. R., Soisson, S. M., & Lumb, K. J. (2011). Structural Basis for Selective Small Molecule Kinase Inhibition of Activated c-Met. Journal of Biological Chemistry, 286(13), 11218–11225. https://doi.org/10.1074/jbc.M110.204404

Santarpia, M., Massafra, M., Gebbia, V., D'Aquino, A., Garipoli, C., Altavilla, G., & Rosell, R. (2021). A narrative review of MET inhibitors in non-small cell lung cancer with MET exon 14 skipping mutations. Translational Lung Cancer Research, 10(3). https://doi.org/10.21037/tlcr-20-1113

Schmid, R., Heuckeroth, S., Korf, A., Smirnov, A., Myers, O., Dyrlund, T. S., Bushuiev, R., Murray, K. J., Hoffmann, N., Lu, M., Sarvepalli, A., Zhang, Z., Fleischauer, M., Dührkop, K., Wesner, M., Hoogstra, S. J., Rudt, E., Mokshyna, O., Brungs, C., … Pluskal, T. (2023).

Integrative analysis of multimodal mass spectrometry data in MZmine 3. Nature Biotechnology, 41(4), Article 4. https://doi.org/10.1038/s41587-023-01690-2

Smyth, E. C., Sclafani, F., & Cunningham, D. (2014). Emerging molecular targets in oncology: Clinical potential of MET/hepatocyte growth-factor inhibitors. OncoTargets and Therapy, 7, 1001–1014. https://doi.org/10.2147/OTT.S44941

Tanizaki, J., Okamoto, I., Okamoto, K., Takezawa, K., Kuwata, K., Yamaguchi, H., & Nakagawa, K. (2011). MET Tyrosine Kinase Inhibitor Crizotinib (PF-02341066) Shows Differential Antitumor Effects in Non-small Cell Lung Cancer According to MET Alterations. Journal of Thoracic Oncology, 6(10), 1624–1631. https://doi.org/10.1097/JTO.0b013e31822591e9

The Cancer Genome Atlas Research Network. (2014). Comprehensive molecular profiling of lung adenocarcinoma. Nature, 511(7511), 543–550. https://doi.org/10.1038/nature13385

Tiedt, R., Degenkolbe, E., Furet, P., Appleton, B. A., Wagner, S., Schoepfer, J., Buck, E., Ruddy, D. A., Monahan, J. E., Jones, M. D., Blank, J., Haasen, D., Drueckes, P., Wartmann, M., McCarthy, C., Sellers, W. R., & Hofmann, F. (2011). A Drug Resistance Screen Using a Selective MET Inhibitor Reveals a Spectrum of Mutations That Partially Overlap with Activating Mutations Found in Cancer Patients. Cancer Research, 71(15), 5255–5264. https://doi.org/10.1158/0008-5472.CAN-10-4433

Trott, O., & Olson, A. J. (2010). AutoDock Vina: Improving the speed and accuracy of docking with a new scoring function, efficient optimization, and multithreading. Journal of Computational Chemistry, 31(2), 455–461. https://doi.org/10.1002/jcc.21334

Wang, C., Li, J., Qu, L., Tang, X., Song, X., Yang, F., Chen, X., Lin, Q., Lin, W., Zhou, Y., Tu, Z., Chen, Y., Zhang, Z., & Lu, X. (2022). Discovery of D6808, a Highly Selective and Potent

Macrocyclic c-Met Inhibitor for Gastric Cancer Harboring MET Gene Alteration Treatment. Journal of Medicinal Chemistry, 65(22), 15140–15164. https://doi.org/10.1021/acs.jmedchem.2c00981

Wang, C., & Lu, X. (2023). Targeting MET: Discovery of Small Molecule Inhibitors as Non-Small Cell Lung Cancer Therapy. Journal of Medicinal Chemistry, 66(12), 7670–7697. https://doi.org/10.1021/acs.jmedchem.3c00028

Wood, G. E., Hockings, H., Hilton, D. M., & Kermorgant, S. (2021). The role of MET in chemotherapy resistance. Oncogene, 40(11), Article 11. https://doi.org/10.1038/s41388-020-01577-5

Yao, Y., Yang, H., Zhu, B., Wang, S., Pang, J., Wu, X., Xu, Y., Zhang, J., Zhang, J., Ou, Q., Tian, H., & Zhao, Z. (2023). Mutations in the MET tyrosine kinase domain and resistance to tyrosine kinase inhibitors in non-small-cell lung cancer. Respiratory Research, 24(1), 28. https://doi.org/10.1186/s12931-023-02329-1

Zhao, Z., & Bourne, P. E. (2020). Overview of Current Type I/II Kinase Inhibitors. In P. Shapiro (Ed.), Next Generation Kinase Inhibitors (pp. 13–28). Springer International Publishing. https://doi.org/10.1007/978-3-030-48283-1_2

Zhou, Y., Xiang, S., Yang, F., & Lu, X. (2022). Targeting Gatekeeper Mutations for Kinase Drug Discovery. Journal of Medicinal Chemistry, 65(23), 15540–15558. https://doi.org/10.1021/acs.jmedchem.2c01361

Zuccotto, F., Ardini, E., Casale, E., & Angiolini, M. (2010). Through the "Gatekeeper Door": Exploiting the Active Kinase Conformation. Journal of Medicinal Chemistry, 53(7), 2681–2694. https://doi.org/10.1021/jm901443h

Publishing Agreement

It is the policy of the University to encourage open access and broad distribution of all theses, dissertations, and manuscripts. The Graduate Division will facilitate the distribution of UCSF theses, dissertations, and manuscripts to the UCSF Library for open access and distribution. UCSF will make such theses, dissertations, and manuscripts accessible to the public and will take reasonable steps to preserve these works in perpetuity.

I hereby grant the non-exclusive, perpetual right to The Regents of the University of California to reproduce, publicly display, distribute, preserve, and publish copies of my thesis, dissertation, or manuscript in any form or media, now existing or later derived, including access online for teaching, research, and public service purposes.

DocuSigned by:
Gabriella Estevam
682E22F089C7433...
Author Signature

11/30/2023
Date